Exploring the influence of sediment heating, thermal maturity and hydrocarbon formation on Hg behaviour in the geological record

Asri Oktavioni Indraswari

Thesis submitted to The University of Oxford for the degree of Doctor of Philosophy in Earth Sciences



Department of Earth Sciences and Exeter College

University of Oxford

Supervised by Professor Tamsin Mather, Professor Hugh Jenkyns and Professor Stuart Robinson

Abstract

The use of sedimentary mercury (Hg) as a proxy for Large Igneous Provinces (LIPs) has become an increasingly important area of research. One key limitation in applying and understanding this proxy is its interaction with thermal maturation. The thermal maturation process is particularly relevant as Hg exhibits a strong affinity for organic-rich shale. When subjected to high temperatures, pressures, and extended burial durations, organic-rich sedimentary rocks undergo chemical transformations, leading to the formation of hydrocarbons. Here, the effect of natural burial-related thermal maturation is investigated using three drill cores with different levels of thermal maturity (immature, mature and post-mature) in Toarcian sediments (Posidonienschiefer Formation) from the Lower Saxony Basin, Germany. It was found that Hg concentrations increased by more than two-fold in mature and post-mature sediments compared to immature sediments, suggesting that thermal maturation may concentrate Hg in organic-rich shale through loss of organic carbon. Additionally, a series of artificial maturation experiments (pyrolysis) on immature Posidonienschiefer was conducted to simulate the natural process and to analyse Hg partitioning into bitumen produced during the early stages of maturation. This analysis was paired with Hg-thermal desorption profiles to monitor changes in Hg speciation throughout the maturation process. Finally, different lithologies representing various depositional environments and organic matter types (organic-rich *vs* organic-lean) were selected to investigate the factors affecting thermal maturation's impact on sedimentary Hg behaviour. The volatility of Hg was observed to be highly temperature- and lithology-dependent, with significant Hg loss in coal and carbonate-rich samples during artificial maturation experiments. Importantly, Hg partitioning into bitumen was minimal, and gaseous Hg was efficiently reabsorbed by the sediments upon cooling. These findings emphasize the critical role of thermal maturation history in interpreting Hg records as proxies for LIPs.

Extended Abstract

In recent decades, sedimentary mercury (Hg) enrichment has been widely used as a proxy for volcanism from Large Igneous Provinces (LIPs). However, there remain many open questions regarding the application of this proxy. For example, little is known about how the Hg contents of different types of sediments are influenced by varying types of organic matter (OM) (e.g., terrestrial vs marine OM) and degrees of thermal maturity. This question becomes significant because Hg tends to be strongly associated with organic-rich material, which, when these organic-rich samples are subjected to prolonged burial, resulting in exposure to high temperatures and pressures, may transform into hydrocarbons. Moreover, at present, the partitioning of sedimentary Hg into hydrocarbons is not well understood. Both burial-related maturation and igneous heating in the subsurface have the potential to generate hydrocarbons and release Hg. Understanding whether subsidence-related thermal maturation affects sedimentary mercury is crucial for comprehending Hg behaviour and mobility in the subsurface. This involves determining if thermal maturation can be replicated in laboratory experiments to better understand the kinetics, exploring how Hg partitions into hydrocarbons, assessing the potential for mobilised Hg to be recaptured by reservoir or host rocks, and identifying the factors that control Hg mobilisation.

This work begins by investigating the influence of thermal maturation on sedimentary Hg using three naturally matured cores (A, B and C) related to basin burial covering a wide range of thermal maturity from Toarcian sediments of the Lower Saxony Basin, Germany. Mercury concentrations, bulk organic geochemistry, and total sulphur data are presented. It is observed that Hg concentrations in the mature and post-mature Toarcian sediments are increased >2-fold relative to the immature material. The reduction in total organic carbon (TOC) suggests that the loss of organic carbon or host-rock mass during thermal maturation

may have facilitated the concentration of Hg in mature shales. Moreover, we argue that the increased Hg concentrations are most likely linked to Hg's 'closed system' behaviour in deep sedimentary basins and the relatively low temperature (70–260 ºC) during maturation, resulting in limited Hg mobility. This argument is further supported by the observation of the very low concentrations of Hg in the produced oil of Posidonienschiefer, indicating limited partitioning of Hg into the produced hydrocarbon – in line with the high Hg concentrations in our mature sediments.

The second study in this thesis examines how Hg partitions into generated gas, bitumen and sediment residues at an early stage of thermal maturation. Using the immature core A from the Lower Jurassic Posidonienschiefer, we conducted a series of isothermal artificial maturation experiments lasting 24–840 hours at 325ºC to quantify Hg volatilization and partitioning into generated bitumen. It is observed that there is a trend of gaseous Hg loss proportional to heating time and that only a small fraction of the Hg was partitioned into the bitumen (≤1% of the total initial Hg). The thermal desorption profiles (TDPs) from these artificially mature samples showed subtle changes to the Hg speciation after pyrolysis and gas escape. In contrast, the TDPs from the naturally matured shales (cores B and C from the Posidonienschiefer) showed that Hg gradually transitions into more stable species over millions of years of relatively low-temperature burial-related maturation. Finally, the reabsorption experiment reveals that gaseous Hg in closed vessels can be efficiently (≥95%) reabsorbed into the sediment within ≤1 hour of cooling, after which both the Hg speciation (derived from TDPs) and concentration values were identical to the original material. This rapid recapture of Hg into low-temperature Hg phases has not previously been observed in experimental settings, but this may mimic critical aspects of Hg behaviour in contact aureoles.

The final part of this work examines how different lithologies affect Hg dynamics during thermal maturation. Through the pyrolysis experiments at 325 °C over varied durations (24, 336, 500, and 840 hours), I added two new samples into the dataset: the Early Jurassic Belemnite Marls, which are carbonate-rich and OM-lean, and the Eocene Tanjung Formation, a coal rich in terrestrial OM. By analysing Hg concentrations, total organic carbon (TOC), hydrogen index (HI), and oxygen index (OI) before and after pyrolysis, and comparing with data from Posidonienschiefer, we found significant Hg losses—over 80% in the coal and marls within the first 24 hours, versus 50% in the Posidonienschiefer. We infer from the data generated here and earlier studies that Hg speciation may strongly impact the efficiency of Hg loss for a specific temperature range. Therefore, the amount of Hg hosted in weakly temperature-resistant *vs* more temperature-resistant species and the specific temperature regime of maturation could be critical parameters to project how Hg might be mobilised.

Combined, these studies give an important insight into multiple key processes regarding Hg behaviour in response to subsurface heating, with implications for Hg cycling during basin burial-related maturation (limited partitioning into bitumen) and contact metamorphism (release and recapture of gaseous Hg). The volatility of Hg in response to specific temperatures also highlights that the thermal maturation history of the sedimentary material is critical for the interpretation of Hg records. Further work with extended-duration thermal experiments at lower temperatures, devising methodology or equipment paired with gas (e.g., CO_2) detectors, and detailed petrographic analysis to look more closely at Hg speciation (e.g., pyrites) could be employed to get better-detailed mechanism and kinetics of Hg in the sediments during thermal maturation.

Acknowledgements

First and foremost, I want to express my deepest gratitude to my supervisors: Professor Tamsin Mather, Professor Hugh Jenkyns, and Professor Stuart Robinson. I'm incredibly grateful to Tamsin for trusting me and giving me the incredible opportunity to work on a DPhil project under her ERC-funded research. I truly can't thank her enough for believing in me and supporting me throughout this journey. A big thank you to Hugh for helping me with my English—his proofreading has been a lifesaver—and for always pointing me to valuable references. Stuart, I can't forget the help with the microwave-sonication solvent extraction training you managed to spare for me despite your very busy days**.** Arriving in such a foreign environment during the unpredictable times of the pandemic back in 2020, I'm incredibly thankful to all three of them for their thoughtful guidance throughout this project. From day one, they've been there, offering advice and encouragement. Their support has been a constant, and I couldn't have made it this far without their help.

Additionally, I would like to thank Professor Alex Dickson and Erdem Idiz for their academic help and technical support in this research and in preparing the draft. Alex's assistance has been invaluable, particularly with the visits to Royal Holloway. Erdem's contributions were equally crucial, offering continuous support with manuscript revisions and updates. His help with core access and the valuable contacts with Shell were indispensable throughout the project.

A special mention to Joost Frieling, whose insightful discussions and generous support have meant so much to my research. I can't thank him enough for reading through my work, offering thoughtful feedback on my English, and helping me sharpen my writing. Our conversations about pyrolysis, Lumex, and Rock-Eval techniques were always enlightening, and his advice really helped me gain a deeper understanding of these methods. Joost also played a huge role in guiding me through the writing process, offering suggestions that made my work much clearer and more concise. I truly appreciate his patience and the help he gave me throughout this journey.

I would also like to thank Steve Wyatt, Darren Hillegond, James Berkeley at Royal Holloway, and Jerry Tian for their generous help in the lab. Their expertise and assistance played a key role in successfully completing this research.

I want to thank the Jardines Foundation for their generous support throughout my studies. Their scholarship has been invaluable in enabling me to pursue my research and complete my DPhil at Oxford.

A special thanks must go to the many friends I've made at Oxford over the past four years. To every Indonesian I've met through PPI Oxford and Pengajian, especially in the final year of writing: Diny, Deva, Aji, Wynne, Tina, Aisha and family, Kak Kaca, Widari, Fay, Oliv, Puspa, Mas Rangga, Bu Yani and family, Mas Fandy, and Mba Jessica—thank you for the hangouts, talks, and random walks that helped me keep my sanity. A special thanks to Wian and Hanifi; without them telling me about Jardine, I wouldn't have even ended up in Oxford in the first place. I also want to thank my postgraduate cohort for sharing these crazy years of research, especially starting a DPhil during such unusual times. And, of course, a big shoutout to my 30.18 mates—Bram, Jack, and Ian—you all have made this journey both enjoyable and unforgettable.

To my parents and my sister, thousands of kilometres away from Oxford, I owe everything to them. Their love and encouragement have been my unwavering source of strength throughout this journey.

Finally, I would like to express my deepest gratitude to Allah SWT for His endless blessings, guidance, and strength that have enabled me to start and complete this journey. All praise is due to Him.

Biggest thanks again to all,

Asri

List of Contents

Abstract ..... **ii**

Extended Abstract ..... **iii**

Acknowledgements ..... **vi**

List of Contents ..... **viii**

List of Figures ..... **xii**

List of Tables ..... **xiii**

1. Sedimentary mercury (Hg) and thermal maturation **1**

1.1. Introduction 1

Sedimentary mercury and its use as a proxy for volcanic activity 1

Effects of thermal maturation on sedimentary mercury 2

1.2. Sedimentary mercury in organic-rich mudrocks (primary deposition) 3

Deposition and association of mercury with other sedimentary phases 3

Deposition of organic-rich facies 4

1.3. Thermal maturation and hydrocarbon production 5

What is thermal maturation? 5

Effect of thermal maturation on metals in organic-rich sedimentary rocks 7

1.4. Mercury speciation, heating temperature, and desorption 10

1.5. Thesis objectives, main findings and outlook 10

2. Investigating the behaviour of sedimentary mercury (Hg) during burial-related thermal maturation **15**

Abstract 16

2.1. Introduction 17

2.1.1. Host phases for sedimentary Hg and its use as a proxy for paleo-volcanic activity 17

2.1.2. The presence of Hg in hydrocarbon reserves 18

2.1.3. Effects of thermal maturation 19

2.1.4. Behaviour of Hg during maturation 20
2.2. Geological Setting and Samples 23
2.3. Methods 26
2.4. Results 28
2.4.1. Bulk sediment chemistry and maturity (TOC, TS, HI and OI) 28
2.4.2. Sedimentary Hg, Hg/TOC and Hg/TS analyses 34
2.4.3. Hg analyses of oils 36
2.5. Discussion 37
2.5.1. Mercury enrichment: differences in OM type and original depositional environmental conditions between cores? 37
2.5.2. Carrier-phase depletion 39
2.5.3. Mobilization and redeposition of Hg 40
2.5.4. Redistribution and mobilization of Hg by fractures and veins 42
2.5.5. Summary of controls on Hg concentrations in cores A, B, and C 43
2.5.6. Implications for the use of the Hg proxy in mature sediments 44
2.6. Conclusions 47
3. Limited mercury (Hg) partitioning into bitumen and efficient gaseous Hg reabsorption in early thermal maturation of organic-rich mudrocks 49
Abstract 50
3.1. Introduction 51
3.2. Material and methods 57
3.2.1. Sample material 57
3.2.2. Solvent extraction 57
3.2.3. Pyrolysis experiments 58
3.2.4. Cooling and reabsorption experiment 59
3.2.5. Total organic carbon and Rock-Eval analysis 60
3.2.6. Mercury analyses for sediments and bitumen 61
3.2.7. Thermal desorption 62
3.3. Results 62
3.3.1. Organic matter maturation 62
3.3.2. Mercury and Hg/TOC in residues, organic extracts, and oils 63

3.3.3 Thermal Desorption Profiles from pyrolysis experiments and natural samples 67
3.3.4. Mercury behaviour during cooling – reabsorption experiments 69
3.4. Discussion 70
3.4.1. Trends in Hg and processes driving Hg loss 70
3.4.2. Mercury partitioning into (hydrocarbon) fluid and gas phases 72
3.4.3. Mercury reabsorption from a gas phase 73
3.4.4. The potential impact of Hg speciation and changes in Hg speciation: natural system *vs* artificial maturation 74
3.5. Conclusions 75
4. The influence of primary depositional conditions on Hg behaviour during early thermal maturation 77
Abstract 78
4.1. Introduction 79
4.2. Material and methods 83
4.2.1. Sample material 83
4.2.2. Methods 86
4.3. Results 90
4.3.1. Organic-matter maturation 90
4.3.2. Mercury (Hg) and Hg/TOC in residues and bitumen 91
4.3.3. Thermal desorption profiles (TDPs) of sedimentary mercury 94
4.4. Discussion 100
4.4.1. Is the rate of Hg release from sediments related to different primary Hg speciation characteristics? 101
4.4.2. Sedimentary Hg speciation and primary depositional environment 102
4.4.3. Thermally induced organic matter transformation and Hg release 104
4.4.4. Relevance to contact aureoles and burial-related maturation 106
4.5. Conclusions and outlook 107
5. Conclusions and Future Work 109
5.1. Summary of results 109
5.2. Conclusions 112

5.3. Future work 114

Bibliography 116

Appendices 141

Appendix 1 - Chapter 2 Supporting Information 141

Appendix 2 - Chapter 3 Supporting Information 145

Appendix 3 – Data tables 146

List of Figures

1.1. Different environmental settings and its related Hg-speciation 6

1.2. Hydrocarbon formation and Hg species temperature desorption 9

2.1. Map of Lower Saxony Basin and location of cores 23

2.2. TOC, HI, TS, Hg, Hg/TOC, Hg/TS, and Mo plots for core A 30

2.3. TOC, HI, TS, Hg, Hg/TOC, and Hg/TS plots for core B 31

2.4. TOC, HI, TS, Hg, Hg/TOC, Hg/TS, and Mo plots for core C 32

2.5. Statistical comparison of TOC, Hg, Hg/TOC, and Hg/TS in different cores 33

2.6. Comparison of TOC, Hg, Hg/TOC, and Hg/TS plots in different cores 33

3.1. Context of pyrolysis experiment 56

3.2. Overview of the experimental procedures 59

3.3. Bulk organic geochemical results from pyrolysis 63

3.4. Hg results from pyrolysis experiments 64

3.5. Distribution of Hg in pyrolysis experiments 66

3.6. Hg concentration in Posidonienschiefer-derived oils 67

3.7. Thermal desorption profiles from pyrolysis experiments 69

3.8. Thermal desorption profiles from reabsorption experiments 70

4.1. Rock-Eval analysis from the three samples 93

4.2. Total Hg (Hg_T) remaining in the residue after pyrolysis 95

4.3. Bitumen produced after pyrolysis 96

4.4. Mercury thermal desorption profiles before and after pyrolysis 99

4.5. Mercury fraction in response to artificial heating 105

List of Tables

2.1. Geochemical data in different cores in this study 34

2.2. Hg in oils derived from the Posidonienschiefer 36

2.3. Summary of Hg processes in cores A, B, and C 44

3.1. Summary of temperature conditions of previous studies 54

3.2. Sub-sample information and pyrolysis condition 59

3.3. Sub-sample information and reabsorption condition 60

3.4. Hg and bitumen data from pyrolysis experiments 65

4.1. Summary of the depositional environments, redox conditions, and lithologies 84

4.2. Geochemical measurements from Tanjung Formation coal and Belemnite Marls 92

4.3. Distribution of Hg in the residues and bitumen 97

1. Sedimentary mercury (Hg) and thermal maturation

1.1. Introduction

Sedimentary mercury and its use as a proxy for volcanic activity

The development of mercury (Hg) as a proxy for volcanic activity has significantly advanced our understanding of Earth's geological and environmental history. Volcanic eruptions emit substantial amounts of Hg into the atmosphere (Pyle & Mather, 2003), where it can disperse globally before depositing in sediments. These characteristics enable Hg concentrations in sedimentary records to serve as indicators of past volcanic events especially when contemporaneous spikes are seen globally (e.g., Sanei et al., 2012; Percival et al., 2015). By analysing Hg levels alongside data on the carbon cycle, climate variations, and environmental changes within the same stratigraphic sequences, a high-resolution reconstruction of periods marked by elevated volcanic activity can potentially be achieved. This approach facilitates a comprehensive examination of the climatic and environmental impacts of volcanism.

However, interpreting sedimentary Hg concentrations is not always straightforward, as Hg records in sediments are influenced by factors such as release pathways (e.g., subaerial versus submarine LIP activity: Percival et al., 2018), and depositional pathways, including local conditions—particularly terrestrial runoff (Them et al., 2019; Dal Corso et al., 2020)—redox conditions, and early diagenesis (Frieling et al., 2023) (Fig. 1.1; e.g., Grasby et al., 2019). Variations due to all these factors are captured in the geological record of sedimentary Hg. A more recent insight is that processes such as thermal maturation and Hg alteration due to dyke

or sill intrusions (Svensen et al., 2023a, Frieling et al. 2024a) in the deep-time records can potentially also significantly modify the Hg signals recovered from the sedimentary record. Both syn-depositional and post-depositional processes can lead to substantial changes in sedimentary Hg records and these have to be constrained prior to its use as a reliable proxy for volcanic activity.

Effects of thermal maturation on sedimentary mercury

Recent studies have examined the effects of high-temperature exposure on Hg in sediments (e.g., Liu et al., 2022; Chen et al., 2022; Svensen et al., 2023a). However, these works have focused primarily on the impact of very high temperatures and pressures, more commonly associated with igneous intrusions and metamorphism, rather than subsidence-related thermal maturation. These studies have not explored the hydrocarbon production part of thermal maturation and how that may influence sedimentary Hg behaviour. Mercury in hydrocarbon (oil, gas, and condensates) is found in various concentrations (1–593 ppb, with the majority of concentrations at the lower end, Wilhelm & Bloom, 2000; Wilhelm et al., 2007; Bryndzia et al., 2023) which highlighted that Hg can be mobilised in subsurface conditions. Moreover, it has been established that high concentrations of Hg are detrimental for hydrocarbon production and refining facilities since Hg can precipitate and cause corrosion to the pipes (Groysman, 2017). These adverse effects for the petroleum industry have stimulated interest in being able to resolve the origin of Hg: where Hg comes from and how it behaves in the subsurface (see, for example, Filby, 1994; Zettlitzer et al., 1997; Liu, 2013; Li et al., 2019; Bryndzia, 2023).

While previous studies have investigated the partitioning of trace metals (e.g., Mo, Cd, V) into the bitumen and asphaltene fractions of oils produced from thermally matured organic-rich rocks (Dickson et al., 2020, 2022; Kendall et al., 2023), the behaviour of Hg in this context

remains unexamined. This thesis addresses this gap by providing the first investigation into the impact of subsidence-related thermal maturation and hydrocarbon production on Hg in sedimentary rocks. One of the key questions addressed in this study is whether Hg is carried away by hydrocarbons during production or redeposited and reabsorbed into sediments after volatilization. These dynamics are not well understood and pose challenges in predicting the mobility and potential recapture of mercury in subsurface environments, relevant to both hydrocarbon and igneous systems. Constraining the mobility of Hg is also key in determining its release efficiency during thermal maturation in the aureoles around igneous intrusions, which have been proposed as important contributors to the Hg and carbon emissions from some large igneous provinces

1.2. Sedimentary mercury in organic-rich mudrocks (primary deposition)

Deposition and association of mercury with other sedimentary phases

Mercury is known to be closely associated with organic matter (OM) in water and soft sediment (Outridge et al., 2007, Gehrke et al., 2009), and it has been suggested that elevated OM deposition may lead to elevated Hg deposition. Therefore, to identify anomalous Hg levels in sediments that may relate to elevated volcanic Hg emissions, Hg concentrations are often normalised to total organic carbon (TOC), a step that aims to correct for the Hg increase associated with high organic matter content (e.g., Sanei et al., 2012; Grasby et al., 2019). However, because Hg can also associate with sulphides and potentially clay minerals, this association can complicate the expected relationship between sedimentary organic matter and Hg (see, for example, Sanei et al., 2012; Charbonnier and Föllmi, 2017; Percival et al., 2018; Shen et al., 2019a, 2020). For this reason, several researchers recommend examining the relationship of Hg not only with TOC but also with clay (often using Al concentrations to quantify clay levels) and total sulphur, which are important controls of Hg association in

various depositional environments (e.g., Grasby et al., 2019; Shen et al., 2020). Indeed, it has been found that there are usually multiple Hg species in a single sample, both in deep-time sedimentary rocks (Frieling et al., 2024b) and recent sediments (Xu et al., 2021). Additionally, the source type of organic matter, whether marine or terrestrial, has been suggested to complicate the Hg-OM relationship, making it challenging to interpret ancient sedimentary Hg records (Grasby et al., 2017; Wang et al., 2018; Them et al., 2019).

Deposition of organic-rich facies

Fine-grained, organic-rich sediments like shales and coals typically contain labile organic matter derived from the original biomass, such as algae and vascular plant matter. These sediments were often deposited under reducing conditions that limited degradation and remineralization, thus promoting the preservation of organic matter (Tissot & Welte, 1984; Bohacs et al., 2020; Dembicki, 2022). This preservation makes these deposits valuable as hydrocarbon source rocks since the labile organic matter can undergo transformation, converting to oil and gas through burial and thermal stress over geological time (Dembicki, 2022). Anoxic or euxinic depositional environments are critical for the preservation of organic-rich mudrocks, as these conditions enhance the presence of hydrogen sulphide (H_2S). When H_2S interacts with mercury (Hg), it can form mercury-sulphide associations, such as pyrite and HgS, which may act as significant Hg hosts (Shen et al., 2020; Frieling et al., 2023). This process complicates the relationship between Hg and its host minerals, posing challenges for using Hg as a straightforward proxy for volcanic activity. For instance, study by Shen et al. (2019a) highlighted how total sulphur (TS), a proxy for sulphide, can appear as a dominant Hg host, where sulphide-bound Hg in sediments from the Ordovician/Silurian boundary may have created false positives in Hg/TOC that could then be misinterpreted as volcanic signals. These complexities underscore the importance of understanding how primary depositional and early diagenetic environments—whether dominated by high sulphide conditions or limited in

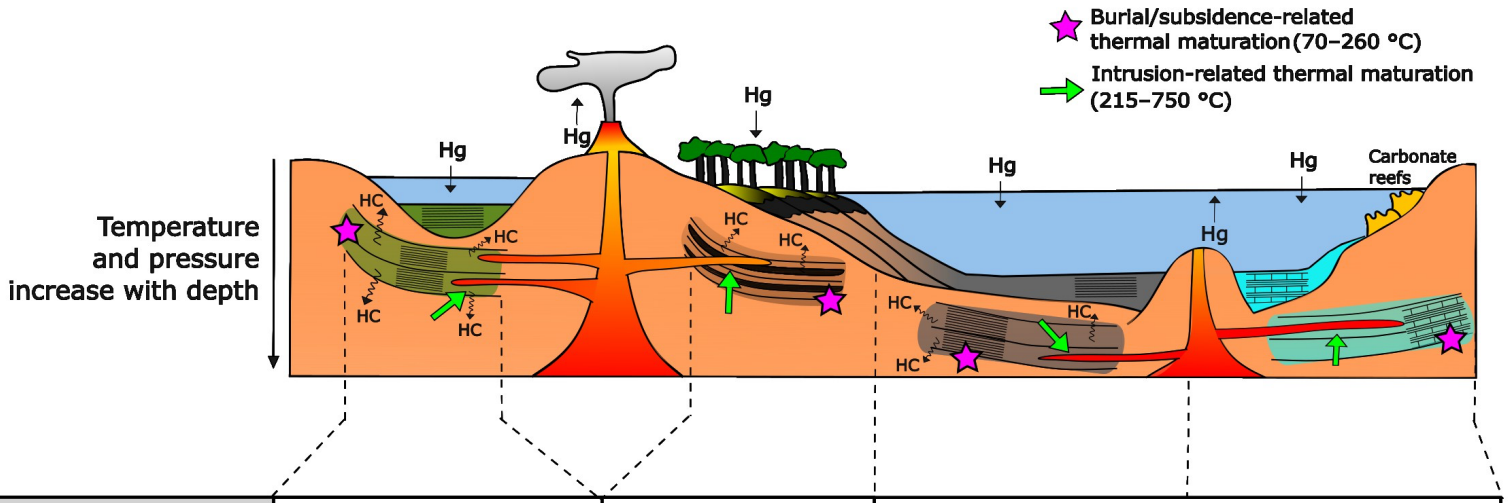
sulphide—affect Hg behaviour during burial and thermal maturation (Fig. 1.1). One of the aims of this thesis to unravel these dynamics, shedding light on how depositional settings influence the geochemical evolution of Hg in organic-rich facies.

1.3. Thermal maturation and hydrocarbon production

What is thermal maturation?

Thermal maturation is the process by which organic matter (OM) in sediments is transformed into hydrocarbons under the influence of temperature, pressure, and time (Tissot & Welte, 1984; Dembicki, 2022). During this process, OM transitions from immature sediments to the oil window at approximately 60°C (oil window), and eventually to the gas window at around 100–120°C (gas window) (Tissot & Welte, 1984) (Fig. 1.2). With increasing temperature, OM is converted into oil and gas through processes called thermal cracking, leaving behind a carbon-rich residue (Tissot & Welte, 1984; Peters et al., 2005; Dembicki, 2022).

Thermal maturation processes in nature involve not only burial- (or subsidence-) related heating but also magmatic intrusion. In burial-related heating, in sedimentary basins with vertical thermal gradients ranging from 20°C/km to 40°C/km (Gluyas & Swarbrick, 2021), and an average surface temperature of 20°C, reaching the oil window requires a burial depth of about 1.5 km, while reaching the gas window necessitates approximately 2.5 km of burial depth. The cracking of kerogen and its conversion into hydrocarbons is governed by temperature and heating duration, typically taking place over millions of years under slow heating rates (Burnham, 2017).



Environment of deposition	Lake	Coal swamps	Marine	
			Clastic	Calcareous
Organic matter type	I Lacustrine algae	III Vitrinite, higher plants (wood)	II Marine phytoplankton, algae	IV Inert
Hydrocarbon generations during thermal maturation	Oil-prone	Gas-prone (condensate)	Oil-prone	Non-source rock (No hydrocarbon generation)
Oxygenation regime	Anoxic–non-euxinic	Suboxic–dysoxic	Anoxic–euxinic	Oxic–suboxic
Associated Hg-compounds in primary deposition (?)	Hg-OM Hg-S (small potential)	Hg-OM Hg-S (small potential)	Hg-OM Hg-S	Hg-OM Hg-Clay minerals(?)

Figure 1.1. Different environmental settings and their associated mercury (Hg) speciation. Adapted from Jones et al. (2019) and Percival et al. (2020). Organic matter type classification and related hydrocarbon products are based on Tissot and Welte (1984).

By contrast, intrusion-related thermal maturation is driven by magmatic intrusions at varied temperatures of contact metamorphism ranging from 300°C to 800°C (Moorcroft & Tonnelier, 2016; Aarnes et al., 2011; Svensen et al., 2023a). The duration of maturation in the intrusion settings is also very rapid compared to the subsidence-related ones, at the scale of ≥ 10^2 years (e.g., see Iyer et al., 2017). When organic-rich sediments are exposed to excessive heat or rapid heating, the organic matter (OM) in the sediments tends to become overmature or "baked" producing hydrocarbons mostly in gaseous form in the contact aureoles (Aarnes et al., 2011). Any oil produced will also experience secondary cracking which is a conversion from liquid phase into gas phase above ~120 °C (Hunt, 1996). In the Karoo basin, this produced hydrocarbons in the gas form that is interpreted to be released from the aureole together with other fluids via breccia pipes (Svensen et al., 2007, 2008, 2009).

Effect of thermal maturation on metals in organic-rich sedimentary rocks

Thermal maturation has been shown to significantly affect trace metals such as Mo, V, and Ni, which are commonly associated with organic matter (OM) in sediments (Lewan & Maynard, 1982; Chappaz et al., 2014; Dahl et al., 2017). Some metals, including Mo, Zn, and Cd, tend to concentrate in the residue after heating due to the combined effects of rock mass loss from bitumen removal, the volatilization of organic matter, and water loss during clay dehydration (Ardakani et al., 2020; Dickson et al., 2020, 2022). Dickson et al. (2020) further observed that only minor (<5%) partitioning of metals into migrated hydrocarbons occurs, leaving relatively immobile elements in the residue that are speculatively held in inorganic phases, predominantly sulphides. Furthermore, the generation of gases such as H_2S during maturation may further influence metal concentrations (Abarghani et al., 2020). They suggested that H_2S released during thermal maturation could enhance pore water–rock

interactions and promote the formation of authigenic Fe-sulphides, thereby increasing the uptake of redox-sensitive trace metals and their concentrations in pore water.

For Hg, its transfer into hydrocarbon fluids during thermal maturation remains uncertain (Bryndzia et al., 2023). Current methods for isolating kerogen-associated metals are limited, as they require dissolving the mineral matrix with strong acids like HF and HCl, which can alter the metal content within kerogen. This limitation complicates assessments of Hg behaviour within organic matter (OM) as sedimentary rocks mature, raising questions about its reliability as a volcanic proxy especially for deeply buried or thermally altered rocks such as those commonly used in geological deep time studies. Understanding how much Hg partitions into produced hydrocarbons and where it may migrate after maturation is critical for determining its host phases. For instance, does Hg primarily associate with inorganic phases like other trace metals (Mo, Cd, Zn), or does it behave differently? These questions are central to evaluating Hg's geochemical behaviour and its potential redistribution during burial and maturation, with implications for interpreting volcanic signals in sedimentary records.

The impact of thermal maturation on Hg varies with geological conditions. Studies on LIP volcanism show that rapid heating from igneous intrusions can cause significant Hg loss, while burial-induced maturation occurs at lower temperatures over millions of years, facilitating kerogen-to-hydrocarbon conversion and possible Hg mobilisation (Liu et al., 2022; Svensen et al., 2023a). Differences in maturation processes and conditions thus underscore the need for caution when using Hg as a geochemical marker, as its behaviour may differ widely between rapid heating and gradual burial scenarios.

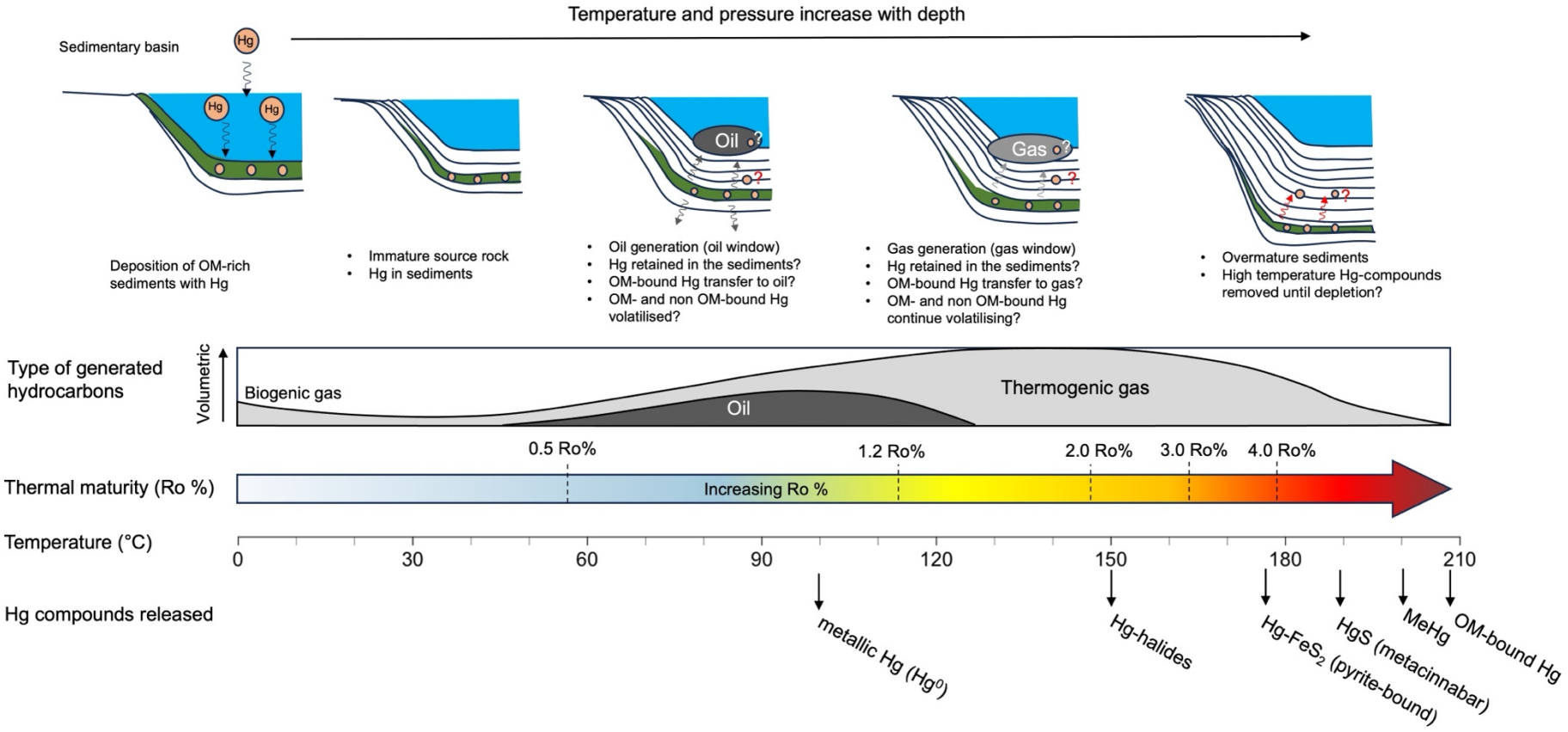


Figure 1.2. Burial-related thermal maturation and hydrocarbon production and thermal stability of chemical Hg species as determined for pure compounds. Mercury halides and metallic Hg are likely very rare in natural sedimentary systems. Adapted from Bjørlykke (1989). Data on thermal desorption temperatures of Hg species compiled by Frieling et al. (2024b).

1.4. Mercury speciation, heating temperature, and desorption

Mercury initially is hosted in different phases (Frieling et al., 2024a, b; Qu et al. 2024), although in general in interpreting LIPs most studies still employ a normalisation to TOC (e.g., Sanei et al., 2012; Percival et al., 2015). But it has been clear for some time that Hg is hosted in other phases too, such as HgS or be hosted by sulphide minerals such as pyrite (Manceau et al., 2018; Pham et al., 2014), HgSe (Mercone et al., 1999), and even has been proposed to be hosted in iron-oxides and clay minerals (e.g., Percival et al., 2018). One of the aims of this thesis is to understand how Hg behaves when heated is related to the temperatures that the sediments are exposed to and what Hg speciation is present in the sediments (Fig. 1.1).

Different Hg species have their own thermal desorption temperatures. By heating certain mercury standard samples, we can track at what temperature that specific Hg phase was volatilized. For example, in modern soil, Hg-OM has been found to desorb at temperature <200°C (Rumayor et al., 2015b; Saniewska and Bełdowska, 2017) while cinnabar HgS needs T >300°C to be volatilized. By exploring thermal desorption profiles (TDPs) in sedimentary rocks, Frieling et al. (2024a, b) demonstrated that a portion of sedimentary Hg is predominantly hosted as higher-temperature Hg species, which are likely not associated with OM or sulphur within OM. These findings challenge the long-standing assumption of a direct Hg-OM relationship in rocks and prompt a re-evaluation of the Hg-host phase normalisation used in paleoenvironmental reconstructions.

1.5. Thesis objectives, main findings and outlook

This study investigates the impact of sediment heating, thermal maturation, and hydrocarbon production on mercury (Hg) behaviour in sedimentary records through three complementary approaches: (1) analysing naturally matured organic-rich sediments (Toarcian

Posidonienschiefer cores) that underwent subsidence-related thermal maturation in the Lower Saxony Basin; (2) conducting laboratory simulations of heating using immature Posidonienschiefer sedimentary rocks to compare Hg behaviour after artificial and natural thermal maturation; and (3) experimenting with other mudrocks from various depositional environments, including the Belemnite Marls and the Tanjung Formation Coal, to evaluate Hg behaviour in different sedimentary rock types impacted by heating. The study employs Hg analysis (including thermal desorption profiles), geochemical characterisation (e.g., Rock-Eval, TOC and TS) in the sedimentary rocks), and measurements of Hg concentrations in oils and bitumen generated during experimental heating to enhance understanding of Hg speciation, mobilisation, and its interaction with organic matter across various depositional settings.

Chapter 2 examines Hg behaviour in the Toarcian Posidonienschiefer Formation in Germany's Lower Saxony Basin to understand how thermal maturation influences sedimentary Hg concentrations. By analysing cores with varying thermal maturities (immature, mature and post-mature), this chapter explores whether Hg remains stable in the sediment or undergoes redistribution during subsidence-related thermal maturation (70–260°C). As the Posidonienschiefer Formation is a prolific source rock known for oil generation, this chapter also investigates Hg concentrations in produced oils to determine whether Hg partitions into hydrocarbons during thermal maturation.

Chapter 3 focuses on isothermal artificial maturation experiments to study subsurface Hg cycling. Using immature Posidonienschiefer sedimentary rocks, pyrolysis experiments were conducted at 325°C for durations ranging from 24 to 840 hours to investigate whether sedimentary Hg in the laboratory behaves similarly to naturally matured samples. The chapter examines Hg transfer to produced bitumen and explores the potential for redeposition/recapture of mobilised Hg into the sediments during cooling—a mechanism hypothesised to explain Hg

capture in igneous contact aureoles. Thermal desorption profiles (TDPs) are used to compare Hg speciation in naturally matured cores from Chapter 2 with artificially matured samples, addressing questions about Hg mobility in low-permeability environments like the Lower Saxony Basin.

Chapter 4 investigates the efficiency of Hg volatilization in different types of sedimentary rocks by conducting pyrolysis experiments on the Belemnite Marls and the Tanjung Formation Coal. These rocks, along with the Posidonienschiefer data from Chapters 2 and 3, represent distinct depositional environments, including variations in redox conditions and organic matter types. The TDPs will allow us to examine how differences in Hg speciation across lithologies influence Hg release efficiency during thermal maturation. Additionally, the hydrocarbons produced from different types of organic matter will help address questions regarding Hg transport and mobilisation after volatilization.

Finally, Chapter 5 integrates findings from all these studies to gain new insight into the following key questions regarding how sediment heating, thermal maturation, and hydrocarbon production influence sedimentary Hg in geological records:

1. **How does natural subsidence-related thermal maturation affect sedimentary mercury?** Cores A, B, and C contain the same sequence of Lower Jurassic Posidonienschiefer from the Lower Saxony Basin, with distinct thermal maturity levels (%Ro) of 0.5–0.7% (immature), 1.5% (mature) and 3.5% (postmature), respectively (Gorbanenko and Ligouis, 2014, 2015). Previous study has examined changes in Mo, Zn, and Cd concentrations in these cores, showing that these trace metals are more concentrated in the mature cores (Dickson et al., 2021). However, Hg has not yet been studied in this context. With the development of the Hg-thermal desorption profiles (Hg-TDPs) method (Frieling et al., 2024a), we can now investigate Hg speciation across

immature, mature, and postmature cores to determine whether thermal maturation alters how Hg is hosted in sediments. This question will be addressed in Chapters 2 and 3.

2. **Does artificial thermal maturation affect sedimentary Hg in the same way as natural thermal maturation?** In Chapters 3 and 4, thermal maturation was simulated in laboratory experiments by heating the immature Core A of Posidonienschiefer, as well as other rocks with different lithologies, such as Tanjung Formation Coal and Belemnite Marls, following the procedure outlined by Dickson et al. (2020). The results were compared with those from previous experimental maturation studies (Liu et al., 2022; Chen et al., 2022) and with the results from Chapter 2 to explain the potential differences between artificial and natural thermal maturation.

3. **Is sedimentary Hg significantly affected by hydrocarbon production during thermal maturation?** In Chapter 2, Hg concentrations in oil produced by the Posidonienschiefer from the Lower Saxony Basin are analysed. Chapters 3 and 4 examine Hg in the bitumen produced during sediment heating to determine whether Hg partitions effectively during early maturation.

4. **What factors control the efficiency of Hg volatilization and reabsorption during thermal maturation?** In Chapter 2, the possibilities and hypotheses regarding the processes by which Hg is mobilised, redistributed, and redeposited or reabsorbed during subsidence-related natural thermal maturation are discussed. In Chapter 3, this question is addressed through open *versus* closed system conditions (reabsorption experiments), which may offer insights into Hg behaviour in natural subsidence-related thermal maturation, as discussed in Chapter 2, and in natural intrusion-related heating (Frieling et al., 2024b). In Chapter 4, it is explored whether OM type and primary depositional

settings influence the initial distribution of Hg speciation across sedimentary rocks and affects volatilization efficiency during thermal maturation.

The answers to these questions are explored in the following chapters, each shedding light on different aspects of Hg behaviour during thermal maturation. Chapter 2 focuses on the naturally subsidence-related maturation of sediments, while Chapter 3 examines the effects of artificial heating. Chapter 4 further investigates Hg volatilization efficiency in different sediment types. Together, these findings provide valuable insights into the complex processes that govern Hg behaviour in sedimentary environments.

2. Investigating the behaviour of sedimentary mercury (Hg) during burial-related thermal maturation

A very similar version of this chapter has been published as Indraswari, *et al*. (2024). Investigating the behavior of sedimentary mercury (Hg) during burial-related thermal maturation. *Geochemistry, Geophysics, Geosystems*, 25, e2024GC011555. https://doi.org/10.1029/2024GC011555. The full authors list as follows:

A. O. Indraswari[1,2], J. Frieling[1], T. A. Mather[1], A. J. Dickson[3], H. C. Jenkyns[1], E. Idiz[1]

[1]Department of Earth Sciences, University of Oxford, South Parks Road, Oxford, OX1 3AN, UK.

[2]Geoscience Study Program, Faculty of Mathematics and Natural Sciences (FMIPA), Universitas Indonesia, Depok 16424, Indonesia.

[3]Centre of Climate, Ocean and Atmosphere, Department of Earth Sciences, Royal Holloway University of London, Egham, Surrey, TW20 0EX, UK.

Abstract

Understanding the behaviour of mercury (Hg) in organic-rich sediments as they undergo thermal maturation is important, for example, because enrichment of Hg in sedimentary deposits has become a widely used proxy for volcanism from Large Igneous Provinces (LIPs). In this study, we evaluate the effects of such processes on sedimentary Hg concentrations by investigating a common stratigraphic interval in three drill cores with different levels of thermal maturity (immature, mature and post-mature) in Toarcian sediments (Posidonienschiefer Formation) from the Lower Saxony Basin, Germany. We present Hg concentrations, bulk organic geochemistry, and total sulphur data. Mercury concentrations in the mature and post-mature sediments are increased >2-fold relative to the immature material, which is greater than any potential differences in original Hg concentrations in the studied successions prior to burial. Organic-carbon and host-rock mass loss during thermal maturation may have concentrated Hg in the mature sediments to some extent, provided Hg is considered effectively immobile. The increased Hg, TOC-normalized Hg, and TS-normalized Hg are most likely linked to the 'closed system' behaviour of Hg in sedimentary basins and the relatively low temperatures (70–260 ºC) during maturation that resulted in limited Hg mobility. More speculatively, a certain degree of redistribution of Hg within the mature sediments is suggested by its enrichment in distinct stratigraphic levels. Regardless of the exact mechanisms at play, the elevated Hg concentrations in mature sediments amplify both Hg/TOC and Hg/TS, implying that thermal effects must be considered when using normalized Hg as a proxy for far-field volcanic activity.

2.1. Introduction

Mercury (Hg) is a highly toxic metal. Thus, understanding its behaviour in shallow- and deep-earth environments, and how it cycles through ecosystems, is of considerable importance (UN Environment, 2019). A major natural source of Hg in the environment is from volcanic exhalations (Pyle & Mather, 2003). Subsequent transport and deposition as dissolved or sorbed species is ultimately followed by removal into biomass in both terrestrial and aquatic settings (e.g., Fitzgerald & Lamborg, 2014; Them et al., 2019; Grasby et al., 2019). Consequently, mercury in the geological record is commonly associated with organic matter in marine, lacustrine, and terrestrial sediments (Sanei et al., 2012; Fitzgerald & Lamborg, 2014; Grasby et al., 2019). It is generally accepted that most Hg will be finally sequestered in sediments containing organic matter (OM) as OM-Hg complexes and associated sulphides. Indeed, field-data show that OM is a very effective scavenging ligand and likely the dominant carrier of Hg in the water column and sediments (Wallace, 1982; Benoit et al., 2001; Outridge et al., 2007).

2.1.1. Host phases for sedimentary Hg and its use as a proxy for paleo-volcanic activity

As volcanoes are amongst the largest natural sources of Hg to the atmosphere (Pyle & Mather, 2003), there has been much recent interest in the potential for its presence in sediments to serve as a proxy for large-scale volcanism, particularly in periods characterized by emplacement of large igneous provinces (LIPs) (Pyle & Mather, 2003; Sanei et al., 2012; Percival et al., 2015, 2021; Grasby et al., 2019). To detect anomalous Hg loading in sedimentary deposits, Hg concentrations are usually normalized with respect to total organic carbon (TOC) to correct for increases associated with larger amounts of organic matter (e.g., Sanei et al., 2012; Grasby et al., 2019). However, Hg can also be bound to sulphides and clay minerals and, in some environments, association with such geochemical species may

complicate the usual relationship found between sedimentary OM and Hg (see e.g., Sanei et al., 2012; Charbonnier & Föllmi, 2017; Percival et al., 2018; Shen et al., 2019a, 2020). Thus, several authors have argued that it is critical to examine the relationship of Hg not only with TOC, but also with clay (Al) and total sulphur (e.g., Grasby et al. 2019, Shen et al. 2020). Moreover, OM source types (i.e., marine- *vs* terrestrially derived OM) may also alter the Hg OM relationship and thus may complicate the interpretation of deep-time sedimentary Hg records (Grasby et al., 2017; Wang et al., 2018; Them et al., 2019).

Fine-grained organic-rich sediments (typically shales and coals) commonly contain labile organic matter inherited from the original biomass (e.g., algal and vascular plant matter). Such sediments were often deposited under reducing conditions that enhanced the preservation of OM by hindering its degradation and remineralization (see e.g., Tissot & Welte, 1984; Bohacs et al., 2020; Dembicki, 2022). These deposits commonly are source rocks for petroleum as the labile organic matter can undergo transformation, converting to oil and gas as a result of burial and exposure to thermal stress (Dembicki, 2022).

2.1.2. The presence of Hg in hydrocarbon reserves

Mercury, in various chemical forms, is commonly found in coals, petroleum and their combustion products in highly varying concentrations (Wilhelm & Bloom, 2000). For example, Hg concentrations range from 7 to 30,000 ppb in fuel oils (Wilhelm, 2001; Mukherjee et al., 2009). However, the presence of Hg in hydrocarbon fluids that are generated and expelled from such source rocks is still not well studied. In fact, there are divergent views as to whether or not the primary depositional environment and OM type is the main driver of Hg enrichment (Liu, 2013; Li et al., 2019; Bryndzia et al., 2022) or whether enhanced mercury concentrations in oil and gas deposits are mainly caused by secondary geological processes, such as interaction of hydrocarbon reservoirs with metal-rich hydrothermal fluids and formation waters (Filby, 1994) and adjacent volcanic rocks (Zettlitzer et al., 1997). High Hg concentrations have also

been observed in hydrocarbon reservoirs associated with deep-faulted basement and mantle degassing (Liu et al., 2020). The intricate interplay between hydrocarbons and mercury (Hg) within a sedimentary basin is crucial to understand, as hydrocarbons have the potential to redistribute Hg across the basin, potentially disrupting the environmental-proxy relationship established by Hg distribution.

2.1.3. Effects of thermal maturation

Thermal maturation of labile sedimentary OM can occur due to increasing temperature with increasing burial depth, with average temperature gradients for sedimentary basins typically ranging between 20°C km^{-1} and 40°C km^{-1} (Gluyas & Swarbrick, 2021). As sediments become buried, the organic matter initially undergoes diagenesis, which eliminates functional groups and moieties that are primarily oxygen- and nitrogen-containing, resulting in a resistant macromolecular residue (kerogen) and sulphur (Tissot & Welte, 1984). This kerogen can be further broken down into lower molecular weight hydrocarbon species, such as oil and gas, through the process of thermal cracking (Tissot & Welte, 1984; Peters et al., 2005; Dembicki, 2022). As the kerogen becomes more thermally 'mature' it progresses through the stages of oil and gas generation and, depending on the type of kerogen, potentially loses up to 60% of its organic-matter mass due to secondary migration of the generated products away from the host rock (Lewan et al., 1979; Tissot & Welte, 1984; Raiswell & Berner, 1987; Dembicki, 2022). With sufficient burial and extended exposure to high basinal temperatures, the original kerogen ultimately ends up as a carbon-rich graphitic residue, having lost most of its labile organic matter as expelled H-rich hydrocarbon species.

Thermal maturation may play a key role in altering the geochemical signature of metals in sediments (e.g., Mo, V, and Ni) due to the close association of these geochemical species with sedimentary OM and the transformations that it undergoes (Lewan & Maynard, 1982;

Chappaz et al., 2014; Dahl et al., 2017). For example, thermal maturation has been shown to lead to progressive enrichment in both the concentration of metals and their TOC-normalized values in sedimentary rocks for Mo, Zn, U and Cd (Ardakani et al., 2020; Dickson et al., 2020, 2022). Such increases can be attributed to the progressive loss of mass caused by the migration of bitumen formed during thermal maturation and only minor partitioning of metals into mobilised organic fluid phases, rendering them effectively immobile in sedimentary strata (Dickson et al., 2020, 2022). Compared to these metals, we do not know how Hg might be expected to transfer into a hydrocarbon fluid phase, especially because data on processes influencing trace elements in hydrocarbons are limited (Bryndzia et al., 2023). The accompanying generation of H_2O, CO_2, and H_2S from both the organic and inorganic phases in such rocks also might play a role in causing additional loss of mass (Abarghani et al., 2020; Dickson et al., 2020). However, it is difficult to directly measure metals bound to kerogen since the primary method to isolate this organic component is by digesting the mineral matrix using strong acids such as HF and HCl, which can also leach metals from the kerogen itself. Consequently, the mechanistic behaviour of metals, including Hg, in OM-rich sediments as they undergo thermal maturation, is still not well understood.

2.1.4. Behaviour of Hg during maturation

Previous studies have investigated various factors influencing sedimentary Hg concentrations (Grasby et al., 2019; Shen et al., 2020), including the effects of contact metamorphism associated with igneous intrusions (Svensen et al., 2023), and by the use of artificial maturation experiments in the laboratory (Li et al., 2016; Liu et al., 2022, Chen et al., 2022). Mass-independent Hg-isotope fractionation signatures are commonly used to determine original depositional pathways of Hg in sedimentary records (e.g., Thibodeau, et al., 2016; Dal Corso, et al., 2020). Recent studies by Chen et al. (2022) and Liu et al. (2022) suggested that

mass-dependent isotope fractionation may occur during heating, but mass-independent fractionation signatures appear to be mostly retained.

Despite efforts to study the behaviour of Hg in experimental settings, the behaviour of Hg in sediments exposed to gradual maturation due to burial in sedimentary basins has not been tested systematically using natural samples. Conditions imposed on sediments in existing (experimental) maturation studies may differ from sediments matured through burial in two critical aspects that may influence Hg mobility. First, the conditions of deeply buried sediments are difficult to replicate in laboratory experiments, e.g., near-impermeable (clay-rich) strata may behave as a closed system, which could limit mobility of hydrocarbons and Hg. Second, the temperatures experienced by the sediments in most maturation experiments (maximum temperature of 610 °C in Liu et al. (2022) and 700 °C in Chen at al. (2022)), as well as sediments sampled from the thermal aureoles of igneous intrusions, might be much higher than experienced during natural burial conditions (60–225 °C; Tissot & Welte, 1984). These considerations require critical attention because most sedimentary Hg species (OM-bound Hg, pyrite and metacinnabar) can be mobilised at temperatures known to be relevant for post-depositional sediment alteration and resulting oil and gas generation (e.g., Rumayor et al., 2013; Saniewska & Bełdowska, 2017; Liu et al., 2022). Indeed, thermal desorption studies and laboratory maturation experiments also showed release of several relevant Hg-species even with short-term exposure to low (~150 ºC) temperatures (Reis et al., 2012, 2015; Saniewska & Bełdowska, 2017). Moreover, Hg is clearly enriched in some, but surprisingly low in other, hydrocarbon fluids (e.g., Wilhelm, 2001; Mukherjee et al., 2009), which might reflect variable release and mobility, this being a function of the original concentration of Hg in the source rocks and its host phase. Extrapolating these observations over geological timescales, we may therefore hypothesize that mature sedimentary strata should contain ubiquitously low Hg concentrations. The extensive geological records of Hg, including those in mature sediments,

shows this is clearly not the case. For example, the outcrop section of the Lower Jurassic Fernie Formation is overmature (T_{max} > 500 ºC) (Them et al., 2017), albeit enriched in Hg (maximum concentration of 232 ppb), which was identified as a signal of Karoo-Ferrar LIP volcanism (Them et al., 2019). The high Hg concentrations found in thermally mature sections suggests that additional processes must play a role in shaping the Hg records of buried strata that were exposed to burial-related maturation, and that these effects are not captured in current experiments (e.g., Liu et al., 2022; Chen at al., 2022).

Unlike most metals, there is evidence from thermal desorption analyses on chemical species of Hg that sediments exposed to temperatures during the burial typical of evolving sedimentary basins could mobilise some Hg compounds. Slow release of many Hg-species during exposure to moderate heating over geological timescales may lead to much more pronounced Hg loss from sedimentary strata, in line with sediments affected by much higher temperatures (e.g., Liu et al., 2022, Chen et al., 2022). While simultaneous mass loss of the host rock may offset some of the Hg release in a similar fashion to other (immobile) elements (see also §2.1.3), the majority of records showing high Hg concentrations in mature sediments suggest that its near-complete loss is very unlikely to have occurred (e.g., Them et al., 2019, Grasby et al., 2019, Bian et al., 2022). The combined effects on Hg of prolonged exposure to the pressure and temperature regimes that typically exist during maturation therefore remain elusive.

Our study explores the influence of thermal maturation on sedimentary Hg using three cores (A, B and C) covering a wide range of thermal maturities from Toarcian sediments of the Lower Saxony Basin, Germany. By investigating Hg concentrations, bulk OM characteristics and total sulphur (TS) concentrations in a stratigraphically constrained interval from a single basin, we examined the role of thermal maturation as a key factor in post-depositional Hg

mobility in sediments. We focus on the Posidonia Shale or Posidonienschiefer Formation (hereafter referred to simply as the Posidonienschiefer).

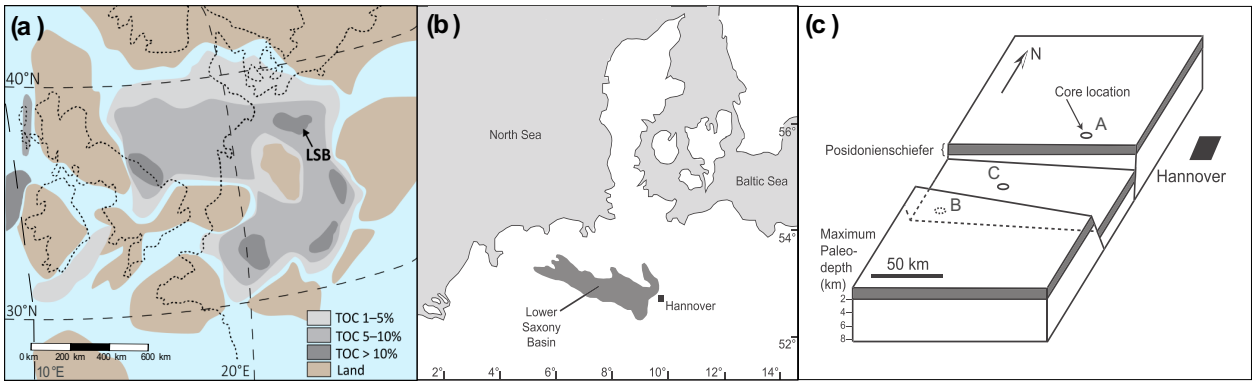


Figure 2.1. (a) Location of the Lower Saxony Basin (LSB) in the Early Jurassic epicontinental seaway of northern Europe (ca. 182 Ma) (after Dickson et al., 2022). Modern shorelines are shown as dashed lines. TOC—total organic carbon– contents in wt% are indicated by grey shading. **(b)** Map of the study area (modified from Kockel et al., 1994 and after Hooker et al., 2020). **(c)** Schematic block diagram showing locations of cores in this study, synthesized from Baldschun et al. (1996). Shaded layer shows approximate maximum paleodepth of the top of the Posidonienschiefer (after Hooker et al., 2020).

2.2. Geological Setting and Samples

The Lower Saxony Basin (LSB) is located in northwestern Germany (Fig. 2.1) and is a 300-km long and 65-km wide E–W-oriented basin formed during the breakup of the supercontinent Pangaea through extension and subsidence (Betz et al., 1987; Brink et al., 1992; Bruns et al., 2013). The Lower Toarcian Posidonienschiefer (also known as Lias Epsilon Formation) is a well-studied, distinct organic-rich unit preserved in the LSB, bracketed by marls and carbonate-rich units of the overlying Lias Delta Formation and underlying Lias Zeta Formation (Littke et al., 1991). It is a prolific source rock for petroleum produced from several significant fields within the LSB (Kockel et al., 1994).

Deposition of the Posidonienschiefer within a restricted basin with high productivity and highly reducing conditions led to preservation of algal and bacterial biomass over a significant stratigraphic interval, resulting in 20–40 meters of sediments with high amounts of

total organic carbon (TOC) and elevated hydrogen indices (HI) (Celestino et al., 2024). A stratigraphically related organic-rich interval was also deposited and preserved in various other fault-bound basins in northwest Europe and elsewhere (Jenkyns, 1985, 1988; Rullkötter et al., 1988; Littke et al., 1988, 1991; Schmid-Röhl et al., 2002; Schwark & Frimmel, 2004). Extensive basin-wide sulfidic conditions and persistent euxinia in the water column during deposition, including indicators of free H_2S in the photic zone, is evidenced by the presence of aryl isoprenoids and other diagnostic carotenoids reported in the Posidonienschiefer from the LSB (Blumenberg et al., 2019) and from other NW European basins (Schwark & Frimmel, 2004; French et al., 2014; Song et al., 2017; Celestino et al., 2024). Further evidence of such basin-wide highly reducing and sulfidic conditions is found in the elevated concentrations and isotope ratios of redox-sensitive metals (Mo, Cd, U, Zn) and Fe-speciation data reported by Celestino (2019) and Dickson et al. (2020; 2022) in the Posidonienschiefer from samples from the LSB, as well as from other basins in Europe (Röhl et al., 2001; Montero-Serrano et al., 2015).

Since its deposition in the Early Jurassic, the Posidonienschiefer has been buried to varying depths due to differential subsidence within the fault bounded LSB, followed by basin inversion during the Paleogene (Betz et al., 1987). As a result, the thermal maturity of the OM contained within the Posidonienschiefer varies significantly over relatively short horizontal distances of tens of kilometres. This variation in maturity, combined with a correlatable interval with very similar organofacies and depositional environmental conditions, makes the Posidonienschiefer in the LSB an ideal candidate for testing the impact of thermal maturation on the concentration of metals such as Hg in organic-rich sedimentary rocks.

Three cores (A, B and C) containing approximately 30-meter-thick stratigraphically equivalent sections of the Posidonienschiefer, as well as sections of the Lias Delta Formation

and Lias Zeta Formation, were studied from different parts of the LSB (Fig. 2.1). These cores have been the focus of a variety of previous studies, including the impact of maturity on the stable-isotope compositions and concentrations of the redox-sensitive and/or chalcophilic trace metals Mo, Zn, Cd and U (Dickson et al., 2020, 2022), and for chemostratigraphy and basic organic and inorganic geochemical parameters (Celestino et al., 2024). Core-to-core correlation of the Posidonienschiefer interval that post-dates the sediments recording the Toarcian Ocean Anoxic Event (T-OAE, see Celestino et al., 2024) was achieved using distinct basin-wide chemostratigraphic trends in the TOC and trace-metal records. We utilize the interval of the Posidonienschiefer that was deposited after the T-OAE (Jenkyns, 2010) to avoid the Hg-cycle perturbation that characterizes this major palaeoceanographic event (Percival et al., 2015; Fantasia et al., 2018; Them et al., 2019; Celestino et al., 2024).

The thermal maturity of each core was previously established by organic petrography yielding vitrinite reflectance (%Ro) measurements of 0.5–0.7%, 1.5% and 3.5% for cores A (immature), B (mature), and C (postmature), respectively (Gorbanenko & Ligouis, 2014, 2015). Cores B and C represent an upper end-member with extremely high maturity, whereas core A represents maturity levels more commonly used in Hg studies and encompasses the hydrocarbon formation window. The present-day depths and subsurface temperatures for the three cores do not represent peak burial and temperatures experienced in the past by the cores due to the significant inversion history of the LSB. The maximum burial depth and exposure temperature data were obtained from a basin modelling study by Bruns et al. (2013), which used a calculated average temperature gradient during maximum subsidence in the central part of the LSB of ~47 ºC/km (Senglaub et al., 2006), and determined maximum burial depths of ~1500 m, ~4300 m and ~5600 m, respectively for cores A, B, and C. Calculated peak burial temperatures for the cores are 70 ºC (core A), 200 ºC (core B), and 260 ºC (core C) were acquired by multiplying maximum burial depth with the basin temperature gradient.

Two key factors postulated to have significant impact on the sequestration and concentrations of Hg (and other metals) in sedimentary systems are redox conditions and type of organic matter (see Grasby et al., 2019; Frieling et al., 2023 and references therein). Trace-metal, organic geochemical and organic petrographic data from previous studies on these 3 cores (Gorbanenko & Ligouis, 2014; 2015; Dickson et al., 2020, 2022; Celestino et al., 2024) show persistent euxinic conditions and input of primarily marine-derived organic matter throughout the deposition of the Posidonienschiefer in the LSB. Consequently, these two variables were not considered a significant factor in our study of long-term maturation effects on Hg concentrations in the LSB cores (see discussion section below, for a more detailed evaluation of these and other variables).

2.3. Methods

A total of 301 sediment samples from the Posidonienschiefer: 217 for core A, 49 for core B, and 35 for core C (Table 2.S1 in Appendix 1), were powdered and analysed for Hg concentrations using a Lumex RA-915 Portable Mercury Analyser coupled to a PYRO-915+ pyrolysis unit at the University of Oxford (Bin et al., 2001). Powdered samples of between 50 and 100 mg were introduced into a sample boat, heated to >700 °C and left for up to 120 seconds to fully volatilize the Hg present. The instrument was calibrated before each run using NIST-SRM2587 (National Institute of Standards and Technology – Standard Reference Material: Trace Elements in Soil Containing Lead from Paint), with a Hg concentration of 290 ± 9 ppb. The same standard was run every ten samples to correct instrument drift. We calculate an external reproducibility of ±8.7% based on the repeat standard measurements (1 standard deviation (S.D.), n=199).

Six different samples of Lower Saxony Basin oils sourced from the Posidonienschiefer (Stock & Littke, 2016) were obtained from the Oil Museum in Germany. These fluids were

analysed for Hg concentrations using the same instrument (Lumex RA-915) used for sediments. An amount (about 0.2 g) of activated charcoal was spread on the inner surface of a quartz boat of the Lumex pyrolyzer. Subsequently, a known mass of oil was added onto the charcoal bed and analysed. Each sample was measured 5 times. The instrument was calibrated before each run using the same paint standard as the sediments above as well as an additional oil standard NIST-SRM2778 (National Institute of Standards and Technology – Standard Reference Material: Mercury in Crude Oil) with a Hg concentration of 39 ppb. The standards were run every seven samples to correct for instrument drift. We calculate an external reproducibility of ±3.64% (1 S.D., n = 12) for the repeat standard measurements of Paint, and ±5.88% (n = 5) for the oil standard. Hydrogen and Oxygen indices (HI, OI) and TOC data from all three cores have been published previously in Celestino (2019), Hooker et al. (2020) and Dickson et al. (2020, 2022). An additional 39 new samples (15 for core A, 21 for core B, and 3 for core C) (annotated in Supplementary Data) were analysed with a Rock-Eval 6, following the methods in Behar et al. (2001), at the University of Oxford. The in-house standard SAB134 (Blue Lias organic-rich marl, 2.74 % TOC) was measured every 8 to 10 samples. The standard deviation of the in-house standard (SAB134) was ~0.03 % TOC (1 S.D.).

Analyses of total sedimentary sulphur (%TS) were undertaken on 155 samples (57 for core A, 50 for core B, and 48 for core C). The samples were selected to cover the full range of Hg concentrations observed within the stratigraphic intervals of interest, to allow the relationship of Hg and S to be quantified. An aliquot of each sample was wrapped in a tin capsule and combusted using an Elemental Cube Elemental Analyzer Vario El III at the Department of Earth Sciences, Royal Holloway University of London. A sulfanilamide reference standard (18.62 % S) was analysed at the start and end of each run and between every ten samples to monitor instrument drift. Within-run reproducibility calculated from the in-house shale standards (1.24 % S) run as unknowns was ±0.12 % S (1 S.D., n = 12).

2.4. Results

2.4.1. Bulk sediment chemistry and maturity (TOC, TS, HI and OI)

The organic-rich intervals of the Posidonienschiefer (PS) in the three cores used in this study are all stratigraphically above the sections that record the negative carbon-isotope excursion characteristic of the T-OAE (Jenkyns, 2010, Celestino 2019, Celestino et al., *submitted*). TOC values in all the cores are relatively elevated in the Posidonienschiefer interval, ranging between ~5–14%. The average TOC values in all the cores are within a comparable range (8.3–9.8 %) despite the differences in maturities, and show a modest increase from core A to core B and from core B to core C (Table 2.1). TOC variability within the Posidonienschiefer section of each core is greater than the variability between the cores. The most notable trend up-section is seen in the immature core A, where there is a decrease from ~14% at the base to a minimum of ~5% in the central section of the Posidonienschiefer before increasing again to ~12% at the top. Hydrogen Index values for the same section in core A are rather high (600–750 mg HC/g TOC), and show little variation, despite the changes in TOC concentrations (Fig. 2.2). Oxygen Index values are low throughout the section, generally below 10 mg CO_2/g TOC. By contrast, in cores B and C, the HI values throughout the Posidonienschiefer are near 0 (Figs. 2.3 and 2.4), in line with their relatively high maturity and negligible to no remaining S2 or hydrocarbon generative potential.

Rock-Eval-determined T_{max} values are around 432–440°C for core A and attest to the immature (onset oil window) stage of conversion of the kerogen, in keeping with the measured vitrinite reflectance (%Ro) data (~0.5–0.7%: Gorbanenko & Ligouis, 2014; 2015). The calculated %Ro equivalents from the T_{max} values (Evenick, 2021) of the immature core A are also in this range. In cores B and C, where the Rock-Eval S2 peak was too low for accurate T_{max} assessment, we relied on petrographically determined %Ro of 1.5% and 3.5%,

respectively for these two cores following Gorbanenko and Ligouis (2014, 2015). In kerogen conversion and hydrocarbon generation terms, core A would be considered immature/onset of generation, core B is in the early dry gas window and core C is post-mature.

Total sulphur (TS) concentrations range from ~2.0 to 4.5 % for the immature core A, and ~2–5.5 % for the mature to post-mature cores B, and C through the Posidonienschiefer (Figs. 2.2, 2.3, and 2.4). These ranges are comparable to data from previous organic geochemical studies of the Posidonienschiefer (e.g., Littke et al., 1991; French et al., 2014; Song et al., 2017) as well as organic petrography (Gorbanenko & Ligouis, 2014; 2015), which identified abundant (framboidal) pyrite and established that both the iron sulphide and organic matter are the primary hosts for the sulphur. Cores B and C show subtle but somewhat higher %TS values in the upper part of the section compared to the lower halves, while the range remains fairly constant for the whole section in core A.

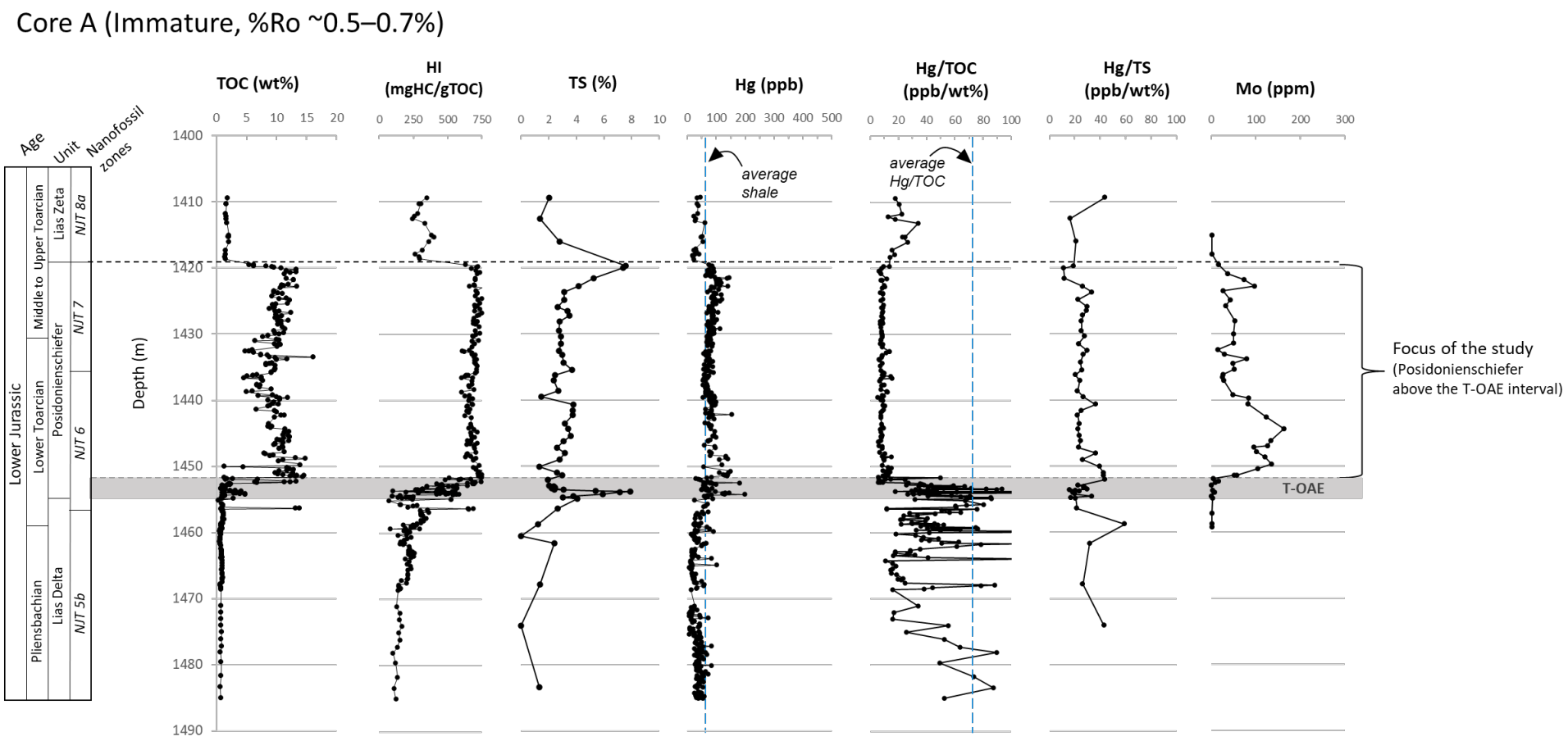


Figure 2.2. Stratigraphic log of the studied core A (immature, vitrinite reflectance, %Ro ~0.5–0.7%) showing the total organic carbon (TOC), hydrogen index (HI), total sulphur (TS), Hg concentration, Hg normalized by TOC, Hg normalized by TS, and Mo concentration. Dashed lines showing average Hg concentration (62.4 ppb) and Hg/TOC (71.9 ppb/%) in shale from Grasby et al. (2019). Mo data are compiled from Dickson et al. (2020, 2022). Rock-Eval data (TOC and HI) include new data generated in this study, as well as compiled data from Hooker et al. (2020), Dickson et al. (2022), and Celestino (2019). Details of individual data sources are annotated in Appendix 3.

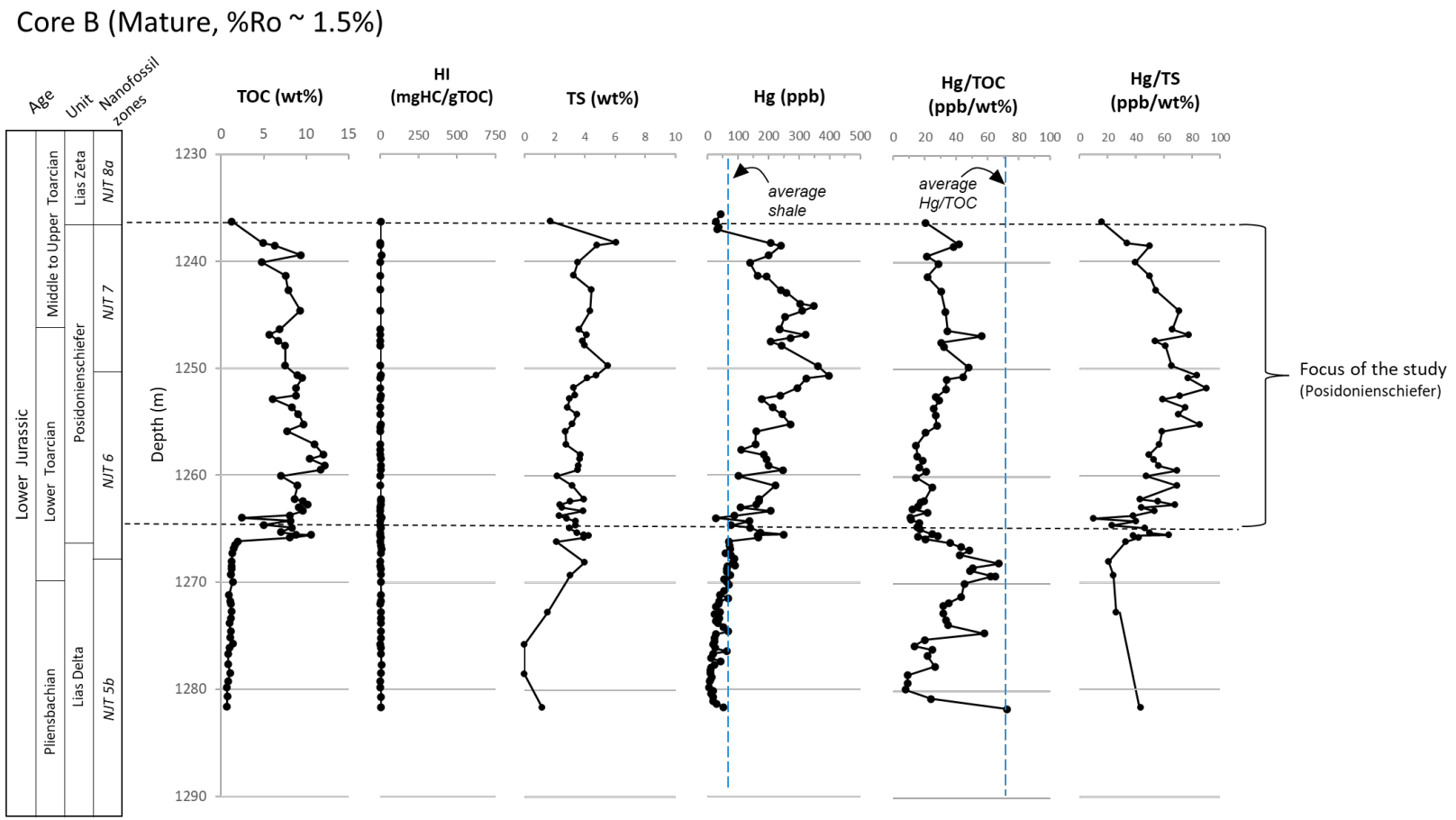


Figure 2.3. Stratigraphic log of the studied core B (mature, vitrinite reflectance, %Ro ~1.5) showing total organic carbon (TOC), hydrogen index (HI), total sulphur (TS), Hg concentration, Hg normalized by TOC, and Hg normalized by TS. Dashed lines showing average Hg concentration (62.4 ppb) and Hg/TOC (71.9 ppb/%) in shale from Grasby et al. (2019). Rock-Eval data (TOC and HI) include new data generated in this study, as well as compiled data from Hooker et al. (2020), Dickson et al. (2022), and Celestino (2019). Details of individual data sources are annotated in Appendix 3.

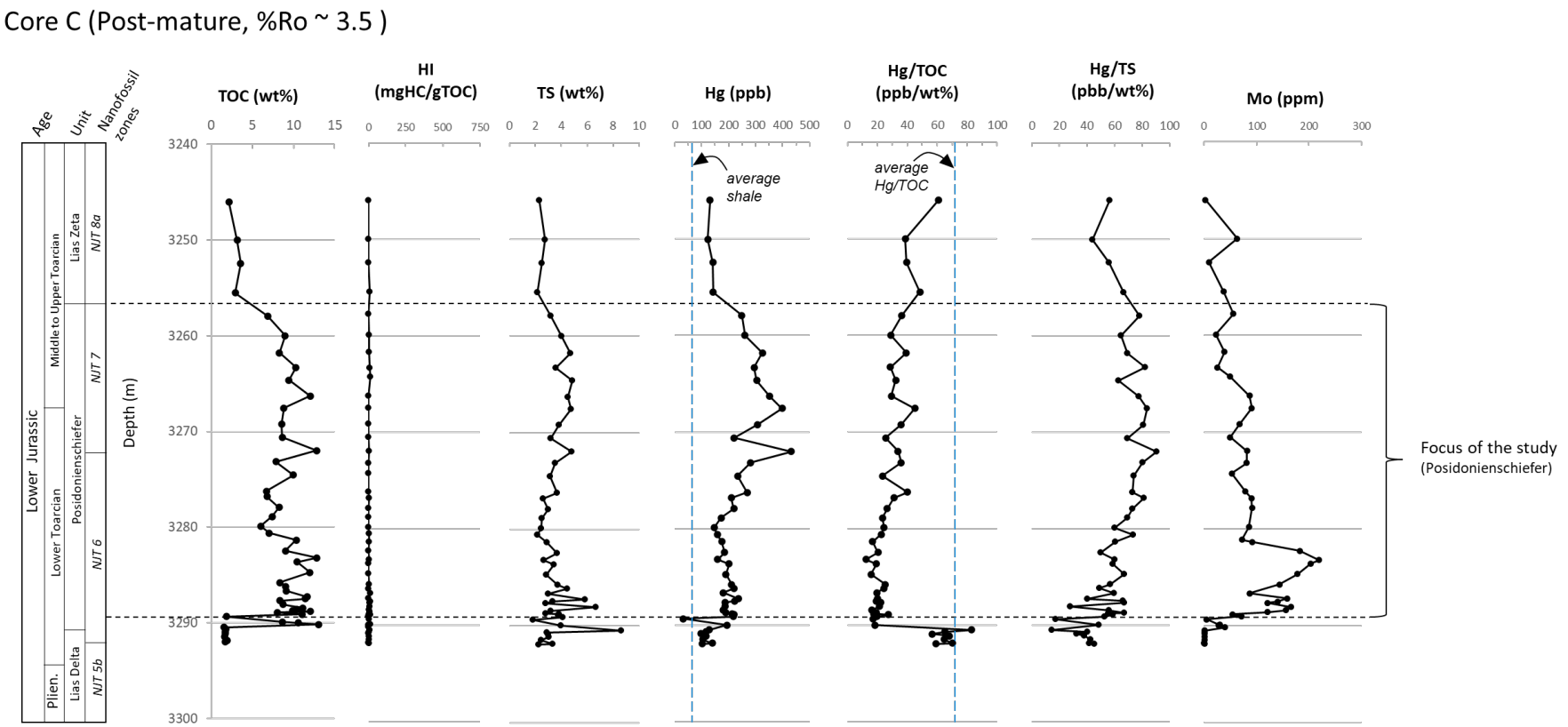


Figure 2.4. Stratigraphic log of the studied core C (post-mature, vitrinite reflectance, %Ro ~3.5) showing total organic carbon (TOC), hydrogen index (HI), total sulphur (TS), Hg concentration, Hg normalized by TOC, Hg normalized by TS, and Mo concentration. Dashed lines showing average Hg concentration (62.4 ppb) and Hg/TOC (71.9 ppb/%) in shale from Grasby et al. (2019). Mo data are compiled from Dickson et al. (2020, 2022). Rock-Eval data (TOC and HI) include new data generated in this study, as well as compiled data from Hooker et al. (2020), Dickson et al. (2022), and Celestino (2019). Details of individual data sources are annotated in Appendix 3.

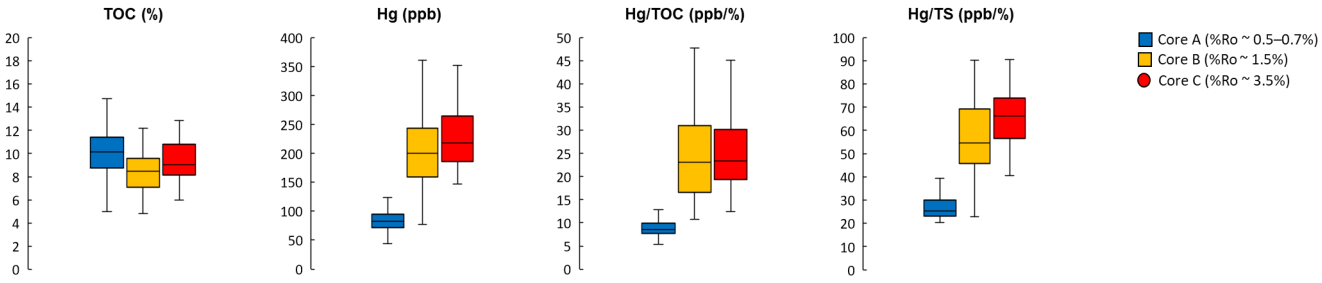


Figure 2.5. Differences between cores A, B and C in the mean (horizontal lines in the box), interquartile range (boxes) and data within 1.5 interquartile range (black lines with bar ends) of TOC (%), Hg (ppb), Hg/TOC (ppb/%), and Hg/TS (ppb/%) in the Posidonienschiefer.

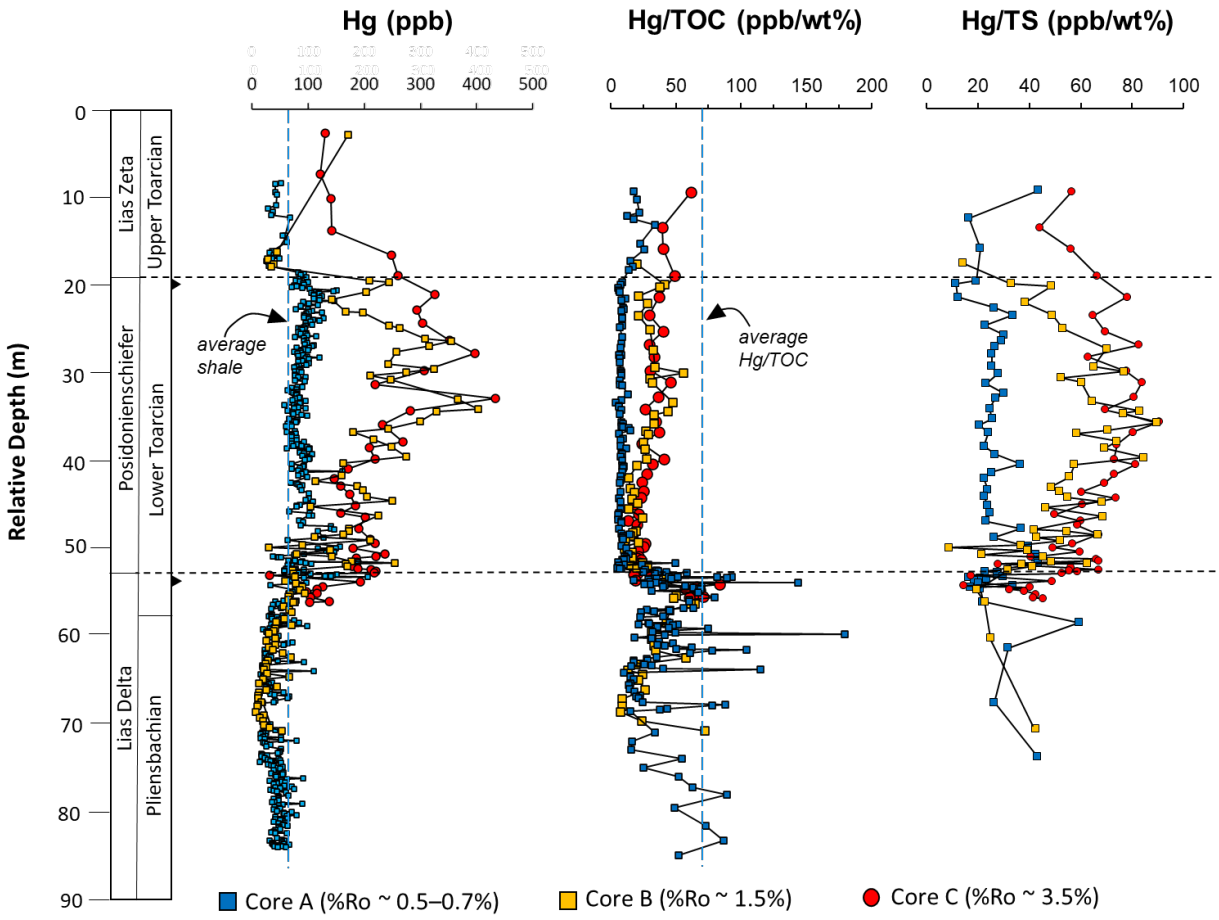


Figure 2.6. Hg concentrations, Hg/TOC, and Hg/TS in cores A, B, and C. Hg concentrations in cores B and C reached maximum amount of ~400 ppb at relative depth 34 m, up to 4 times the Hg concentrations in core A at the same depth. The Hg/TOC and Hg/TS ratios in core A diverge from those for cores B and C around a relative depth of ~50 m, with values increasing to 4 times the values of core A. Dashed lines showing average Hg concentration (62.4 ppb) and Hg/TOC (71.9 ppb/%) in shale from Grasby et al. (2019). The Hg/TOC profile in the Posidonienschiefer shows homogeneity, especially in core A. TOC includes new data generated in this study, as well as compiled data from Hooker et al. (2020), Dickson et al. (2022), and Celestino (2019).

Table 2.1. TOC, Hg, TS, HI, OI and trace-metal data for cores A, B and C from the Posidonienschiefer. Symbols + indicate data from Hooker et al. (2020) and * from Dickson et al. (2022).

		Core		
		A	B	C
Hg (ppb)	Mean	85.88	209.49	234.37
	Std. Dev.	21.76	76.77	67.39
TOC (%)	Mean	9.81	8.33	9.40
	Std. Dev.	2.21	2.00	1.82
TS (%)	Mean	3.32	3.61	3.64
	Std. Dev.	1.26	0.81	0.98
Hg/TOC (ppb/%)	Mean	9.08	25.13	25.72
	Std. Dev.	2.08	10.35	7.81
Hg/TS (ppb/%)	Mean	27.19	56.07	65.70
	Std. Dev.	7.50	16.63	12.98
Hydrogen Index^{+} (mgHC/gTOC)	Mean	690	1	3
	Std. Dev.	36	1	3
Oxygen Index^{+} ($mgCO_2$/gTOC)	Mean	6	11	12
	Std. Dev.	2	2	2
Cd* (ppm)	Mean	1.7		1.8
	Std. Dev.	1.1		0.6
Zn* (ppm)	Mean	178		217
	Std. Dev.	97		80
U* (ppm)	Mean	5.7		16.1
	Std. Dev.	2.4		11.8
Mo* (ppm)	Mean	70.45		101.9
	Std. Dev.	39.9		52.3

2.4.2. Sedimentary Hg, Hg/TOC and Hg/TS analyses

Within the Posidonienschiefer interval of the three cores, Hg concentrations fluctuate between 32–433 ppb, which are generally elevated above the typical mean values of Hg found in sedimentary rocks (62.4 ppb from the compilation in Grasby et al., 2019). In the correlated Posidonienschiefer intervals of cores A, B and C, the ranges of Hg concentrations are 53–154 ppb (Fig. 2.2), 28–397 ppb (Fig. 2.3) and 32–433 ppb (Fig. 2.4), respectively. The mean Hg concentration increases from 85 ppb (core A) to 203 ppb (B) and 225 ppb (C) (Table 2.1, Fig. 2.5). Cores B and C have, on average, ~2.3–2.6-fold higher Hg than core A. Notably, the Hg

concentrations in cores B and C show larger variability than core A and have clear maxima in the central and upper part of the core before decreasing again towards the top of the Posidonienschiefer (Fig. 2.6). In cores B and C, Hg concentrations show remarkably similar patterns (Fig. 2.6), with close correlation in the trends (peaks and troughs) between the two cores. In both the B and C cores, overall Hg concentrations are higher in the upper half of the section compared to the lower. This trend in Hg mimics the subtle differences in %TS (Figs. 2.2, 2.3, and 2.4) between the upper and lower halves of cores B and C noted in the previous section (§2.4.1).

Hg/TOC values in core A are in the range of 5–15 ppb/TOC%, 10–56 ppb/TOC% in core B, and 12–45 ppb/TOC% in core C. Hg/TOC ratios in core A vary over a narrow range around an average of ~10 ppb/TOC% throughout the Posidonienschiefer (Fig. 2.2) whereas, in cores B and C, these values are overall higher and show significantly more variation in ranges (Figs. 2.2, 2.3, and 2.4). As with the Hg and TS concentrations and TOC/TS values, Hg/TOC ratios in cores B and C (Fig. 2.6) again have persistently higher values in the upper halves of the section compared to the lower.

The Hg/TS ratio in core A is relatively constant throughout the organic-rich Posidonienschiefer section (~20–40 ppb/TS%) while cores B and C have higher ratios (~38–90 ppb/TS% and ~42–90 ppb/TS%, respectively) and show more variability (Table 2.1 and Figs. 2.5 and 2.6). Cores B and C have higher Hg/TS ratios in the upper half of the sections, with the former showing a decrease in the uppermost part. (Fig. 2.6). Overall, as with the Hg concentrations, the Hg/TS profiles for core B and C are quite similar in their changes up-section.

The Hg *vs* TOC shows a weak correlation ($R^2 = 0.395$) in core A and essentially none in cores B and C ($R^2 = 0.065$ and 0.032, respectively) (Table 2.S2, Fig. 2.S2 in Appendix 1).

Compared to Hg-TOC, Hg correlates only slightly better with TS for core B (R^2 = 0.139, 0.363, 0.010, for core A, B, C, respectively) (see Table 2.S2 and Fig. 2.S2 in Appendix 1). There is a weak general trend of higher Hg with higher TS when the data from all three cores are taken together, with the higher maturity ones showing the most elevated values of Hg and TS (Fig. 2.S2 in Appendix 1). However, individual correlations between Hg, TOC and TS each explain less than 50% (R^2 <0.5) of the observed variance, likely signalling that Hg is hosted by both TOC and sulphide phases and/or that neither strongly controls Hg variability. This pattern is expected because, for high-TOC, high-TS sediments, the Hg supply is often limiting (e.g., Schuster et al., 2018; Frieling et al., 2023; Fendley et al., 2024).

2.4.3. Hg analyses of oils

The results of Hg measurements in LSB oils are shown in Table 2.2. The mean concentration of Hg in Posidonienschiefer-derived oils is 3.4 ± 1.1 ppb (1 S.D.), which is at the lower end of the range of Hg reported in fuel oils (7 to 30,000 ppb; Wilhelm & Bloom, 2000). The amount of Hg found in produced oils is also significantly lower than Hg concentration in the sediments, both mature and immature.

Table 2.2. Average and standard deviation for Hg in oils derived from the Posidonienschiefer.

Sample	Average Hg concentration (ppb)	n replicates
066.02	4.0 ± 1.9	5
066.05	2.6 ± 0.9	5
066.06	2.8 ± 2.1	5
066.09	5.2 ± 1.9	5
066.18	3.0 ± 2.9	5
066.21	2.5 ± 1.9	5
Mean	3.4 ± 1.1	

2.5. Discussion

2.5.1. Mercury enrichment: differences in OM type and original depositional environmental conditions between cores?

In all three cores in our study, Hg concentrations in the organic-rich section of the Posidonienschiefer are higher than in the underlying Lias Delta and the overlying Upper Toarcian unit (Lias Zeta) (Figs. 2.2, 2.3, and 2.4). Increased Hg concentrations are coincident with the much higher TOC (measured and calculated original values) in the Posidonienschiefer and is marked by a change from the marls and carbonate-dominated lithologies stratigraphically above and below, differences that reflect very pronounced changes in depositional redox and sedimentary conditions (Dickson et al., 2022) as well as type and preservation of organic matter.

Differences in the original organic-matter concentration of the cores are evident, given that the mature and post-mature cores B and C have residual TOC values that are still in the same range as the immature core A, despite having undergone significant conversion of labile organic matter into hydrocarbons. Reconstructing original TOC for these two mature/post-mature cores using the method of Jarvie (2012) yields calculated original TOCs in cores B and C before thermal maturation of around ~16% and ~19%, respectively, which is significantly higher than the average TOC value in core A (~10%). This pattern of higher initial OM concentration in cores B and C could be the result of their more distal position relative to the paleo-shoreline (Fig. 2.1; Dickson et al., 2022), with higher productivity and subdued siliciclastic input relative to supply of organic matter.

With HI values around 600–750 and oxygen index (OI) values under 20 in core A (Fig. 2.2), the Posidonienschiefer is a Type I/II kerogen (Fig. 2.S1 in Appendix 1), with a primary algal organic-matter-dominated maceral assemblage confirmed by organic geochemical and

petrographic studies on these cores (Gorbanenko & Ligouis 2014; 2015; Blumenberg et al., 2019; Celestino et al., 2024). These features are comparable to those in Toarcian sediments from other sections in the LSB and adjoining NW European basins (e.g., Littke et al.,1988, 1991; Schwark & Frimmel, 2004; French et al., 2014; Song et al., 2017). Analysis of the residual organic matter in Cores B and C (Celestino, 2019) indicate that they also contained original organofacies that were comparable to those in core A; there is therefore no evidence that depositional conditions favouring high productivity and preservation of organic matter in the Posidonienschiefer varied significantly across the basin.

Another factor resulting in the differences of TOC, and therefore organic-matter-related Hg, could be varied redox conditions in the paleogeographic locations of the 3 cores. Although the basin was generally characterized by anoxia and extensive euxinic depositional conditions, the presumed greater paleo-water depths of cores B and C and subtle variations in the intensity of euxinia and/or vertical extent of the euxinic water column may have resulted in higher TOC preservation efficiency and observed differences in TS and redox-sensitive and/or chalcophilic trace elements at the time of deposition. However, trace-element concentration profiles, iron-speciation data and organic petrography (Gorbanenko & Ligouis, 2014; 2015; Celestino, 2019; Dickson et al., 2020; 2022) demonstrate persistent anoxic/sulfidic conditions. Molybdenum concentration profiles for cores A and C (Figs. 2.2 and 2.4) show remarkably similar trends up-section, implying that equivalent changes in depositional redox conditions through time affected both cores, despite the geographic distance between them. The similarity in Mo profiles between the cores and previous studies on the effects of maturation on concentrations and stable isotopes of Mo, Cd, U, and Zn in cores A and C (core B was not analysed for Mo) found no evidence for significant differences in depositional redox conditions (Dickson et al., 2020; 2022). Hence, it is unlikely that redox conditions favouring preservation of the biomass varied significantly between the three core locations and within each Posidonienschiefer

section, at least not to the extent that it could have appreciably influenced Hg deposition (Gorbanenko & Ligouis, 2014; 2015; Celestino, 2019; Dickson et al., 2020; 2022, Frieling et al. 2023).

The clay content differences between cores A, B, and C could be a possible alternative explanation related to Hg loading difference, as well as TOC and TS. While clay is another commonly invoked Hg host phase (Shen et al., 2020), its importance as a Hg host phase seems limited to organic- and sulphur-lean sediments (e.g., Shen et al., 2019b). The higher original TOC in Cores B and C suggest that the organic-matter at these localities was less diluted, indicating these depositional settings may have received less detrital matter, not more. Collectively, differences in clay content appear an unlikely explanation for causing any primary differences in Hg loading.

2.5.2. Carrier-phase depletion

It is generally accepted that Hg is hosted in both organic matter and in sulphide minerals in organic-rich sedimentary rocks such as the Posidonienschiefer (e.g., Grasby et al., 2017; Them et al., 2019; Frieling et al., 2023). Nonetheless, the weak relationships between Hg concentrations and TOC or TS exhibited in the Posidonienschiefer sections may be a function of variable amounts of Hg being hosted in these two phases. Both elevated TOC and TS values are typical in sediments rich in labile organic matter, which may also contain substantial amounts of Hg. As discussed previously, labile organic matter can undergo transformation as a result of thermal stress (burial) and form mobile hydrocarbon and non-hydrocarbon phases that can be expelled from the sedimentary section where they are formed, resulting in an overall decrease in the amount of original TOC and consequent rock-mass loss (Lewan et al., 1979; Tissot & Welte, 1984; Raiswell & Berner, 1987; Dembicki, 2022). Although it is difficult to know precisely how much of the original organic-carbon of the Posidonienschiefer sediments

in our study has been lost during maturation, using the reconstruction method of Jarvie (2012) we estimate that up to 50% of the original TOC in cores B and C may have been reduced as a result of kerogen conversion and hydrocarbon expulsion. Consequently, loss of organic carbon may have resulted in a significant (relative) enrichment in trace elements, if these were retained in the host rock and not removed in a mobile fluid phase.

Such significant loss of TOC as a result of thermal maturation would result in proxies such as Hg/TOC shifting to higher ratios in mature and post-mature OM-rich rocks (Figs. 2.5 and 2.6) compared to their immature equivalents if Hg were not significantly remobilised and expelled. Previous studies on these cores demonstrated that this process has also affected the concentrations of Cd, Zn, Mo, and U, which increased by as much as ~10% (Cd), ~20% (Zn), ~45% (Mo), and, although more uncertain, 185% (U) from core A to core C (Dickson et al., 2022) (see Table 2.1). In addition to TOC loss, the expulsion of water from the dehydration of clays during burial and maturation also would have contributed to the loss of rock-mass (Peters & Cassa, 1994). The combination of TOC loss and host-rock mass loss from inorganic compounds would potentially result in a bias in both measured Hg and normalized Hg relative to the original signal stored in the rock record. As an example of this pitfall, one might infer a higher (> 2 times) original Hg mass accumulation rate in cores B and C compared with core A, if one did not take the thermal maturity level of each core into account, especially since the thicknesses of the Posidonienschiefer sections do not vary significantly.

2.5.3. Mobilisation and redeposition of Hg

The magnitude of change in Hg concentration compared to previously determined TOC loss (Dickson et al., 2020) shows that the increase in Hg can be partially explained by mass loss during catagenesis if Hg is considered nearly immobile. However, the notion that Hg is immobile during maturation appears at odds with previous findings from maturation

experiments (Liu et al., 2022; Chen et al., 2022), and data from metamorphic aureoles around igneous intrusions (Svensen et al., 2023), that showed progressive Hg loss with heating. Such distinct differences in Hg mobility between our naturally matured materials and previous studies (e.g., Liu et al., 2022; Chen et al., 2022, Svensen et al., 2023) might be explained by the fact i) that our cores were deeply buried shale units with very limited permeability and ii) that Hg in the LSB does not seem to partition strongly into evolved fluids (Table 2.2). The oil contains ≤5 ppb Hg, compared to the 50–150 ppb sedimentary Hg concentrations found in core A, supporting very limited partitioning. Compacted low-permeability shale units might have behaved more akin to a closed-system, whereby Hg released from its original host might have been re-sequestered by other phases over time. The effective mobility of Hg might have been further limited by the relatively low geological maximum temperatures (70–260 ºC) experienced by our material and abundance of scavenging ligands (OM, sulphur), that might have permitted re-capture in pyrite, as HgS or as secondary Hg-OM complexes.

In addition to the constant-sum effects and speculative release–recapture in a closed system, as discussed above, other processes could also have played a role in elevating Hg concentrations in the mature cores. Such processes could include, for example, internal (lateral or, more unlikely, vertical) redistribution of Hg as a fluid or gas phase in the sediment column or capture of externally sourced Hg within the Posidonienschiefer. Even if net Hg mobility in these sedimentary strata was effectively zero, some degree of Hg release from its initial host-phase is to be expected during maturation. For example, the burial temperatures experienced by cores B and C (as much as 200 and 260 ºC, respectively) would have allowed (partial) release of Hg from common known sedimentary host phases such as OM and pyrite (Reis et al., 2012, 2015; Rumayor et al., 2013; Saniewska & Bełdowska, 2017). Mercury concentrations in core A are approximately stable within the Posidonienschiefer, whereas a distinct up-section increase is observed in cores B and C (Fig. 2.6). While this chemostratigraphic pattern might

be explained by Hg migration and (partial) re-capture in cores B and C, such a process is difficult to envisage in lithologies such as the Posidonienschiefer that have extremely low matrix porosity and permeability, especially after burial to depths of ~5600 m (Bruns et al., 2013). Furthermore, the likelihood of 2 cores (B and C), which are separated by 10s of kilometres, resulting in similar Hg profiles after such a proposed redistribution seems very low.

2.5.4. Redistribution and mobilisation of Hg by fractures and veins

The maturation of organic matter and heating of sediments ultimately can lead to fluid overpressures and fracturing of low-porosity/permeability rocks (see Hooker et al., 2020 and references therein). For example, according to Meissner (1978), the catagenesis of solid kerogen into liquid hydrocarbons, gas, refractory carbon (e.g., graphite), and other by-products can increase local fluid pressures and result in hydraulic fracturing of the host lithology, and in the formation of veins (e.g., Mandl & Harkness, 1987; Lash & Engelder, 2005). Shale layers in highly mature to post-mature cores B and C contain abundant layer-parallel and oblique veins, mostly filled by calcite cement, with traces of pyrite crystals (Hooker et al., 2020). These oblique and bedding-parallel fractures containing so-called ‘beef’ calcite may have played an important role in the primary migration of petroleum fluids within and from the Posidonienschiefer (Leythaeuser et al., 1988). These calcite veins in the mature cores also demonstrate that fluid passed through the stratigraphy at some point in the basin history and could have been the means of transport for a volatile or dissolved Hg phase, either during thermal maturation or afterwards. However, Hooker et al. (2020) indicated that the potential for vertical migration of fluids through the fractures that are filled with calcite is low, as well as the postulated porosity and permeability within the fracture fill itself. Although we cannot indicate whether finer or larger scale fractures in the cores themselves or outside the core intervals have indeed played a role in redistributing Hg, the observation of diverging up-section Hg trends within some of the highly fractured intervals warrants caution.

2.5.5. Summary of controls on Hg concentrations in cores A, B, and C

From the above discussions, we compiled a summary table of known syn- and post-sedimentary processes that might have influenced sedimentary Hg concentration in cores A, B, and C (Table 2.3). For these high-productivity, anoxic conditions, Hg burial is effectively limited to the Hg supply from atmospheric and riverine sources (Schuster et al., 2018, Frieling et al., 2023; Fendley et al., 2024). The Hg supply limitation during deposition is also supported by the correlation, albeit weak, between Hg and Mo concentrations (Fig. 2.S4 in Appendix 1, Bian et al., 2024). When the Hg supply is limiting, Hg concentrations can no longer increase at the same rate as TOC, expressed as decreasing Hg/TOC with increasing TOC, as for example seen in the Hg/TOC between the Lias Delta and Posidonienschiefer in core A (4-fold increase in TOC concentration but only 2-fold increase in Hg, Fig. 2.2). In order to explain the observed differences (Fig. 2.5), the local Hg supply to cores B and C would have needed to be approximately twice as high as for core A. All three cores were in the same latitudinal band with similar rainfall patterns and rates of wet and dry Hg deposition (e.g., Jiskra et al., 2021); therefore, no major differences are expected between the cores in terms of the atmospheric Hg supply. Riverine Hg supply could have been important locally, but because of the more distal position of core B and C relative to the palaeoshoreline (cf. Zimmermann et al., 2018; Fig. 2.1), this would likely have reduced the supply to B and C relative to A, resulting in a lower, not higher, total Hg supply for more distal parts of the basin. Thus, the increase in Hg concentration or changes in stratigraphic trends cannot be simply explained by differences in starting concentrations. This observation suggests that other, perhaps unlikely, maturation-related effects such as redistribution via fractures and veins may have to be considered.

Table 2.3. Summary of all processes involved in sedimentary Hg concentrations in cores A, B, and C in this study

Time	Process	Difference between cores (core A, B to C)	Range of possible changes	Data
Syn-deposition	Hg in atmosphere (atmospheric deposition)	None expected		
	Hg from terrestrial material (land-derived OM)	Reduced in core B & C because of distance from palaeoshoreline	Unknown	Zimmermann et al., 2018
	Hg binding with marine organic-matter (algae in shallow marine environment)	Higher in core B & C because of higher TOC content	max. ~200%	Frieling et al., 2023; Fendley et al., 2024
	Redox in water column and sediment	None expected		Dickson et al., 2020
Post-deposition	Hydrocarbon generation/organic-matter loss	Core A: none, Core B & C: maximum organic mass loss ~50%		Hooker et al., 2020
	Non organic-matter mass loss (dehydration)	Core A: none, Core B & C: ~5–10%		Peters & Cassa, 1994
	Fracturing and fluid migration through fractures	Unknown		
	Hydrocarbon migration	None expected		This study (Hg in oil)
Observed Result	Catagenesis (oil window & gas window)	Increase from core A to B	~200%	This study
	Metagenesis (dry gas zone)	Increase from core B to C	10%	

2.5.6. Implications for the use of the Hg proxy in mature sediments

The Hg concentration of an average clastic sedimentary rock is 62.4 ppb according to the compilation in Grasby et al. (2019), and Hg/TOC values from the global inventory from the same study average around 71.9 ppb/%. Mercury concentrations in the Posidonienschiefer sections of much of core A and all of cores B and C are above the reported global averages (Figs. 2.3 and 2.4) and are well within the range of anomalous “Hg spikes” in the geological

record previously interpreted to result from LIP activity. However, because of the very high TOC, the TOC-normalized Hg data in all the cores in this study are significantly lower (Fig 2, 3, 4, 6, and Fig. 2.S3 in Appendix 1) than the range of recorded Hg/TOC values that are generally considered anomalous and interpreted as volcanic signatures.

In this study, we inferred a rise in Hg/TOC with maturation that is not easily explained away by differences in starting Hg concentrations or by intra-basinal differences in depositional conditions. We consider this effect important for workers utilizing Hg/TOC ratios as a proxy for volcanism, as maturity-related changes may alter an interpretation where volcanic threshold values are used. Therefore, we consider it important to highlight the fact that maturation can result in a higher Hg/TOC signal, which could then be misinterpreted as consistent with enhanced volcanic loading. Very few published studies report the maturity level or exposure temperatures of their samples, but our observations show a cautious approach when using samples that have been substantially matured is warranted. It is also worth noting that the effects of maturity become more important further back in the geological record, increasing the likelihood of the bias but nonetheless in many cases represent valuable targets for study.

Our findings further highlight that it is important to note that the use of normalized Hg as a volcanic proxy must be used with caution as Hg does not linearly scale with TOC due to a variety of (syn-)depositional processes (e.g. Schuster et al., 2018; Grasby et al., 2019; Frieling et al., 2023; 2024; Fendley et al., 2024). In addition, we must consider similar processes acting on relatively low-TOC samples; maturation in such settings could easily lead to values that (far) exceed the Hg/TOC shale value. As previously discussed, the variability in the Hg and Hg/TOC and Hg/TS profiles between the three cores, and within the Posidonienschiefer section of each core is, at this stage, difficult to explain without invoking unlikely factors such as Hg migration through low-permeability shales. The loss of rock mass during thermal maturation,

and variation in hydrocarbon production may explain some of the variance in TOC and Hg/TOC ratios. However, the changes in Hg concentrations within the Posidonienschiefer sections of each core are likely related to other processes that we do not fully understand as yet. Redistribution of Hg cannot be ruled out; however, the similarity in profiles of cores B and C, and the extremely low permeability of the current overall Posidonienschiefer lithology, make such a process difficult to envisage. Regardless of the exact mechanisms, the change in pattern of Hg concentration, and Hg/TOC and Hg/TS ratios between the three cores (Fig. 2.6) shows that thermal maturation can displace, introduce, or remove Hg "spikes" in the geological record.

Assessing the extent of signal alteration caused by thermal maturation is more challenging, as it requires extremely detailed knowledge of the original depositional and paleoenvironmental conditions of the examined sequence. In the current study, we have the advantage of evidence from the three cores with comparable biomass input and preservation, persistent and comparable redox conditions and high sampling resolution to compare, in detail, the correlated sections. Despite possible minor differences in initial Hg concentrations, we infer a clear rise in Hg/TOC ratios (and potentially also Hg) with maturation that is important for the proxy to be used for assessing anomalous Hg concentrations in the sedimentary record. Regardless of the precise mechanisms involved, the increase in Hg/TOC from TOC loss alone implies that knowledge of thermal maturation history of the material becomes critical for the interpretation of Hg records when analysing sediments that have undergone significant burial and exposure to different maximum temperatures.

For periods when all records are thermally mature, as would be progressively more likely with sediment deposited further back in time, systematic changes might occur to Hg and normalized Hg values. These changes might include potential Hg spiking through

remobilisation and recapture, concentration or other enrichment processes (as explored here) or, after extreme heating, Hg depletion via mobilisation and escape (Liu et al., 2022; Chen et al., 2022). Together, these potential changes lead to much increased uncertainties in terms of estimating volcanic (Hg) emissions from thermally mature sedimentary successions, although despite these challenges many still yield very important data and insights.

2.6. Conclusions

Understanding Hg behaviour during the thermal maturation of sediments is important in terms of our broader knowledge of its global cycling. It also further highlights how the thermal history of sediments is a necessary consideration when looking for anomalous Hg enrichments with the intention to use Hg as a proxy for volcanism. We have studied three cores with different levels of thermal maturity from the Lower Toarcian Posidonienschiefer in the Lower Saxony Basin, Germany. In contrast with other studies that show progressive Hg loss with heating in the thermal aureoles of sill intrusions or in laboratory experiments, maturation here appears to be associated with higher Hg concentrations. Mercury concentrations recorded in mature core B and post-mature core C were +132% to +157% higher than in immature core A. The very low Hg concentrations (≤5 ppb) in Posidonienschiefer-derived oils compared to the immature sediments (50 – 150 ppb) support the conclusion that Hg did not effectively partition into hydrocarbons during maturation and may be considered nearly immobile under these circumstances. At the same time, thermal maturation and hydrocarbon generation-migration reduced the TOC concentration of the host rock by up to ~50% at the high levels of maturity in Core B and C. As a consequence, Hg/TOC ratios from those mature sediments are considerably inflated relative to the immature material. Nonetheless, the observed increase in Hg concentrations with maturation cannot be easily explained by TOC or host-rock mass loss alone.

In search of a mechanism that may have resulted in differences between the three cores, we therefore discuss a suite of syn-depositional processes (i.e., atmospheric Hg and riverine Hg supply, distance from palaeoshoreline, and redox conditions) and post-depositional (i.e. maturation related) processes. None of the known syn-depositional or post-depositional processes can satisfactorily explain the Hg increase from core A to core B and C. As syn-depositional processes are unlikely to have resulted in all the observed differences between core A and core B and C, we speculate that, to some degree, the pronounced difference in the variability of stratigraphic signals of Hg between cores A and core B and C, is related to maturation effects, including Hg redistribution. Although the precise mechanisms of Hg mobilisation and re-sequestration remain elusive, the calcite- and pyrite-filled fractures and veins that occur in certain intervals of cores B and C may hint at Hg migration into specific stratigraphic levels, during or after hydrocarbon mobilisation. Regardless of the exact mechanisms of Hg enrichment, and inflation of Hg/TOC, our results show that thermal maturation effects mean that a cautious approach is warranted when using (post)mature and especially fractured sedimentary successions as an archive for far-field subaerial volcanic activity. Our data show that in a broader sense sediment maturation processes are complex in terms of their contributions to Hg cycling and behaviour.

3. Limited mercury (Hg) partitioning into bitumen and efficient gaseous Hg reabsorption in early thermal maturation of organic-rich mudrocks

A very similar version of this chapter has been submitted to *Geochimica et Cosmochimica Acta* and is under review. The full authors list as follows:

A. O. Indraswari[1,2], J. Frieling[1], E. Idiz[1], T. A. Mather[1], H. C. Jenkyns[1], S.A. Robinson[1], A. J. Dickson[3]

[1]*Department of Earth Sciences, University of Oxford, South Parks Road, Oxford, OX1 3AN, UK.*

[2]*Geoscience Study Program, Faculty of Mathematics and Natural Sciences (FMIPA), Universitas Indonesia, Depok 16424, Indonesia.*

[3]*Centre of Climate, Ocean and Atmosphere, Department of Earth Sciences, Royal Holloway University of London, Egham, Surrey, TW20 0EX, UK.*

Abstract

Recent studies have looked into the impact of exposure to extremely high temperature, such as typifies contact metamorphism, on mercury (Hg) in sediments, and observed significant Hg loss with increasing temperature. By contrast, sediment cores of Lower Jurassic organic-rich Posidonienschiefer (also known as Posidonia Shale) from the Lower Saxony Basin, Germany seemingly showed Hg enrichment after maturation related to basin subsidence and burial under more typical geothermal gradients. To investigate the apparent differences in Hg behaviour, we conducted a series of artificial maturation experiments on immature Posidonienschiefer, analysing Hg concentrations within rock residues and partitioning into generated bitumen during early maturation stages. Thermal desorption profiles were used to track Hg speciation changes in the matured sediment. Our results show a progressive decrease in Hg concentrations in sediments with increasing thermal maturity throughout the experiments, which dominantly relates to released gaseous Hg with only a fraction of the Hg being partitioned into the bitumen (≤1% of the total initial Hg). Further experiments on the dynamics of Hg after mobilisation showed that gaseous Hg in closed vessels was rapidly (≤1 hour) and efficiently (≥95%) reabsorbed into the sediment during cooling. We speculate that our experiments may simulate some of the processes that drive Hg mobilisation and recapture occurring in contact aureoles, such as the rapid release and recapture of gaseous Hg. However, the Hg speciation changes that occur in our experiments and during natural burial maturation clearly differ. Specifically, the changes in Hg speciation in the natural system with burial-related maturation suggest that under those conditions organic matter associated Hg may instead transition into more thermally stable phases, such as HgS, that may form during pyritization, especially in organic-rich sediments with Fe availability.

3.1. Introduction

Understanding the processes associated with Hg behaviour during thermal evolution of sediments is key to understanding its concentration in hydrocarbon reserves (Bryndzia et al., 2023). It also pertains to its use in the sedimentary record as a proxy for large igneous province (LIP) volcanism (e.g., Sanei et al., 2012; Percival et al., 2015, 2021; Grasby et al., 2019; Indraswari et al., 2024) and aids in reconstructing Hg emissions from volcanic activity, especially those resulting from contact metamorphism of intruded sediments (Svensen et al., 2023; Fendley et al., 2024; Frieling et al., 2024a).

Sediments rich in labile organic matter undergo chemical changes in response to burial-related heating in basins, often resulting in the production of hydrocarbons, through the process of thermal maturation (Tissot & Welte, 1984; Peters et al., 2004; Dembicki, 2022). Organic matter (OM) has been widely recognised as the dominant carrier of Hg in the water column and sediments (Wallace, 1982; Benoit et al., 2001; Outridge et al., 2007), although other phases may be important in the rock record (Shen et al., 2020; Qu et al., 2024; Frieling at al., 2024b). Because of its high affinity with OM, Hg concentrations are typically normalised to total organic carbon (TOC) to account for increases linked to higher OM content when identifying anomalous Hg loading in sedimentary deposits (e.g., Grasby et al., 2019; Sanei et al., 2012). As Hg is commonly associated with organic matter, which is transformed during thermal maturation, this process may result in re-distribution of Hg between solid and fluid phases, and potentially mobilises Hg that may facilitate transport out of the host rock. Previous studies have shown that thermal maturation of sediments with labile organic matter produces fluids, both hydrocarbon and non-hydrocarbon, into which metals such as Mo, Zn, U, and Cd have minor partitioning (Dickson et al., 2020, 2022). Similarly, only limited concentrations of Hg have been found in crude oils and hydrocarbon gases with most values falling between 1 and 20 ppb (Wilhelm & Bloom, 2000; Wilhelm et al., 2007; Bryndzia et al., 2023), with some exceptions

(e.g., 593 ppb in condensate liquids in Thailand; Wilhelm et al. 2007). These Hg concentrations are below those typically found in bulk average shale (~62 ppb, Grasby et al. 2019). As a result, the Hg/TOC ratio of hydrocarbons (≤0.24 ppb/%, given that hydrocarbons contain 82–87% carbon by weight, Berkowitz, 1997) is significantly lower than that of sediments (72 ppb/% Hg/TOC; Grasby et al., 2019). However, we note that the shale average is partly derived from datasets representing periods of large igneous province (LIP) volcanism, during which Hg concentrations may be elevated.

Thermal maturation of labile sedimentary OM can occur due to increasing temperature with increasing burial depth, with average temperature gradients for sedimentary basins typically ranging between 20°C km^{-1} and 40°C km^{-1} (Gluyas & Swarbrick, 2021). Through the process of thermal cracking, sedimentary OM (kerogen) is broken down into lower molecular weight hydrocarbon phases, such as oil and gas, often beginning at around 100–120°C (Tissot & Welte, 1984; Peters et al., 2004; Dembicki, 2022). The kerogen becomes more thermally mature as it experiences continued burial and exposure to higher temperatures within the basin and can eventually end up as a carbon-rich graphitic residue, having lost most of its labile OM as separate hydrocarbon phases. This transformation of OM during maturation raises intriguing questions regarding the fate of Hg, which has a high affinity with OM, particularly whether Hg remains associated with the original phase in which it was deposited.

There are several previous studies investigating how thermal maturation has influenced sedimentary Hg concentrations (Table 3.1) (Li et al., 2016; Liu et al., 2022; Chen et al., 2022; Svensen et al., 2023; Indraswari et al., 2024). The various studies yielded insights for Hg and hydrocarbon systematics but particularly for Hg release associated with LIP volcanism. LIP-associated Hg release has been proposed to result from a combination of emissions from the magma itself and, in some cases, crustal rocks such as coals and shales that were heated directly by the LIP intrusions or by associated thermal anomalies affecting whole basins as a result of

crustal thinning (Jones et al., 2019; Svensen et al., 2023a, 2023b). The observations from artificial maturation (pyrolysis) experiments at various temperatures, as well as from field studies of contact aureoles show that rapid heating linked to igneous intrusion in general can cause significant and potentially complete Hg loss from sediments (Liu et al., 2022; Svensen et al., 2023). Quantifying these processes is important in terms of the use of the Hg proxy and what it tells us about LIP-driven perturbations of the global carbon cycle (Svensen et al., 2023; Fendley et al., 2004; Frieling et al., 2024a). As a consequence, most previous studies have focused on replicating thermal conditions relevant to contact metamorphism and thermal anomalies from igneous intrusions, involving steep heating rates to a very high final temperatures (up to a maximum temperature of 750 ºC) (Table 3.1).

In contrast to igneous intrusions, thermal maturation related to basin subsidence generally occurs at a lower (maximum) temperature regime (70–260ºC) and over much longer periods of time (commonly millions of years), resulting in the conversion of whole stratigraphic sequences of organic-rich sediments (Tissot & Welte, 1984; Gluyas & Swarbrick, 2021). The associated conversion of the organic matter (kerogen) into large volumes of hydrocarbon (oil and gas) and non-hydrocarbon (CO_2, H_2S, N_2) fluids may have a significant role in the release, mobilisation and further sequestration of Hg – processes that are not well understood to date. The contrast between apparent increases in Hg with maturation during burial maturation (Indraswari et al., 2024) and Hg loss in most pyrolysis experiments and field observations from contact aureoles may be attributed to the different experimental conditions (open *vs* closed, isothermal *vs* non-isothermal) and the high temperatures (up to 700ºC) the samples were subjected to in the laboratory or in contact metamorphic aureoles (Fig. 3.1).

Table 3.1. Summary of temperature conditions of previous studies of the relationship between thermal maturation and sedimentary Hg concentrations.

Author(s)	Method	Temperature	Maturation Time	Final maturity reached (max %Ro)	Hg concentration final condition (maximum change %)
Liu et al., 2022	Experimental	240–610°C	10–28.5 hours	up to 3.27%	-99
Chen et al., 2022	Experimental, high pressure (0.3 GPa)	50–700°C	18 hours	Unknown	-76
Svensen et al., 2023	Observations from contact aureoles	215–750°C (modelled temperature)	up to millennia for thick sills	up to 5%	-100 (dyke)
					-90 (sill)
Indraswari et al., 2024	Observations from burial natural cores	70–260°C (modelled temperature)	90 Ma	3.5%	+302
This study	Experimental	325°C	24–840 hours	~0.88%	-62

To improve understanding of the impact of maturation and re-distribution of Hg between solid and fluid phases, we performed isothermal artificial maturation experiments to more closely simulate the process of organic matter transformation and hydrocarbon generation (Lewan et al., 1979), especially in the initial to peak generation stages where significant liquid hydrocarbons are mobilised. These experiments were designed to investigate the effects of kerogen conversion and the specific physicochemical conditions that influence sedimentary Hg behaviour (Fig. 3.1). Kerogen cracking and conversion to hydrocarbons is a function of heating time and temperature (Burnham, 2017), occurring over millions of years at slow heating rates. Therefore, laboratory maturation experiments aimed at producing hydrocarbons generally require a compromise between practical (fast) heating times (weeks) combined with the lowest temperatures that still result in appreciable OM conversion (≥300ºC).

We performed isothermal pyrolysis experiments at 325ºC, using established protocols (see Dickson et al. 2020) for periods of up to 5 weeks, using sediment samples rich in immature labile organic matter, reaching conditions that simulate levels of early thermal maturation

stages in sedimentary basins. Mercury concentrations and Hg/TOC values from bulk immature samples were measured before the pyrolysis experiments. We then measured both these parameters in bulk and solvent-extracted residues as well as thermal desorption profiles (Frieling at al., 2024b) to track changes in Hg speciation. The differences between the parameters measured in the original immature samples and the matured pyrolysis samples were examined to determine the change in the bulk Hg concentrations and Hg/TOC values. Finally, Hg has been hypothesised to be recaptured into secondary host phases or reprecipitate with sulfides at lower temperature after mobilisation (Bryndzia et al., 2023; Indraswari et al., 2024; Frieling et al., 2024a). We therefore also performed a small number of experiments whereby closed pyrolysed samples were left to cool for a short while (1–60 minutes) before opening to test whether Hg recapture had occurred.

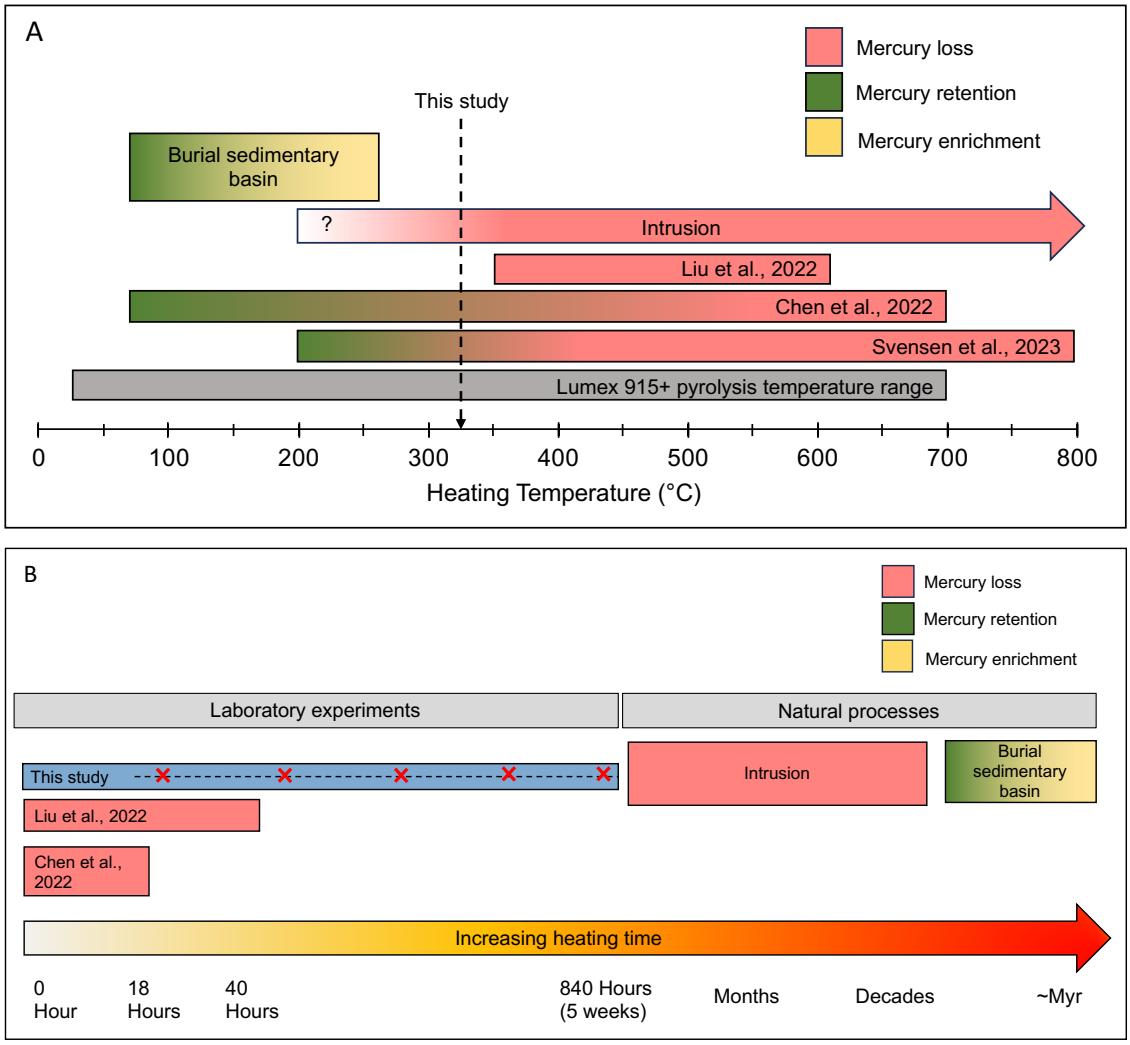


Figure 3.1. (A) The context of this study compared to other previous studies looking at the effect of thermal maturation on sedimentary Hg, focusing on the influence of experimental temperature. **(B)** As panel A, for heating time. Mercury loss, retention, and enrichment represent the observed effects on sedimentary mercury (Hg) after experiments or geological processes, relative to its initial concentration in the sediment.

3.2. Material and methods

3.2.1. Sample material

This study used one sample (ca. 25 grams) from immature, organic matter-rich Lower Jurassic Posidonienschiefer from the Lower Saxony Basin (drill Core A in Indraswari et al., 2024). The immature sample material was taken at relative depth of 34.65 m in core A, homogenised, and divided into ~1 g sub-samples for the experiments. The Posidonienschiefer, a well-known hydrocarbon source rock, is thought to have been deposited in an anoxic marine environment, locally euxinic in nature (Röhl et al., 2001; Schmid-Röhl et al., 2002; Frimmel et al., 2004; Schwark & Frimmel, 2004; Gorbanenko & Ligouis, 2014, 2015; Song et al., 2017; Celestino et al., 2024). The selected sample has a total organic carbon (TOC) value of 8.85 wt% and a hydrogen index (HI) of 701 mgHC/g TOC. Rock-Eval derived T_{max} values of 437°C (vitrinite reflectance equivalent of 0.5% Ro), puts them in the immature to earliest stage of hydrocarbon generation.

3.2.2. Solvent extraction

To obtain an accurate estimate for the amount of generated hydrocarbons during artificial maturation, all sediment aliquots were solvent-extracted prior to pyrolysis. The newly generated hydrocarbon fraction was isolated by a second solvent extraction using the same procedure after pyrolysis. The solvent-extractable organic matter fraction from the sediments was obtained via microwave-sonication using an Analytix Advanced Microwave Digestion System at the University of Oxford following methods described in O'Connor et al. (2019). Sediment powders (~1 g dry mass) from both the original bulk samples, and the post-pyrolysis residues were extracted using 20 mL of dichloromethane (CH_2Cl_2, hereafter DCM): methanol (9:1; volume/volume). The microwave temperature settings were configured to gradually rise from room temperature to 70°C in 10 minutes, isotherm at 70°C for 10 minutes, and then

decrease to 25°C over 20 minutes. After centrifugation, the extracted rock residues were separated from the extracts and dried under N_2. The total lipid extracts (TLE) were then set aside and dried under N_2 and weighed. The TLEs were re-dissolved and homogenised in DCM:MeOH (9:1) prior to Hg analyses. The extraction typically yielded between 8–10 mg of TLE per gram of sediment. After two microwave extraction cycles, no significant additional yield (≤ 1 mg) was observed, indicating that the extraction process had reached its optimal efficiency.

3.2.3. Pyrolysis experiments

The pyrolysis experiments were performed in glass Carius tubes using established procedures (Tannenbaum & Kaplan, 1985; Lu & Kaplan, 1989; Dickson et al., 2020). Carius tubes were initially sterilized at 500°C in a furnace overnight before soaking in hot 10% HNO_3 and rinsed with hot ultra-pure 18.2 MΩ·cm water. The dry extracted rock residues (~1 g) were loaded into clean Carius tubes. Each Carius tube was connected to a vacuum extraction line and flame-sealed after the internal pressure was reduced to 10^{-2} atm. It is important to note that the pressure used in these experiments is not representative of the conditions that these rocks would experience in a real geological setting. This low pressure was selected specifically to minimize oxidation, and also because pyrolysis reactions produce gases, which could lead to tube rupture if high pressure were allowed to build up. The tubes were then loaded into stainless steel containment vessels for heating.

The experiments were carried out under isothermal conditions, with each sub-sample subjected to heating at 325°C for either 24 hours (1 day), 168 hours (7 days), 336 hours (2 weeks), 500 hours (3 weeks) or 840 hours (5 weeks) (Fig. 3.2). Each experiment was performed in triplicate to assess reproducibility. The experimental conditions are shown in Table 3.1. Upon removal from the furnace, Carius tubes were taken from their stainless-steel jackets and broken

open immediately to allow the gaseous component to escape. Microwave-sonication extraction was then carried out (described in §3.2.2) to remove any solvent-extractable organic matter (bitumen) evolved during pyrolysis. The extracted rock residues were dried under a stream of N_2 to remove any remaining solvents and re-homogenised before Hg and Rock-Eval measurements were made (for details see §3.2.5 and 3.2.6).

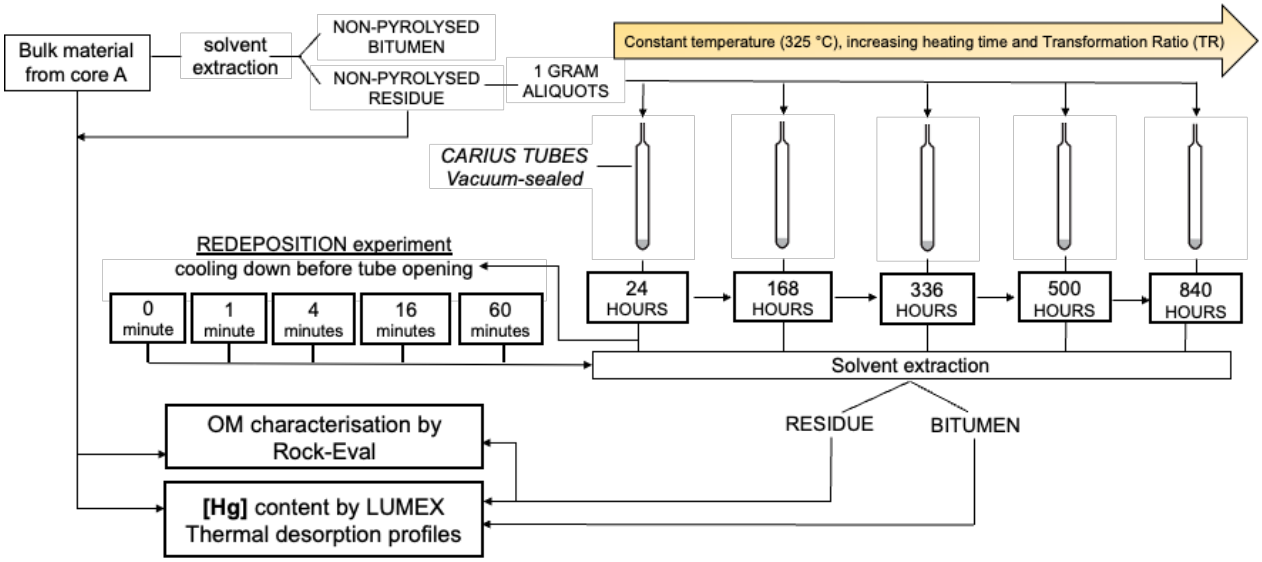


Figure 3.2. Overview of the experimental procedures and analytical approaches in this study modified from Dickson et al. (2020).

Table 3.2. Sub-sample information and specific experimental conditions during pyrolysis experiments.

Sub-sample ID	Rock type	Temperature (°C)	Pressure (atm)	Heating time (hours)
PS-0	Black shale	20	1	0
PS-1	Black shale	325	0.01	24
PS-2	Black shale	325	0.01	24
PS-3	Black shale	325	0.01	168
PS-4	Black shale	325	0.01	336
PS-5	Black shale	325	0.01	500
PS-6	Black shale	325	0.01	840

3.2.4. Cooling and reabsorption experiments

To assess the reabsorption or uptake of generated volatile Hg compounds as a result of cooling to ambient temperature, a new set of four original sub-samples were heated in the furnace for 24 hours and then left to cool in the fume hood for variable amounts of time (1, 4, 16, and 60 minutes) before being opened (Fig. 3.2). For each sub-sample, the temperature of the tube at the time of opening was measured using an infrared thermometer. The specific conditions for cooling time and opening temperature are detailed in Table 3.3. After opening, microwave-sonication extraction, Hg measurements, and Rock-Eval analysis were performed as described above.

Table 3.3. Sub-sample information and specific experimental conditions during cooling and reabsorption experiments.

Sub-sample ID	Heating time (hours)	Cooling time (minutes)	Opening temperature (°C)
PS-0-min	24	0	280
PS-1-min	24	1	211
PS-4-min	24	4	63
PS-16-min	24	16	16
PS-60-min	24	60	16

3.2.5. Total organic carbon and Rock-Eval analysis

The amount, composition and thermal maturity of the organic matter in bulk rocks and solvent-extracted bulk rocks was characterised prior to pyrolysis using a Rock-Eval 6 at the University of Oxford (Behar et al., 2001) (Fig. 3.2). After pyrolysis and subsequent solvent-extraction, sub-samples of residues were measured in Rock-Eval in duplicate, and the precision of the measurements was monitored using in-house standard SAB134 (Lower Jurassic organic-rich marl from St. Audries Bay, Somerset, UK, 2.7 wt% TOC) for every 8 to 10 samples. The standard deviation of the in-house standard over the period of analysis (SAB134) was ±0.03 wt% TOC

3.2.6. Mercury analyses for sediments and bitumen

Mercury (Hg) analyses were conducted with a Lumex RA 915M device, attached to a pyrolysis unit (PYRO-915+) at the University of Oxford (Bin et al., 2001). Powdered solvent-extracted and unextracted sediments of ~50 ± 5 mg were introduced into sample boats, heated to ~700°C and left for up to 120 seconds to fully volatilize the Hg present. The instrument was calibrated before each run using NIST-SRM2587 (National Institute of Standards and Technology – Standard Reference Material: Trace Elements in Soil Containing Lead from Paint) with a Hg concentration of 290 ± 9 ppb. The long-term accuracy of the Hg concentration measurements, based on the SRM2587 standard, was ±5% of the measured value. The manufacturer-specified detection limit for the Lumex RA 915M is ~0.1 ng Hg.

Mercury concentrations of Lower Saxony Basin oils sourced from the Posidonienschiefer were previously measured by Indraswari et al. (2024) on samples obtained from the Lower Saxony Oil Museum (Stock & Littke, 2016). Mercury concentrations in total lipid extracts (TLE) were analysed using a Lumex RA-915M instrument using similar methods as those used to analyse the oils, as described in Indraswari et al. (2024). Following pyrolysis, the solvent-extractable fractions (TLE) were isolated (§3.2.2), dried under a N_2 stream and the solvent-free weight of the TLE from each sub-sample was measured. Prior to Hg analyses, the TLE was redissolved and homogenised in a mixture of dichloromethane and methanol (9:1). An aliquot of 250 µL of the diluted TLE was pipetted into a quartz boat, dried with nitrogen (N_2), and subsequently weighed before adding a food-grade activated charcoal bed to prevent generated smoke affecting the Hg analyses. Mercury concentrations in the activated charcoal were analysed to correct for trace amounts of Hg present in the TLE. Repeat measurements of the charcoal (n = 15) showed an average concentration of 0.4 ± 0.07 ppb (standard error of the mean), or 0.04 ± 0.007 ng Hg for a 100 mg bed. Finally, we analysed Hg concentrations in the

TLE for each sub-sample in duplicate and subtracted the trace amounts of Hg added by the charcoal bed to obtain an accurate estimate of Hg in the bitumen fraction.

3.2.7. Thermal desorption

Mercury thermal desorption profiles (TDPs) were generated for all sub-samples (n = 7) with duplicates and compared with TDPs from a selection of naturally matured samples in Posidonienschiefer from Core B (n = 5) and C (n =5) (Indraswari et al., 2024). The samples taken from Cores B and C are close stratigraphic equivalents to the sample PS-0 from Core A used in the pyrolysis experiments (all within ± 1 m from a relative depth of 34.65 m). The TDPs were obtained using a Lumex RA-915M set up with a PYRO-915+ at the University of Oxford following methods described in Frieling et al. (2024b). The desorption profiles were obtained concurrently with the total mercury concentration measurements within the pyrolysis chamber in Mode 1 (stable temperature of ~700°C). The weight of each sample was held constant at 50 ± 5 mg to avoid the effects of variable sample mass.

3.3. Results

3.3.1. Organic matter maturation

The results of the bulk organic geochemical measurements are shown in Figure 3.3. The decrease in hydrogen index (HI) from 701 to 317 mgHC/gTOC in the extracted residues highlights the increasing conversion of the kerogen as a result of maturation, representing a 55% loss (Figs. 3.3A, B). The highest T_{max} of 443°C, and the HI of 323 mgHC/g TOC in sub-sample PS-6 (840 hours heating time) makes it equivalent to the naturally matured Posidonienschiefer in the Harderode Well in the Hils Syncline, Northern Germany with a measured vitrinite reflectance of ~0.88% Ro (Poetz et al., 2014). The maturity levels of the pyrolysis samples range from immature to the early/peak-oil window stages of kerogen conversion. A simplified transformation ratio (TR), defined as $[(HI_{original} – HI_{measured})/HI_{original}]$,

was used to calculate the proportion of HI change from the original immature kerogen sample to that measured on the individual pyrolysed samples. The TR attains a value of 0.55 for the longest heated sample (840 hours), showing that about 55% of the labile organic matter in this sample has undergone conversion into hydrocarbons compared to the original immature kerogen (Fig. 3.3B).

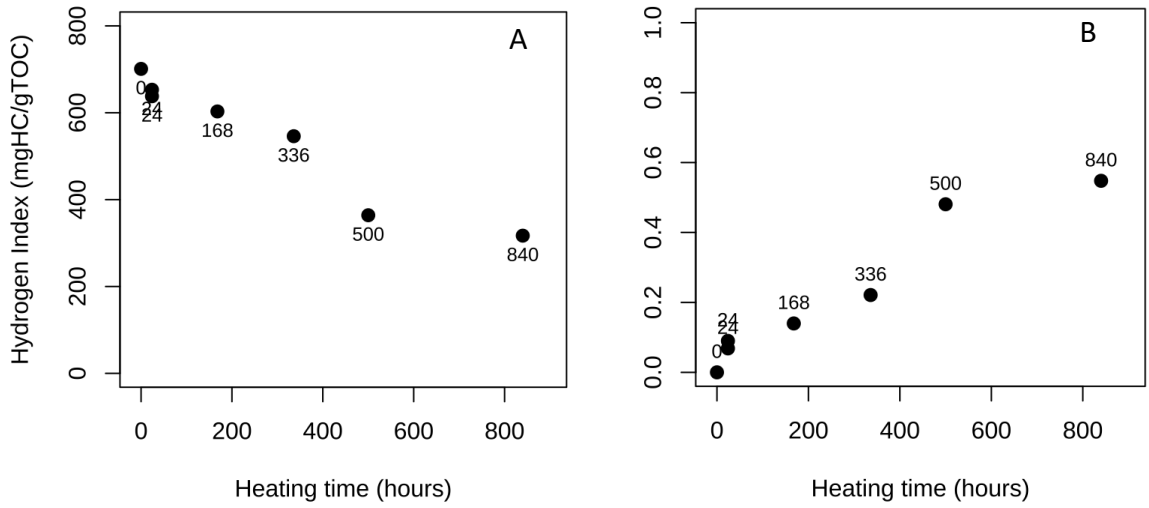


Figure 3.3. Bulk organic geochemical results. **(A)** Hydrogen Index versus heating time in hours showing decreasing hydrogen content/conversion of kerogen into hydrocarbons during maturation; **(B)** Transformation Ratio versus heating time in hours showing how much organic matter (kerogen) has undergone primary cracking into hydrocarbons. Number labels by points show heating time in hours.

3.3.2. Mercury and Hg/TOC in residues, organic extracts, and oils

The results of the pyrolysis experiments show a net loss of Hg, corresponding to a decrease of ~65% of the original yield in sub-samples with the greatest proportion of transformed organic matter (Fig. 3C). Similar to Hg concentration, the Hg/TOC values for the sub-samples also show a decreasing trend due to the relatively large variation of Hg concentration compared to more limited TOC change (e.g., ~65% loss for Hg *vs* ~30% loss for TOC, Fig. 3.3A), and particularly the pronounced Hg loss in the first 24 hrs. As organic matter

conversion progresses, the interpretation of Hg/TOC could become complicated because of progressive Hg and TOC loss at different rates.

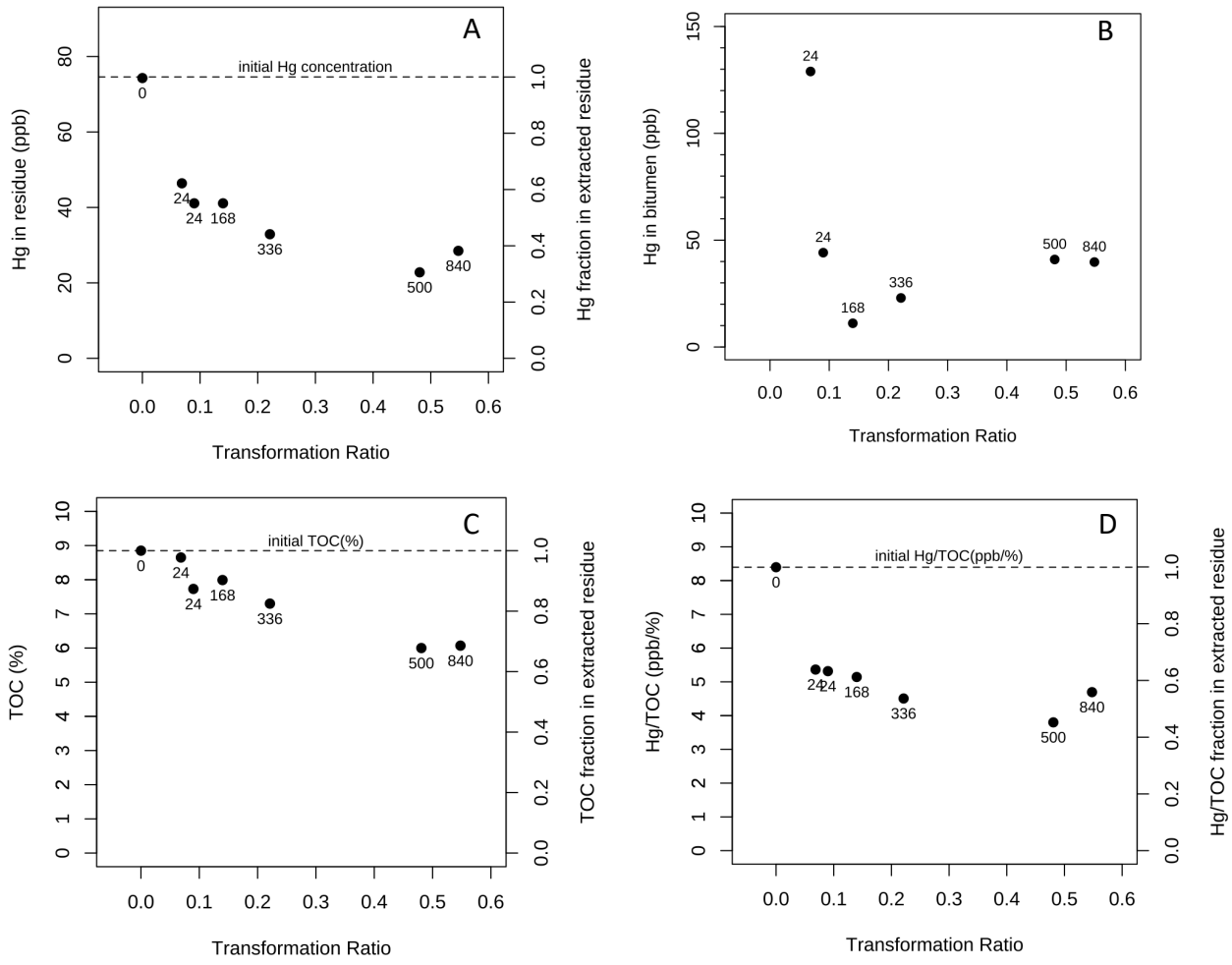


Figure 3.4. (A) Total Hg concentration and fraction of Hg remaining of the original Hg concentration of the sub-samples (dashed line, 74.6 ppb) in the extracted sediments after artificial maturation. **(B)** Total Hg concentration in the produced bitumen. **(C)** As panel A and B with TOC in the residue (dashed line, 8.85%). **(D)** Hg/TOC in the residue (dashed line, 8.43 ppb/%). Number labels by points show heating time in hours.

Table 3.4. Geochemical data from the Posidonienschiefer analysed in this study (also shown in Figure 3.2). HI: Hydrogen Index. TOC: Total Organic Carbon. Tmax: temperature of maximum hydrocarbon yield during pyrolysis. TR: transformation ratio (change in Hydrogen Index during pyrolysis). Extracted Residue: pyrolysed bulk rock residue after solvent extraction. Bitumen: the total solvent-extractable organic matter. The gas loss is calculated using the difference: Hg loss as gas = 100% − %Hg in bitumen − %Hg in the sediments.

Heating time (hours)	HI	TOC (%)	T_{max} (°C)	TR	TLE (mg/g sediment)	Hg				
0	701	8.85	437	0	0.44	74.6 ppb				
						Extracted Residues		Bitumen		Loss (as gas)
						ppb	% of total Hg	ppb	% of total Hg	% of total Hg
24	653	8.65	436	0.07	3.16	48.00	64.34	128.95	0.36	35.29
24	638	7.73	440	0.09	9.02	41.10	55.09	44.15	0.38	44.53
168	603	7.99	440	0.14	11.58	41.45	55.56	11.10	0.04	44.40
336	546	7.3	441	0.22	14.89	33.05	44.30	22.95	0.33	55.36
500	364	6	443	0.48	22.58	22.55	30.23	40.95	1.00	68.77
840	317	6.07	440	0.55	18.31	28.50	38.20	39.75	0.76	61.04

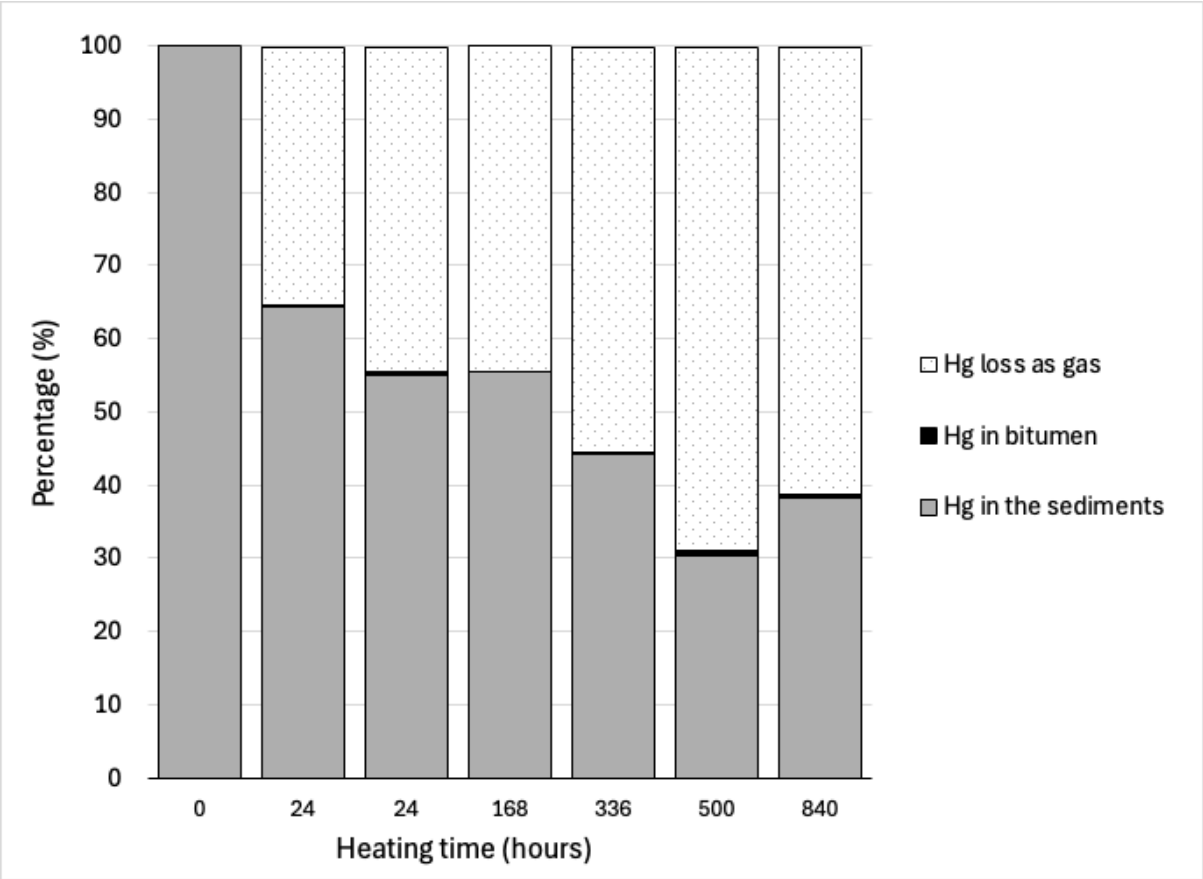


Figure 3.5. Distribution of Hg in pyrolysis experiments showing Hg loss in the longer heated samples. Mercury in bitumen does not show a clear trend with maturation.

The results of Hg measurements in the TLE from pyrolysis are shown in Table 3.4. Hg contents of Posidonienschiefer-derived oils range from 2.5 – 5.2 ppb (Indraswari et al., 2024), which is at the lower end of the range of Hg reported in oils globally (1 – 20 ppb; Wilhelm & Bloom, 2000; Wilhelm et al., 2007; Bryndzia et al., 2023). The Hg concentrations in the Posidonienschiefer-derived oils appear to show a strong correlation with the polar and heteroatomic fraction of Lower Saxony Basin oils analysed in Stock and Littke (2016) using saturate, aromatic, resin and asphaltene (SARA) chromatography analyses (Fig. 3.6). This relationship between Hg and polar and heteroatomic fraction of the oils suggests that the association is mainly with the nitrogen, sulphur and oxygen (NSO) containing heteroatomic compounds in the heavy fraction, as previously observed by Wilhelm et al. (2006). These

results, and the data from the Posidonienschiefer-derived oils in our experimental pyrolysis study, suggest that Hg can be mobilised in a liquid hydrocarbon fraction, particularly at the stage of peak oil generation where NSO and polar compounds are still present in abundance. Although the Hg concentrations in the TLE from the artificially matured sediments are higher (average ~50 ppb) than the natural oils, these levels are still below the bulk value of the untreated immature sediment (74.6 ppb). The greatest proportion of Hg (≥ 99%) in the artificially matured sediments appears to be held in the sediment residue or escapes as released gases (Table 3.2; Fig. 3.5). The gas loss is calculated using the difference: Hg loss as gas = 100% − %Hg in bitumen − %Hg in the sediment residue. To calculate these values, Hg concentrations (in ppb) from the untreated sample, the heated sediment residue, and the extracted bitumen were used to determine the mass of Hg in each fraction. The remaining mass—assumed to be lost as gas—was then expressed as a percentage of the initial Hg content in the untreated sample.

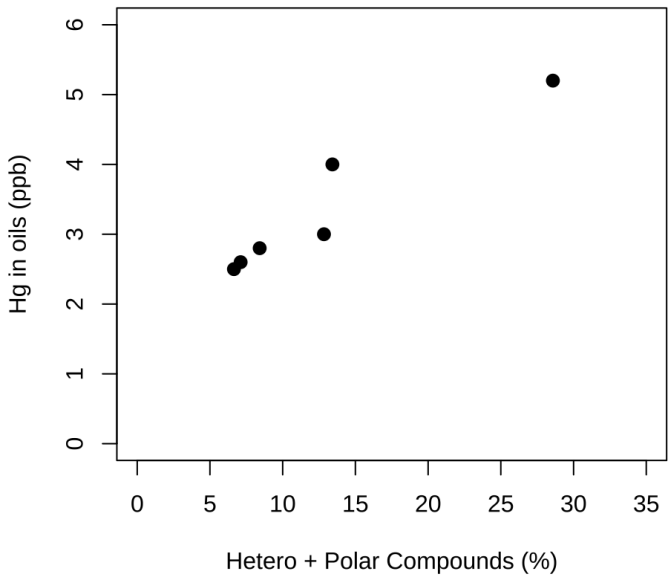


Figure 3.6. Hg concentration in Posidonienschiefer-derived oils (data from Indraswari et al., 2024) showing a strong correlation with the polar and heteroatomic fraction of the oils (data from Stock & Littke, 2016), suggesting, for the Lower Saxony Basin, that the association is mainly with the NSO compounds in the heavy fraction (as also observed by Wilhelm et al. (2006)).

3.3.3 Thermal Desorption Profiles from pyrolysis experiments and natural samples

Thermal desorption profiles (TDPs) of sub-samples from pyrolysis experiments reported here can be compared with averaged TDPs from naturally matured samples, 5 samples from different depths (± 1 m from relative depth 34.65 m) each in the Posidonienschiefer from Cores B and C (Indraswari et al., 2024) and stratigraphically equivalent to the Core A used in all pyrolysis experiments. The TDPs of these two different sample sets (artificially and naturally matured) are presented in Figure 3.7. It is important to note that the thermal maturity achieved in our pyrolysis experiments (%Ro ~0.5% to ~0.88%) did not reach the higher levels of maturity observed in Core B (%Ro ~1.5%) and Core C (%Ro ~3.5%).

The original, untreated sub-samples from Core A (PS-0, Fig. 3.7) display a dominant, single-phase Hg release early in the TDP. The position of this phase in the TDP suggests it might be associated with Hg bound to organic matter (OM) or OM-associated sulphides, as proposed by Frieling et al. (2024b). By contrast, sub-samples with %Ro > 0.64% exhibit more complex TDPs, indicating two-phase, or perhaps even more intricate, Hg release patterns, suggesting the presence of multiple Hg species (PS-5 and PS-6, Figs. 3.7A, B). The artificially matured sub-samples are distinguished from the immature original sediment by two key features: lower overall Hg concentrations (Table 3.2) and a shift from a single dominant release peak to release patterns with a more pronounced 'shoulder' and bimodal peaks (Figs. 3.7A, B).

The naturally matured samples from Cores B and C differ from the artificially matured sub-samples, exhibiting higher Hg concentrations and peaks that appear later in the TDP (Fig. 3.7C). A clear trend of delayed peak Hg release with increasing natural maturity is observed, progressing from Core A (at 26 seconds) to Core B (33 s) to Core C (40 s) (Figs. 3.7C, D). Though the Hg concentrations in Cores B and C are relatively similar, delayed Hg desorption with increasing maturation suggests progressive changes in Hg speciation may occur with

increasing maturity even beyond the oil/gas window. Indeed, limited hydrocarbon generation is expected during the maturation from Core B (%Ro ~1.5%, entering dry gas window) to Core C (%Ro ~3.5%, overmature post-gas window) (Indraswari et al., 2024).

Moreover, the samples from Core B exhibits a more prolonged Hg release compared to material from both Core A and Core C, resulting in lower amplitude peaks in area-normalised Hg (Fig. 3.7D). The variation in release duration and the shift towards later Hg release across the different sample sets (from Core A to Cores B and C) underscore the possibility that there may be appreciable and predictable Hg speciation changes with increasing maturity.

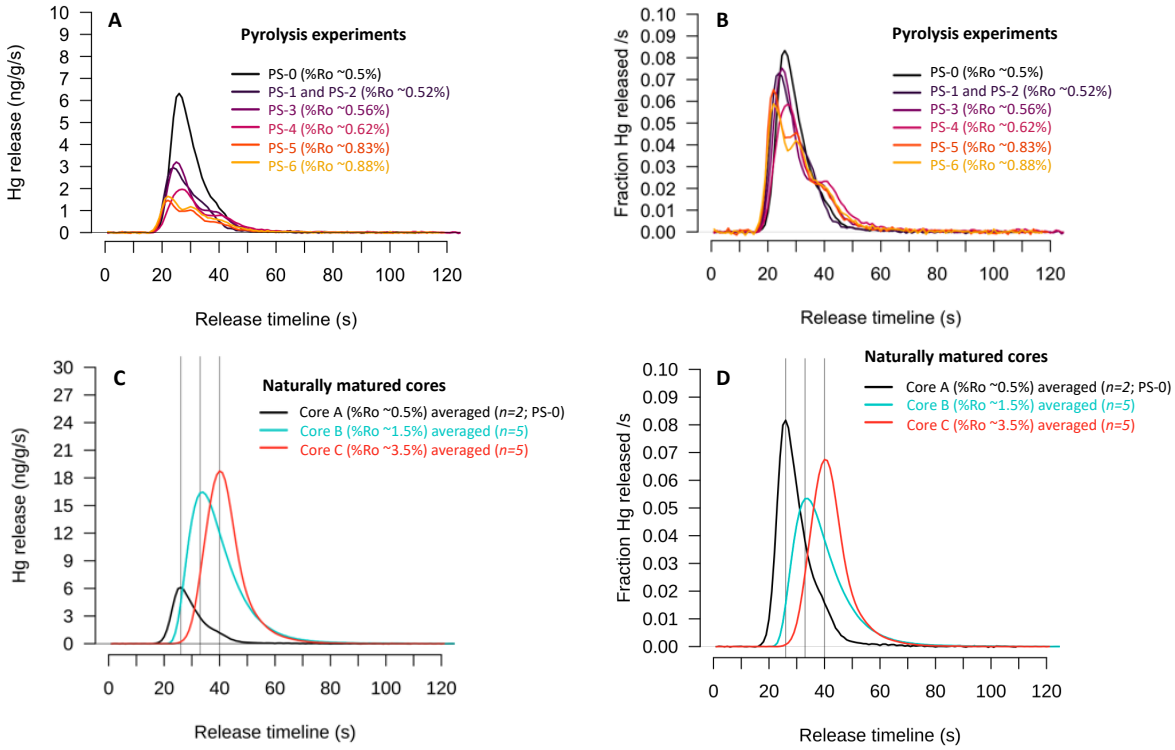


Figure 3.7. Thermal desorption profiles of artificially matured sub-samples from pyrolysis experiments and naturally matured samples from Cores B and C. **(A)** Hg release rate per second for artificially matured sub-samples from Core A (PS-0) in pyrolysis experiments. **(B)** Fraction of total Hg released per second) for pyrolysis sub-samples. **(C)** Hg release rate per second for samples selected from Cores A, B, and C. **(D)** Average Hg release intensity normalised to total release for samples selected from Cores A, B, and C. Peak Hg release shifts from 26 s in averaged PS-0 (untreated sub-sample from Core A used in this study) to 33 s in averaged samples from Core B and 40 s in averaged samples from Core C selected in this study (grey vertical lines on each peak), observed in both the total release and normalised plots.

3.3.4. Mercury behaviour during cooling – reabsorption experiments

Upon opening a sub-sample at the highest temperature at 280°C (0 minutes of cooling, inside the oven with the door open), a significant decrease in Hg concentration in the residue was observed, indicating substantial Hg loss as a gas phase (Fig. 3.8). Specifically, Hg concentrations remaining in the residue were 32% and 26% of the untreated sub-sample value when opened at 280°C (0 minute) and 211°C (1 minute), respectively. Subsequent openings after sealed cooling to 63°C (4 minutes) and 16°C (16 and 60 minutes at room temperature) showed Hg concentrations returning to 38%, 66%, and 96% of the original values, suggesting appreciable and ultimately near complete Hg reabsorption at lower temperatures, from a gas phase, into sediments.

In the TDPs from the reabsorption experiments, the Hg release peaks for PS-0 (untreated), PS-4-min, and PS-16-min were consistently observed at 26 seconds (Fig. 3.8B). By contrast, the peak Hg release for PS-0-min and PS-1-min are more extended, similar to the artificially matured sub-samples that were not allowed to cool down (§3.3.3). Regarding the Hg fraction release profiles (Fig. 3.8C), the curves for PS-0 (untreated), PS-16-min and PS-60-min were nearly identical, overlapping each other.

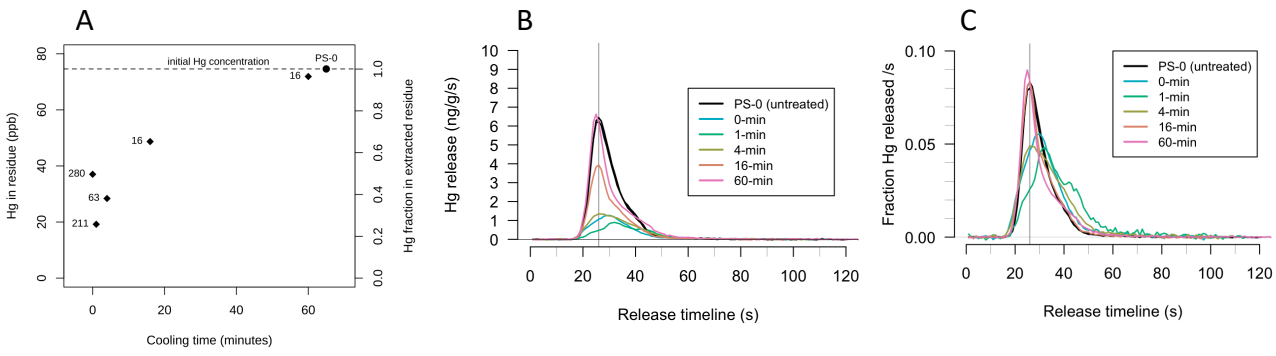


Figure 3.8. (A) Mercury concentration and fraction of original Hg concentrations from reabsorption experiments with progressive cooling (filled diamonds). Number labels by points show opening temperature in °C. The top right point (filled dot) represents the untreated sub-sample (PS-0). **(B)** Thermal desorption profile for reabsorption experiments. **(C)** Average release intensity normalised to

total Hg release. Grey vertical line in panel B and C shows peak Hg release of PS-0 (untreated), PS-4-min, and PS-16-min at 26 seconds.

3.4. Discussion

3.4.1. Trends in Hg and processes driving Hg loss

We observed Hg loss across all isothermal maturation experiments, with the most pronounced decrease occurring within the first 24 hours (Fig. 3.4A). Mercury concentrations in bitumen were found to be low (≤1% of total initial Hg) while Hg in the gas phase (Hg lost during opening inferred by difference, see §3.3.2) was significant (>35% of total initial Hg) (Table 3.4, Fig. 3.5). This result indicates that, under these experimental conditions, most of the mobilised Hg is present in the gas phase rather than in the bitumen after maturation. The pyrolysis temperature used in our experiments (325ºC) would allow the decomposition of the most common sedimentary Hg species, such as organic matter and sulphide-bound Hg, followed by subsequent release as gas from the sediments. Previous studies have shown Hg desorption from sediments occurring at temperatures as low as ~150ºC (Rumayor, et al., 2015a; Saniewska and Bełdowska, 2017). Other potentially relevant sedimentary Hg species that may decompose below the experimental pyrolysis temperature experienced by the sample include pyrite-bound Hg and HgS (Rumayor et al., 2015b, 2016).

Similar to previous experimental studies (Liu et al., 2022; Chen et al., 2022), we observe Hg loss with heating. In our experiments, the main mechanism is thought to be escape of gaseous Hg during opening of the hot, sealed, tubes. The maximum Hg loss observed in this study (35–69%) is lower than the Hg losses reported in Liu et al. (2022), which exceeded 99% at their maximum temperature of 610°C, and in Chen et al. (2022), which reached 76% Hg loss at their maximum temperature of 700°C. However, when examining similar temperature points, the findings become more comparable, with Hg losses ranging from 5–25% at 300°C (0.3 GPa) for Chen et al. (2022), and 30–65% at 350°C for Liu et al. (2022). Altogether, the experiments

are, however, difficult to compare in detail even at similar temperature settings because they include a number of different conditions/set-ups used for the experiments (Table 3.1).

Besides the differences in temperature regime, we find that sample-specific Hg speciation is a likely candidate to explain the substantial differences in the behaviour for various shales in Liu et al. (2022) and Chen et al. (2022) for experiments conducted at the same temperature (experiments become more similar ≥450 ºC because of complete Hg loss). Mercury speciation therefore can be a crucial factor in Hg mobilisation, as is the overall openness of the system and pressure (sealed tubes *vs* semi-closed anvil cell), that might impact Hg loss and reabsorption potential. Further, we note that some materials of the maturation vessels used in previous experiments (gold tubes in Liu et al., 2022; graphite in Chen et al., 2022) might be more conducive to absorbing Hg from a gas phase compared to the glass used in our experiments (e.g., gold-amalgamation used in direct Hg analysers: Schroeder, et al., 1985; Lee & Park, 2003). Altogether, we find the results for Hg loss are broadly comparable to previous works and not unexpected given the temperature regime employed here.

3.4.2. Mercury partitioning into (hydrocarbon) fluid and gas phases

As kerogen cracks and forms bitumen and a mobile fluid phase, Hg associated with organic matter may selectively move to specific organic fractions (e.g., polar, asphaltene-fractions and natural gas condensates) (Wilhelm et al., 2006). Interestingly, Hg did not show a strong tendency to partition into the extractable (oil) phase, with the concentration of Hg in extracted hydrocarbons typically at or below the sediment average (Table 3.2). It follows that the Hg/TOC of the bitumen (≤ 1.5 ppb/%, with bitumen contains typically ca. 82–87% C by mass, Berkowitz, 1997) is below that of the average sediment (8.43 ppb/%). These data imply that only a very small fraction (≤1%) of the total Hg present in the sediment is hosted in the extracted bitumen. In contrast to the Hg in bitumen, Hg in the gas phase (potentially as Hg^0) is

lost from the artificially matured sub-samples upon opening the hot tubes and this process appears to be the dominant pathway for removal of mobilised Hg in these experiments. To what extent this experimental process replicates Hg dynamics in burial-driven thermal maturation is less certain, as temperature is likely to be a strongly controlling factor in Hg mobility and the majority of sedimentary Hg species would not be stable at the temperatures employed here (325ºC). However, the observations from our experiments may become more relevant near igneous intrusions, which also produce hydrocarbons (e.g., Svensen et al. 2015) and mobilise Hg (e.g., Liu et al. 2022, Svensen et al. 2023), both of which can migrate out of contact aureoles. The limited partitioning into liquid hydrocarbons or other solvent-extractable fractions in our experiments suggests that Hg would likely experience limited transport by hydrocarbons in contact aureoles, and that Hg transport might be dominated by the gas phase in such settings. This observation aligns with previous inferences on the formational mechanism of mercury ore deposits that were believed to be transported as Hg in a gas phase (Varekamp & Buseck, 1984; Bryndzia et al., 2023; Frieling et al., 2024a), although some bitumen may be present and provide an additional supply of Hg (Bryndzia, 2023).

3.4.3. Mercury reabsorption from a gas phase

In a previous study of the same Posidonienschiefer sequences from the Lower Saxony Basin, we observed a 2- to 3-fold increase in Hg concentrations and Hg/TOC due to burial-related maturation of sediments compared to the more immature stratigraphic equivalent section (Indraswari et al., 2024). We attributed the increase in Hg concentrations in the natural system to loss of rock mass, particularly TOC and water and perhaps subtly elevated original sedimentary Hg concentrations. In most sediments, rock mass loss during maturation would be relatively small but in organic-rich shales mass loss may have influenced a significant fraction of the total rock mass, which implies that, if Hg is effectively immobile during thermal maturation, Hg concentrations increase through the closed-sum effect. There is also the

possibility that Hg was temporarily partitioned into a gas or fluid phase but ultimately remained in the host-rock, reabsorbed with residual organic matter fractions or sulphides, its mobility being limited primarily by the very low permeability of the Posidonienschiefer.

In our experiments at 325ºC, a substantial proportion of the original Hg was initially desorbed from sediments and moved into a gas phase. The simple reabsorption experiments conducted here serve to illustrate the fate of mobilised (gaseous) Hg during cooling, and to test whether the result may match the observations from burial or igneous heating. Remarkably, we find that a substantial part of the desorbed, gaseous, Hg is recaptured in the sediment after only a very limited time (minutes) at lower temperature. Moreover, most of the recaptured Hg is not extractable with organic solvents (Table 3.S1 in Appendix 2), effectively excluding the possibility that it has been taken up into hydrocarbons or formed (thermogenic) methylmercury (Zettlitzer et al., 1997, Wilhelm et al., 2006). Finally, a heating experiment where we exposed the sub-samples marked by Hg recapture overnight at 80ºC in an open vessel showed no concentration changes. This experiment excludes the presence of appreciable amounts of extremely volatile Hg species, such as condensed Hg^0 (e.g., Windmöller et al. 1996). We therefore argue that volatilized Hg can be rapidly and efficiently reabsorbed into or onto organic particles and sulphides after cooling; an observation that seems to align with previous observations of retained Hg in thermally altered rocks around igneous intrusions (Frieling et al., 2024a).

3.4.4. The potential impact of Hg speciation and changes in Hg speciation: natural system *vs* artificial maturation

The response of sedimentary Hg to heating and maturation can vary significantly across different shales (terrestrial *vs* marine *vs* lacustrine organic matter), as demonstrated in Liu et al. (2022). These variations may, in part, be attributed to differences in the nature of the chemical species of Hg present in the shales. The results obtained from the naturally matured

Core B and C samples (Figs. 3.7C, D), as well as the experimental data (Figs. 3.7A, B), suggest that during burial-maturation Hg speciation evolves with temperature and time, ultimately leading to a more significant proportion of temperature-resistant species. This suggestion could imply that processes accompanying burial maturation, such as pyritization, may limit Hg mobility during and after hydrocarbon formation.

While helpful in understanding Hg mobilisation and phase transformation at high temperatures, the controlled conditions of artificial maturation experiments thus cannot fully replicate the complexities of natural burial maturation. These experiments lack the extended timescales and pressures characteristics of natural burial maturation and are conducted at slightly higher temperatures than would occur in the hydrocarbon window. These practical compromises required by artificial maturation experiments result in Hg behaviour that appears to differ from the transformations observed in natural burial maturation. The differences in TDPs between our experimental and natural Posidonienschiefer sub-samples (Fig. 3.7) highlight the fact that our experiments probably cannot fully mimic Hg phase changes that occur during burial maturation.

However, we propose that our experiments better simulate certain processes driving Hg mobilisation and recapture in contact aureoles, such as the rapid release and reabsorption of gaseous Hg. The TDPs from our reabsorption experiments in this study (Fig. 3.8C, D), where Hg is reabsorbed into sediments as a low-temperature phase are similar to shales observed in contact aureoles (Frieling et al., 2024a).

3.5. Conclusions

Artificial maturation experiments, designed to simulate the natural process of thermal transformation of labile organic matter, demonstrated a drop of ~65% in Hg concentration with increasing heating time, mainly due to the release of volatilized gaseous Hg. Most importantly,

Hg in bitumen extracted from the sediments indicates that Hg does not have a significant tendency to partition into hydrocarbon fluids produced during thermal maturation. After heating, only a minor fraction (≤1%) of initial Hg in the untreated sediments was transferred to the bitumen. In comparison, 64–30% of initial Hg was retained in the rock residue, and 35–69% of as volatilized gas.

Further, we studied the potential for Hg reabsorption during cooling using artificially matured sediments. These experiments showed that once mobilised, gaseous Hg in a closed system can be efficiently (≥95%) reabsorbed back into the sediment within an hour during cooling to room temperature (16°C).

While our experiments simulate some processes that drive mobilisation and recapture, we also find distinct differences between our experiments and burial-related naturally matured core shales. In particular, observed changes in Hg speciation with maturation suggest that, during burial maturation, mobilised Hg from organic matter may not reabsorb into a similar phase but, over time, progressively transition into more thermally stable phases. Using core material that represents various stages of burial-related maturation in the Posidonienschiefer (Lower Saxony Basin), we previously observed that Hg concentrations increased with maturity and loss of rock mass. Our new analyses suggest that the limited partitioning of Hg into bitumen and progressive transformation of Hg species into more thermally stable phases are processes that can limit Hg mobility both during and after hydrocarbon formation.

Together, the limited partitioning of Hg into bitumen and changing Hg speciation may explain the inefficient transport of Hg in the low-permeability and relatively low-temperature environments that generate hydrocarbons. However, our artificial maturation experiments perhaps more closely mimic the conditions in contact aureoles, particularly the rapid volatilization and reabsorption of gaseous Hg.

4. The influence of primary depositional conditions on Hg behaviour during early thermal maturation

This chapter is currently in preparation for publication with the following author list:

A. O. Indraswari[1,2], J. Frieling[1], E. Idiz[1], T. A. Mather[1], A. J. Dickson[3], H. C. Jenkyns[1], S.A. Robinson[1], I. M. Fendley[1,4], O. Neilson[4]

[1]Department of Earth Sciences, University of Oxford, South Parks Road, Oxford, OX1 3AN, UK.

[2]Geoscience Study Program, Faculty of Mathematics and Natural Sciences (FMIPA), Universitas Indonesia, Depok 16424, Indonesia.

[3]Centre of Climate, Ocean and Atmosphere, Department of Earth Sciences, Royal Holloway University of London, Egham, Surrey, TW20 0EX, UK.

[4]Department of Geosciences, Pennsylvania State University, University Park, PA, USA.

Abstract

Mercury (Hg) behaviour in sedimentary rocks is important to understand both in terms of its potential volatilization during magmatic intrusions (e.g., those associated with large igneous province activity) and its redistribution during thermal maturation associated with burial and, in some cases, hydrocarbon generation. Mercury behaviour varies significantly across different lithologies, likely influenced by the amount and type of organic matter present and sulphur chemistry. This study investigates the effects of lithology on Hg dynamics during thermal maturation through pyrolysis experiments at isothermal conditions of 325°C for various durations (24, 336, 500, and 840 hours). To study Hg behaviour in different lithologies, representing different depositional environments and OM-types (organic-rich *vs* organic-lean), we analysed a relatively Hg-rich sample from the Lower Jurassic (Pliensbachian) Belemnite Marls, a marine carbonate-rich sequence exposed in southern England, and a coal from the Eocene Tanjung Formation, Indonesia composed of terrestrial organic matter. Before and after pyrolysis, we generated data on Hg concentrations, total organic carbon (TOC), hydrogen index (HI), and oxygen index (OI) and compared our results with existing data from the Posidonienschiefer, a marine, highly organic-rich, black shale of Toarcian age from Germany. Results indicate substantial Hg loss, with the coal and Belemnite Marls samples losing over 80% of their Hg in the first 24 hours, compared to a 50% loss in the Posidonienschiefer. Thermal desorption profiles (TDPs) allow us to align the Hg losses in the isothermal heating experiments with the initial Hg speciation in the sedimentary rocks. Both the Belemnite Marls sample and Tanjung Formation coal are dominated by lower temperature Hg species, potentially bound to or associated with organic matter. These findings enhance our understanding of the interplay between lithology, thermal maturation, and Hg behaviour, which is critical for interpreting historical Hg cycling and the environmental impacts associated with the formation of large igneous provinces (LIPs).

4.1. Introduction

Mercury (Hg) anomalies in sedimentary record are increasingly recognized as a valuable proxy for studying large igneous provinces (LIPs) and their environmental impacts (Sanei et al., 2012; Grasby et al., 2019; Percival et al., 2021). While this proxy has been mostly used as a qualitative metric of LIP activity, under the right circumstances it might be possible to use Hg to estimate carbon emissions during carbon-cycle perturbation events by scaling up carbon emissions based on Hg sedimentary contents via realistic Hg/C ratios (Fendley et al., 2024). A proportion of both carbon and Hg emissions associated with LIPs is potentially sourced from thermogenic release from intruded sediments as well as the magmatic volatile load (Ganino and Arndt, 2009; Svensen et al., 2023a; Frieling et al., 2024a). This proportion depends on the scale of the intrusions and the nature of the intruded rocks. Specifically, the intruded rocks may vary not only in both organic-matter and Hg content but also in their potential to generate fluids and gases, and their potential for Hg release may depend on its speciation as well as the feasibility of the fluids generated escaping to the surface. There is growing interest in understanding how Hg and C behave near intrusives within LIPs (Svensen et al., 2023a; Frieling et al., 2024a): a comprehensive overview of Hg and organic-matter behaviour with thermal maturation can be used to inform how intrusions into specific rock-types or environmental conditions may influence Hg/C of thermogenic gases and refine Hg-based LIP emissions.

The volatiles produced and released along with Hg by these intrusives can range from hydrocarbon gases and CO_2, to larger molecular weight hydrocarbons (Svensen et al., 2023b and references therein), influenced by the temperature (i.e., distance from the intrusion) and the bulk compositions of the intruded rocks. Close to the igneous intrusion, the sediments may be exposed to very high temperatures and, with increasing exposure temperature, the resulting products will gradually become more enriched in dry gases (CH_4 and CO_2) as a result of

cracking of the sedimentary organic matter and generated heavier hydrocarbons (Goodarzi et al., 2018). Furthermore, the behaviour of Hg during subsidence-related (burial) thermal maturation has also gained attention, with a focus on understanding Hg in generated and mobilized fluids (e.g., Bryndzia et al., 2023; Indraswari et al., 2024; *submitted*).

Mercury can be hosted in various sedimentary phases, for example, organic matter (OM) and metal sulfides (e.g., pyrite, (meta-)cinnabar HgS) (Grasby et al., 2019; Shen et al., 2019). Whether influenced by magmatic intrusions or basin subsidence, sedimentary OM and other components (i.e., water, clays) undergo transformation (thermal maturation) in response to elevated temperature and pressure, which can result in, for example, the redistribution of carbon and Hg between solid and fluid phases (both hydrocarbon and non-hydrocarbon). The generated fluids provide a potential pathway for mobilizing and facilitating Hg transport between geological rock reservoirs and the surface (see e.g., Filby, 1994; Indraswari et al., 2024). Although metals are often assumed to be closely associated with OM, previous studies have observed only minor partitioning of elements such as Mo, Zn, U, and Cd into the hydrocarbon fluids during maturation (Dickson et al., 2020, 2022; Kendall et al., 2023). We have recently found evidence via isothermal pyrolysis experiments that the same situation applies to Hg (Indraswari et al., *submitted*), which showed only very limited (≤ 1 %) partitioning into a hydrocarbon phase during maturation, at least for a highly organic-rich marine shale.

The type and concentration of organic matter (OM) in sediments strongly influences the quantity and composition of fluids generated and expelled during thermal maturation (Tissot and Welte, 1984). This principle may also extend to the behaviour of sediment-hosted mercury (Hg). Recent studies, including artificial maturation experiments and investigations of sedimentary rocks affected by igneous intrusions, have explored the isotopic variations of Hg under thermal maturation (e.g., Liu et al., 2022; Chen et al., 2022). However, these studies have

not focused on the depositional environments of the samples that may have had an influence on Hg behaviour during maturation through differences in both OM type and concentration as well as Hg speciation. Consequently, the influence of varying depositional environments on sedimentary Hg behaviour during thermal maturation remains poorly understood. This study aims to contribute to addressing this gap by examining how different depositional settings affect the thermal behaviour of Hg in sedimentary rocks.

Table 4.1 outlines the different depositional settings of samples previous researchers have used when looking at the effect of thermal maturation, both burial- and intrusion-related, on Hg. The sediments in question consist mainly of marine black shales (Liu et al., 2022; Chen et al., 2022; Svensen et al., 2023a; Frieling et al., 2024a), but also lacustrine shales and calcareous mudstones (Liu et al., 2022), as well as a Recent soil (Chen et al., 2022) (Table 4.1). These studies all showed significant Hg loss due to the high potential for sedimentary Hg species to decompose, especially in a temperature range of 200–300ºC (Chen et al., 2022; Liu et al., 2022; Svensen et al., 2023a, Frieling et al., 2024a; Indraswari et al., *submitted*). However, between different sample types, we find there are significant differences in Hg behaviour. This result is not unexpected as different sediment types and depositional settings will likely cover a range of variations in OM types, and organic and inorganic S-containing species (sulfides, sulfates, thiols) and Hg species (OM-bound, pyrite-bound, (meta-)cinnabar) – all factors that we hypothesize play an important role in the sequestration, release and mobilization of Hg in response to thermal maturation.

In order to address the role of the depositional environment and organic-matter variability on Hg behaviour during thermal maturation, and to complement a previous study carried out on a Jurassic marine organic-rich marly sediment (Posidonienschiefer) with Type II kerogen (Indraswari et al., *submitted*), we performed pyrolysis experiments on two additional types of samples. The first is carbonate-rich organic-lean marl sample from the Lower Jurassic

Belemnite Marls sequence that has atypically elevated Hg contents (>300 ppb). The organic matter of the Belemnite Marls is Type IV kerogen (non-source rock) and the sediment was deposited in a shallow-marine epicontinental basin. Although the Belemnite Marls sequence has significant variability in both TOC content and quality (Lang et al., 1928; Weedon and Jenkyns, 1990, 1999; Hesselbo and Jenkyns, 1995), the organic-lean and Hg enriched material we selected provides an end-member so far unrepresented in maturation experiments. The second sample, from the Eocene Tanjung Formation, is a terrestrial coal deposited in a tidally influenced lower coastal plain (Type II/III Kerogen) with moderate Hg but high organic-carbon. As in our previous study (Indraswari et al., *submitted)*, we conducted artificial maturation experiments under isothermal conditions at 325°C for 24, 168, 336, 500, and 840 hours. These new datasets were compared with existing pyrolysis data from the Posidonienschiefer (Indraswari et al., *submitted*) and published data on Hg in artificially and naturally matured marine shales, lacustrine shales and marine carbonate-rich mudstones (Liu et al, 2022; Chen et al., 2022, Frieling et al., 2024a).

The heating temperature used in the experiments is particularly significant, as the primary range for Hg loss, between 200–300°C, is also where the greatest variability in Hg behaviour has been observed during pyrolysis analysis (see e.g., Frieling et al., 2024a). To build on previous studies that typically used shorter durations of around 24 hours, we conducted longer term isothermal analyses. These extended experiments provide valuable insights into how Hg loss progresses under stable temperature conditions, a closer (albeit still limited) representation of situations that occur near igneous intrusions or in deeply buried sediments (Indraswari et al., *submitted*). We specifically focus on how different environmental conditions during deposition may have influenced sedimentary Hg behaviour during thermal maturation by examining the differences in redox state, availability of sulfur (which affects the presence of specific sulfide minerals) and organic-matter type.

4.2. Material and methods

4.2.1. Sample material

We conducted maturation experiments for two new samples (organic-lean Belemnite Marls sample and organic-rich Tanjung Formation coal) and compare these to material used in previous studies looking at the effect of thermal maturation on Hg (Table 4.1). Comparative material includes the marine mudrocks of the Lower Jurassic Posidonienschiefer (Indraswari et al., *submitted*), the Proterozoic Xiamaling Formation, the Permian Talung Formation (Liu et al., 2022), Cryogenian Datangpo Formation (Chen et al., 2022), lacustrine shales from the Eocene Shahejie Formation (Liu et al., 2022), and highly contaminated recent GSS-4 soil standard reference material (Chen et al., 2022) (Table 4.1).

4.2.1.1. Depositional setting of the Belemnite Marls

The Belemnite Marls comprise a cyclically bedded alternation of light and dark marls and rare concretionary limestones packaged in decimetre-scale couplets and metre-scale bundles. The sequence is of Pliensbachian (Early Jurassic) age and was deposited in the Wessex Basin of southern England. The samples were collected from outcrops on the Dorset coast (Lang et al., 1928; Weedon & Jenkyns, 1990, 1999). Key sedimentary components are varying amounts of calcium carbonate, partially coccolith-derived, clay minerals (dominantly illite), organic matter and pyrite. The sequence is rich in body fossils such as belemnites, ammonites, bivalves, brachiopods and crinoids, signifying that the depositional environment was fully marine (Sellwood, 1970, 1972). The presence of *Chondrites* burrows throughout the section, signals relatively low oxygen (dysoxic) conditions (Bromley & Ekdale, 1984; Buatois & Mángano, 2016; Baucon et al., 2020). The burrowing mixed light-coloured sediment into dark and *vice versa*, and together with the local presence of black laminated shale in the succession,

Table 4.1. Summary of the depositional environments, redox conditions, and lithologies used in experimental studies examining the effects of thermal maturation, both burial- and intrusion-related, on sedimentary Hg.

Age	Formation /Member Name	Environment of deposition	Oxygenation regime	Potential for sulphide production	Kerogen Type	Lithology	Initial bulk TOC (%)	Initial Total Hg (ppb)	Reference
Mesoprotero-zoic	Xiamaling Formation	Marine	Suboxic	Moderate to high	Oil-prone (II)	Black shale	4.09	326.8	Liu et al., 2022
							13.35	107.3	
Permian	Talung Formation	Marine	Suboxic-anoxic	Moderate	Oil-prone (II)	Calcareous mudstone	5.56	238.7	
Eocene	Shahejie Formation	Lacustrine	Anoxic	Moderate to high	Oil-prone (I/II)	Black shale	3.45	272.4	
							4.83	178.1	
Proterozoic (Cryogenian)	Datangpo Formation	Marine	Anoxic	High	Oil-prone (I/II)	Black shale	1.91	375	Chen et al., 2022
Recent	-	Limestone-weathered soil	Unknown	Unknown, likely low	Unknown	Contaminated soil	0.62	563	
Lower Jurassic	Posidonienschiefer	Marine	Euxinic	High	Oil-prone (II)	Black shale	8.85	74.6	Indraswari et al., *submitted*
Lower Jurassic	Belemnite Marls	Marine	Dysoxic	Moderate	Inert (IV)	Calcareous mudstone	0.85	325.4	**This study**
Eocene	Tanjung Formation	Terrestrial/Coastal swamps	Dysoxic	Low but non-zero	Oil and gas-prone (II/III)	Coal	24.73	44.2	

indicates the primarily nature of the sedimentary cyclicity, attributed to astronomical (Milankovitch) forcing (Weedon & Jenkyns, 1990, 1999).

The specific sample used in this study is from sample BM-15, taken from the 15.09 m level in the section (Top 113c Bed) according to the numbering system of Lang et al. (1928) and stratigraphic log of Weedon and Jenkyns (1999). This specific layer is a light marl that is carbonate-rich and relatively poor in organic matter. In general, the light marls in the sequence have mean TOC of 0.94% and $CaCO_3$ of 58.8% (Weedon & Jenkyns, 1990).

4.2.1.2. Depositional setting of Tanjung Formation

The Tanjung Formation, deposited in the Barito Basin during the Middle Eocene to Early Oligocene in the Sundaland margin, is characterized by thick, laterally extensive planar coals formed in fluvial-tidal and marginal marine environments (Witts et al., 2012; Anggara et al., 2024). The coals in the Tanjung Formation contain mixed fresh- and brackish-water palynomorph assemblages and were interpreted as estuarine (non-deltaic) coastal swamp deposits due to their lateral continuity and stability (Witts et al., 2012). The coal is mainly composed of huminite macerals, with significant amounts of cutinite and resinite, along with inorganic constituents such as clay (kaolinite), pyrite, and carbonate minerals (Fikri et al., 2022; Anggara et al., 2024). Anggara et al. (2024) performed proximate and ultimate analyses of Tanjung Formation coals (n = 35). The proximate analysis, which measures moisture, fixed carbon, volatile matter, and ash content, revealed an average volatile matter of 44.6%, fixed carbon of 40.1%, and low moisture content (4.2%). The ultimate analysis, which determines the chemical composition of coal (i.e., percentages of carbon, hydrogen, nitrogen, oxygen, and sulphur) on a moisture- and volatile matter-free basis, showed high carbon (80%), hydrogen (6.3%), nitrogen (1.5%), and total sulphur (1.6%) contents. Vitrinite reflectance values of 0.52–0.59% Ro (Fikri et al., 2022) indicate that the coals are at the subbituminous A or high volatile

bituminous C stage and are immature with respect to hydrocarbon generation (Tissot & Welte, 1984). Patria et al. (2024) observed that framboidal pyrite in Tanjung Formation coals predominantly exceeded 5 μm in size and interpreted redox conditions in the water column during deposition as dysoxic, with some sulphide production in pore-waters.

4.2.1.3. Depositional setting of Posidonienschiefer

All data for the Toarcian (Lower Jurassic) Posidonienschiefer in this study are taken from Indraswari et al. (*submitted*) that used one sample from a relative depth of 34.65 m in core A. This sample is thermally immature (0.5% Ro, T_{max} 437ºC) and rich in organic matter. The Posidonienschiefer is a prolific hydrocarbon source rock in the Lower Saxony Basin of Northern Germany. This sequence is interpreted to have been deposited in an euxinic (free H_2S in the water column) marine environment based on the size distribution of framboidal pyrite, with limited terrestrial detrital and organic-matter input (Röhl et al., 2001; Schmid-Röhl et al., 2002; Frimmel et al., 2004; Schwark & Frimmel, 2004; Gorbanenko & Ligouis, 2014, 2015; Celestino et al., 2024). The selected sample has a total organic carbon (TOC) value of 8.85 % and a hydrogen index (HI) of 701 mgHC/g TOC.

4.2.2. Methods

Experimental setups follow those detailed in Indraswari et al. (*submitted*). In short, aliquots of ~ 6 g each of the Belemnite Marls and Tanjung Formation coal were solvent-extracted and subsequently analysed for Hg concentrations and Rock-Eval measurements before pyrolysis (outlined below). Each of the ~6 g solvent-extracted samples of Belemnite Marls and Tanjung Formation coal was divided into six sub-samples, resulting in a total of 12 sub-samples. Each sub-sample weighed approximately 1 g and was loaded into clean glass tubes to be heated in the furnace following Tannenbaum and Kaplan (1985), Lu and Kaplan (1989), and Dickson et al. (2020). Each glass tube was flame-sealed after removing

atmospheric air using a vacuum extraction line. Each sub-sample was put into a stainless-steel jacket and heated in the furnace isothermally at 325°C for either 1 day, 7 days, 2 weeks, 3 weeks, or 5 weeks. After heating according to the designated time, each sub-sample was opened instantly to let the gaseous component out. The sediments, after heating, were solvent-extracted again to isolate the bitumen that evolved during thermal maturation. After centrifugation, the bitumen and solvent-extracted residues were separated and dried under N_2. The extracted rock residues were subsequently re-homogenised before Hg and Rock-Eval analyses. The bitumen generated during pyrolysis was extracted, dried under nitrogen and weighed, then re-dissolved and homogenised in dichloromethane (DCM): methanol (MeOH) (9:1, volume/volume) prior to Hg analyses.

4.2.2.1. Solvent extraction

Solvent extraction of the sediments before and after pyrolysis was undertaken using an Analytix Advanced Microwave Digestion System at the University of Oxford, following methods described in O'Connor et al. (2019). Before pyrolysis, existing free hydrocarbons were solvent-extracted from ~6 g sub-samples using 120 mL of DCM:MeOH (9:1, v/v). The microwave temperature settings were configured to gradually rise from room temperature to 70°C in 10 minutes, isotherm at 70°C for 10 minutes, and then decrease to 25°C over 20 minutes. The sub-samples were then centrifuged and the sediments were separated from the solvent. The sediments were dried under a N_2 stream and divided into glass tubes for the pyrolysis experiment. After pyrolysis, each sub-sample of ~ 1 g was solvent-extracted using 20 mL of dichloromethane (DCM)/methanol (9:1, v/v). After centrifugation, the bitumen and solvent-extracted residues were separated and dried under N_2 to be analysed for Hg concentrations and Rock-Eval measurements.

4.2.2.2. Rock-Eval analysis

Analysis using the Rock-Eval 6 at the University of Oxford (Behar et al., 2001) was performed on solvent-extracted samples prior to pyrolysis and solvent-extracted sub-samples after pyrolysis. This analysis returns data on the total organic carbon (TOC), pyrolysable carbon in the rocks (S2, in mg HC per g rocks), hydrogen index (HI), and oxygen index (OI) in the sub-samples before and after pyrolysis. HI values are calculated as (100×S2)/TOC (mg HC per g TOC). The HI is then used to determine the thermal maturity parameter as a simplified transformation ratio (TR), defined as $[(HI_{original} - HI_{measured})/HI_{original}]$. The reproducibility of the measurements was monitored using in-house standard SAB134 (Lower Jurassic organic-rich marl from St. Audries Bay, Somerset, UK, 2.7% TOC and HI 660 $mgCO_2$/gTOC) for every 8 to 10 samples. The standard deviation of the in-house standard over the period of analysis (SAB134) was ±0.1% TOC and ±15 mgHC/gTOC for HI.

4.2.2.3. Mercury analysis for sediments and bitumen

Mercury (Hg) concentration analyses for solvent-extracted sediments before and after pyrolysis were conducted with a Lumex RA 915M device, attached to a pyrolysis unit (PYRO-915+) at the University of Oxford (Bin et al., 2001). Powdered sub-samples of 50 ± 5 mg in sample boats were rapidly heated from ~20 to ~700ºC, during which Hg was released. Before each run, the instrument was calibrated using NIST-SRM2587 (National Institute of Standards and Technology – Standard Reference Material: Trace Elements in Soil Containing Lead from Paint), with a mercury (Hg) concentration of 290 ± 9 ppb. The long-term analyses of the SRM2587 standard indicate reproducibility of Hg concentration within ±5% of the measured value. The manufacturer-specified detection limit for the Lumex RA 915M is ~0.1 ng Hg for solid samples weighing 100–200 mg (1 ng g^{-1} or ppb by weight).

Mercury concentrations in bitumen were also analysed using a Lumex RA-915M, following methods similar to those used for oil analysis as detailed in Indraswari et al. (2024; *submitted*). After pyrolysis, the solvent-extractable fractions (bitumen) were isolated (§2.2), dried under a nitrogen (N_2) stream, and the solvent-free weight of each bitumen sub-sample was recorded. Before Hg analysis, the bitumen was redissolved and homogenized in 9:1 (v:v) DCM:MeOH. A 250 µL aliquot of the diluted bitumen was pipetted into a quartz boat, dried under nitrogen, and weighed. A food-grade activated charcoal bed was added to minimise oil smoke interference in Hg analyses. Mercury concentrations in the activated charcoal were also analysed to correct bitumen data for trace Hg present in the charcoal bed, with repeat measurements (n = 15) showing an average concentration of 0.44 ± 0.06 ppb (standard error of the mean), equating to 0.044 ± 0.006 ng Hg for a 100 mg charcoal bed. Finally, duplicate measurements of Hg concentration in each bitumen sub-sample were taken, with the trace Hg from the charcoal bed subtracted to obtain accurate Hg estimates in the bitumen fraction.

4.2.2.4. Thermal desorption profiles (TDPs) for mercury

Thermal desorption profiles (TDPs) for sedimentary Hg from solvent-extracted sediments before and after pyrolysis were obtained using a Lumex RA-915M set up with a PYRO-915+ at the University of Oxford, according to the procedures described in Frieling et al. (2024b). These TDPs allow us to examine whether changes in Hg speciation occur in the sediment residues during maturation. The desorption profiles were obtained concurrently with the total mercury concentration measurements within the pyrolysis chamber in Mode 1 (stable temperature of ~700°C). The weight of each sample was held constant at 50 ± 5 mg to avoid the effects of variable sample mass. In addition to these standard steps, Saniewska and Bełdowska (2017) highlighted the fact that samples with high OM content (Loss on Ignition (LOI) > 20%, equivalent to > ~9.4% TOC) such as coals can experience spontaneous combustion between 225 and 250°C. Self-ignition may result in an instantaneous uncontrolled

rise in temperature, that, in turn, could result in small differences in the heating rate between the desorption measurements. We therefore analysed the Tanjung coal over a slow temperature ramp (150–300ºC with 5-minute plateaus every 25ºC step), including the critical 225–250ºC range with a Lumex 915Lab at the University of Oxford, and monitored the temperature of the combustion cell. These measurements did not show any anomalous temperature rises that might signal self-ignition.

4.3. Results

4.3.1. Organic-matter maturation

4.3.1.1. Initial conditions

The results of the bulk organic geochemical measurements are shown in Figure 4.1. The untreated sub-sample of Tanjung Formation coal has a high hydrogen index (HI) of 290 mg HC/g TOC and a low oxygen index (OI) of 16 mg CO_2/g TOC. By contrast, the original untreated Belemnite Marls sub-sample has a lower HI value of 100 and a higher OI value of 125.

4.3.1.2. Effects of maturation on OM characteristics

The effect of artificial thermal maturation on the three different samples is shown in Table 4.2 and the modified van Krevelen diagram (Fig. 4.1A). The maturation of all samples with increasing heating time is demonstrated, as expected, by the reduction in the HI, as a result of transformation of kerogen into bitumen and gas. Compared to the original HI values for the samples, the decrease in HI is 55% for the Posidonienschiefer, 36% for the Tanjung Formation coal and 68% for the Belemnite Marls. It is important to note that the original HI of the Belemnite Marls is already quite low prior to maturation and the longer experiments result in S2 peaks near the analytical limit for quantification (0.2 mg HC/g). As for TOC, the

Posidonienschiefer experienced largest loss with a 32% reduction of the original TOC concentration (Fig. 4.1B). The loss of TOC in Tanjung Formation coal is minimal (3%) and in the Belemnite Marls all samples were within analytical error of each other.

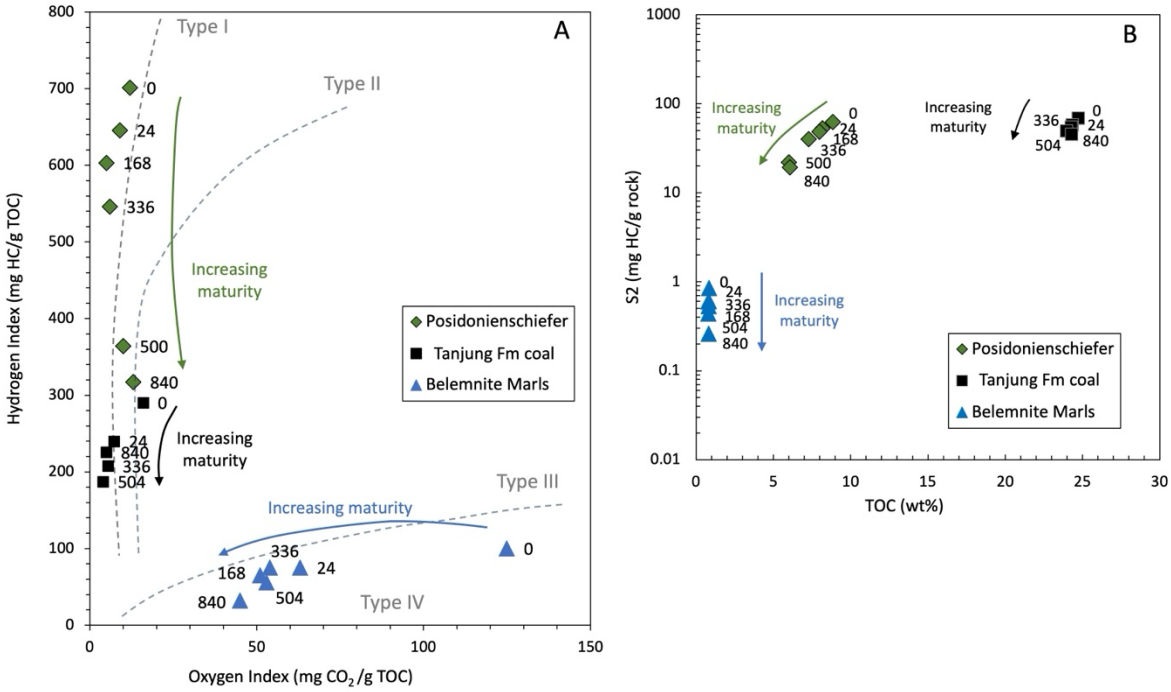


Figure 4.1. A. Modified van Krevelen diagram showing the maturity evolution of samples in this study. **B.** S2-TOC plot showing S2 decrease as samples mature for all samples. Number labels by points show heating time in hours.

4.3.2. Mercury (Hg) and Hg/TOC in residues and bitumen

All three samples (the Posidonienschiefer, the Belemnite Marls, and the Tanjung Formation coal) show systematic Hg loss with increasing pyrolysis times, but to different degrees. The original untreated Belemnite Marls sub-sample has an initial total Hg (Hg_T) concentration of 325.4 ppb and the sub-sample heated after 840 hours lost ~83% of its Hg_T (Table 4.2, Fig. 4.2). The original untreated Tanjung Formation coal sub-sample has an initial Hg_T concentration of 44.2 ppb and the 840-hour sub-sample shows a loss of 93% of the initial Hg_T. The previously analysed original untreated Posidonienschiefer sub-sample has an initial Hg_T concentration of 74.6 ppb (Indraswari et al. *submitted*) with 63% initial Hg_T loss after 840

Table 4.2. The geochemical measurements from Tanjung Formation coal and Belemnite Marls analysed in this study (also shown in Figures 4.1 and 4.2). HI: Hydrogen Index. OI: Oxygen Index. TOC: Total Organic Carbon. TR: transformation ratio, change in Hydrogen Index during pyrolysis, defined as $[(HI_{original} - HI_{measured})/HI_{original}]$. T_{max}: temperature of maximum hydrocarbon yield during pyrolysis. S2: pyrolysable carbon in the rocks.

Sample	Heating time (hour)	HI (mg HC/g TOC)	OI (mg CO_2/g TOC)	TOC (%)	TR	T_{max} (°C)	S2 (mg HC/g rock)	Total Hg (ppb)	Hg_T/TOC (ppb/%)
Tanjung Formation coal	0	290	16	24.7	0	428	68.76	44.2	1.79
	24	240	7	24.3	0.17	432	58.29	12.7	0.52
	336	208	5.5	24	0.28	439	49.78	10.8	0.45
	500	187	4	24.3	0.36	446	45.44	3.6	0.15
	840	226	5	24.3	0.22	437	54.47	5.4	0.22
Belemnite Marls	0	100	125	0.85	0	432	0.85	325.4	382.76
	24	75	63	0.81	0.25	433	0.61	78.7	97.16
	168	65	51	0.82	0.35	437	0.53	65.9	80.37
	336	75	54	0.8	0.25	437	0.6	74.7	93.38
	500	56	53	0.79	0.44	439	0.44	60.8	76.96
	840	32	45	0.82	0.68	439	0.26	55.3	67.44

hours heating. Because of the different rates of change of TOC and Hg_T in the sample sets through the pyrolysis experiments, we also observe a distinct decrease in Hg_T/TOC in all samples (Table 4.1 and Fig. 4.2B). The Belemnite Marls sub-sample showed a reduction in Hg_T/TOC from ~383 ppb/% (0-hour heating) to ~67 ppb/% (840 hours heating) whereas the Tanjung Formation coal started with 1.79 ppb/% Hg_T/TOC in the non-heated sub-sample and ended up with 0.22 ppb/% in the sub-sample heated after 840 hours. The Posidonienschiefer started with an initial Hg_T/TOC of 8.43 ppb/% in the original sub-sample and declined to 4.70 ppb/% after 840 hours of pyrolysis.

Clear differences between the sample types appear when examining the rate of Hg_T loss over heating time. The rate of Hg_T loss, especially after the first 24 hours of isothermal heating, is similar for the Belemnite Marls and the Tanjung Formation coal, with the Belemnite Marls having 24% of Hg_T retained in the sediment residue and the Tanjung Formation coal 29% (Fig. 4.2C, Table 4.3). original untreated the Posidonienschiefer retained 64% of Hg_T after 24 hours heating, signifying a much slower Hg release. Continued isothermal heating of the Posidonienschiefer resulted in progressive Hg loss but at a reduced rate compared to that of the first 24 hours (Fig. 4.2C) reaching a minimum of 30% at 500 hours. The Tanjung Formation coal also still continued to release Hg after the first 24 hours (~10% Hg_T retained after 500–840 hours heating) while the Belemnite Marls experienced only a more subtle decrease (17% of the original Hg_T after 840 hours of heating) (Fig. 4.2C).

The amount of bitumen produced after heating for each sub-sample varies (Fig. 4.3A). There is an observed trend of increasing bitumen mass produced in the more mature sub-samples for the Posidonienschiefer and Tanjung Formation coal. On the other hand, the Belemnite Marls, with a high proportion of inert OM (type IV kerogen), produced no bitumen during heating. In the earlier stage of maturation level (TR <0.3), the Posidoniencshiefer generated a slightly higher amount of bitumen (~15 mg bitumen/g sediment, Indraswari et al.,

submitted) compared to the Tanjung Formation coal (~13 mg bitumen/g sediment, Table 4.3). However, at the higher maturity level (TR ~0.4), both the Posidonienschiefer and the Tanjung Formation coal generated a similar amount of bitumen: 22–23 mg/g sediment (Fig. 4.3A).

The results of Hg concentration measurements in the bitumen from the Tanjung Formation coal corresponding to its transformation ratio are shown in Figure 4.3B. These results plotted together with the ones from Posidonienschiefer (Indraswari et al., *submitted*) show the absence of a strong correlation between Hg concentration in the bitumen and maturity level. When the proportion of the Hg mass in the bitumen is calculated from the Hg_T, we find that the percentage of mercury that partitioned into the bitumen after pyrolysis ranges from 0.05% to 0.8% of Hg_T in Tanjung Formation coal, similar to what is observed for the Posidonienschiefer (0.04%–1%) (Indraswari et al., *submitted*) (Fig. 4.3C).

4.3.3. Thermal desorption profiles (TDPs) of sedimentary mercury

The thermal desorption profiles (TDP) show Hg release over time (seconds) as the sample is heated in the furnace. From statistical analyses, Frieling et al. (2024b) proposed that the relatively low-temperature Hg release peak relates to Hg bound to organic matter (OM) or OM-associated sulphides, and the later release as other Hg release phases (which may include, e.g., red HgS (cinnabar)). We follow the same methodological approach as Frieling et al. (2024a), who used a cut-off to separate the distinct low-temperature Hg phase (Hg_{LT}) from the higher temperature Hg phases (Hg_{HT}) (note that $Hg_{LT} + Hg_{HT} = Hg_T$) to illustrate how Hg speciation relates to Hg mobilization in the vicinity of a contact aureole. We here use a cut-off at 35 seconds. The Hg-TDP results from the Posidonienschiefer, the Belemnite Marls, and the Tanjung Formation coal used in this study show distinct behaviour in Hg release as a response to isothermal heating (Fig. 4.4). Each curve in Figures 4.5A, 4.5B, and 4.5C represents Hg release (ng) per gram of sample material per second and the curves in Figures 4.5D, 4.5E, and

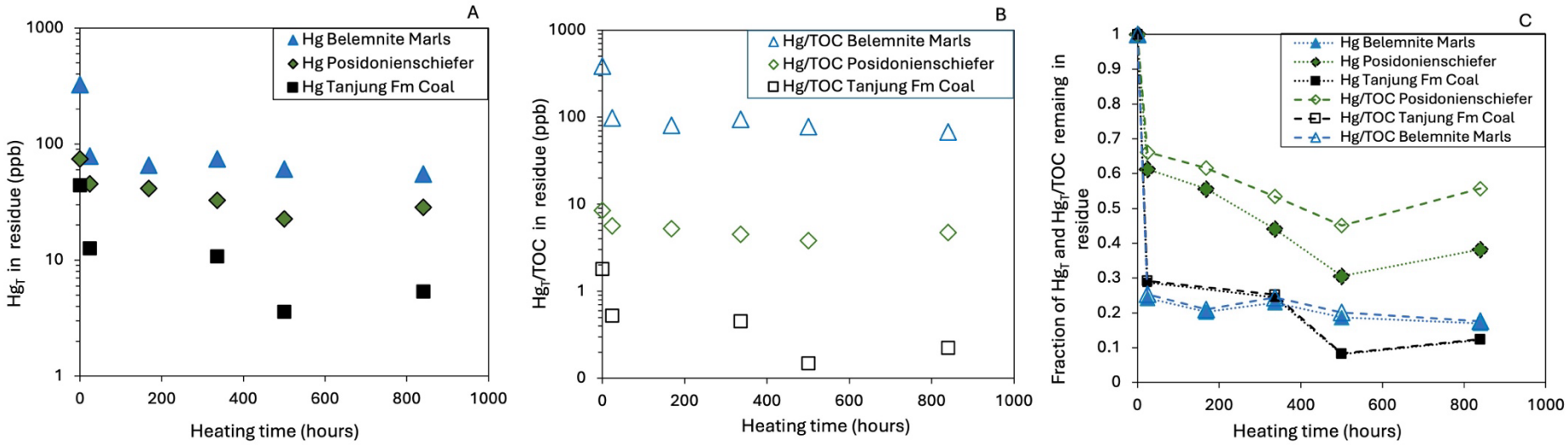


Figure 4.2. A. Total Hg (Hg_T) concentration remaining in the residue after pyrolysis. **B.** Hg_T/TOC in the residue. **C.** Fraction of Hg_T and Hg_T/TOC of the original Hg_T concentration and original Hg_T/ TOC in the residue. Note that the y-axes in A and B are logarithmic.

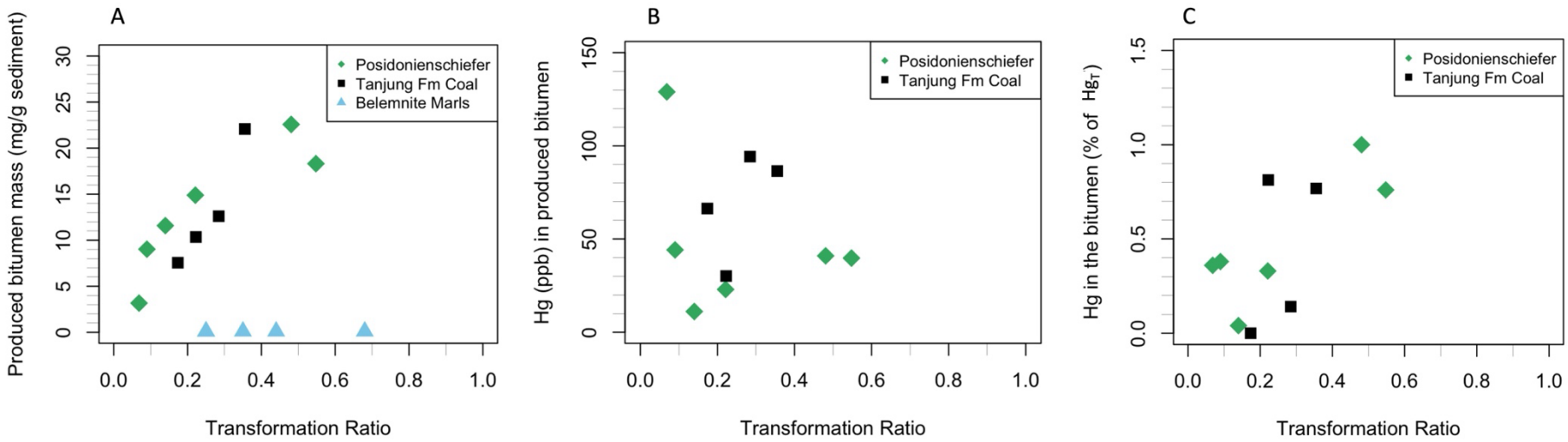


Figure 4.3. A. Bitumen mass produced from heated samples in this study with respect to their transformation ratio. There is an observed trend of increasing bitumen mass produced in the more mature samples for the Posidonienschiefer and Tanjung Formation coal sub-samples. The Belemnite Marls sub-samples did not generate enough bitumen for Hg analyses. **B.** Mercury concentration in the produced bitumen from pyrolysis. **C.** Fraction of Hg (% of Hg_T) in the original samples partitioned to the bitumen.

Table 4.3. Distribution of Hg in the residues and bitumen from the Tanjung Formation coal and Belemnite Marls sub-samples analysed in this study (also shown in Figure 4.3). HI: Hydrogen Index. TOC: Total Organic Carbon. T_{max}: temperature of maximum hydrocarbon yield (S2) during pyrolysis. TR: transformation ratio (change in Hydrogen Index during pyrolysis). Extracted Residue: pyrolysed bulk-rock residue after solvent extraction. Bitumen: the total solvent-extractable organic matter. The gas loss is calculated using the difference: Hg loss as gas = 100% − %Hg in bitumen − %Hg in the sediments. N.D.: not determined. No measurable amount of TLE could be obtained from the Belemnite Marls.

Sample	Heating time (hours)	HI (mg HC/g TOC)	TOC (%)	TR	TLE (mg/g sediment)	Total Hg				
Tanjung Formation coal	0	290	24.7	0	0.16	44.2 ppb				
						Extracted Residues		Bitumen		Loss (as gas)
						ppb	% of Total Hg	ppb	% of Total Hg	% of Total Hg
	24	240	24.3	0.17	7.55	12.70	28.73	66.35	0.14	71.13
	336	208	24	0.28	12.61	10.80	24.43	94.25	0.77	74.80
	500	187	24.3	0.36	22.08	3.60	8.14	86.45	0.81	91.04
	840	226	24.3	0.22	10.35	5.40	12.22	30.15	0.06	87.72
Belemnite Marls	0	100	0.85	0	-	325.4 ppb				
						Extracted Residues		Bitumen		Loss (as gas)
						ppb	% of Total Hg	ppb	% of Total Hg	% of Total Hg
	24	75	0.81	0.25	-	78.7	24.19	n.d.	0	75.81
	168	65	0.82	0.35	-	65.9	20.26	n.d.	0	79.74
	336	75	0.8	0.25	-	74.7	22.96	n.d.	0	77.04
	500	56	0.79	0.44	-	60.8	18.69	n.d.	0	81.31
	840	32	0.82	0.68	-	55.3	17.00	n.d.	0	83.00

4.3.3.1. Belemnite Marls Hg behaviour

In the original untreated (i.e., prior to artificial maturation) Belemnite Marls sub-sample, a prominent Hg release peak occurs around 30 seconds (Fig. 4.4A, darkest blue line), which is likely associated with OM based on its position early in the TDP (Frieling et al., 2024b). After 24 hours of heating, however, this Hg release peak is no longer prominent, and the maximum Hg release significantly decreases from 35 ng/g/s to 5 ng/g/s, which corresponds with the reduction in Hg concentration observed in the 24-hour sub-sample (Fig. 4.2, Table 4.3). The concentration-normalised plot of Belemnite Marls sub-samples heated for ≥ 24 hours shows a delayed and more prolonged Hg release (Fig. 4.4D), with a consistent release profile across these sub-samples and only minimal further reduction in Hg release (Fig. 4.4A, D). This sharp decrease in the early, lower temperature Hg release phase (Hg_{LT}) indicates that this is the dominant phase that was volatilized in the first 24 hours of isothermal maturation, while the sub-samples that were heated for longer show a later, more stable peak, around 40 seconds and strongly reduced rate of Hg loss.

Before maturation, the Belemnite Marls sub-sample is dominated by the low-temperature Hg phase, with 87% Hg_{LT} and 13% Hg_{HT} (Fig. 4.4G). After 24 hours of heating, the proportion of Hg_{LT} to Hg_{HT} in the Belemnite Marls sub-sample changed to 51:49. This ratio subsequently exhibited slight fluctuations in the proportion, with Hg_{HT} making up 68%, 58%, and 54% after 336, 500, and 840 hours of heating, respectively.

4.3.3.2. Tanjung Formation coal Hg behaviour

For the Tanjung Formation coal, the Hg release signals from the untreated sub-sample show a single peak (Fig. 4.4C). The signals from the heated (≥ 24 hours) sub-samples are identical to the untreated sub-sample but with lower overall Hg concentrations (Fig. 4.4C, F, Table 4.3). This characteristic is further demonstrated in the normalised plots of the Tanjung

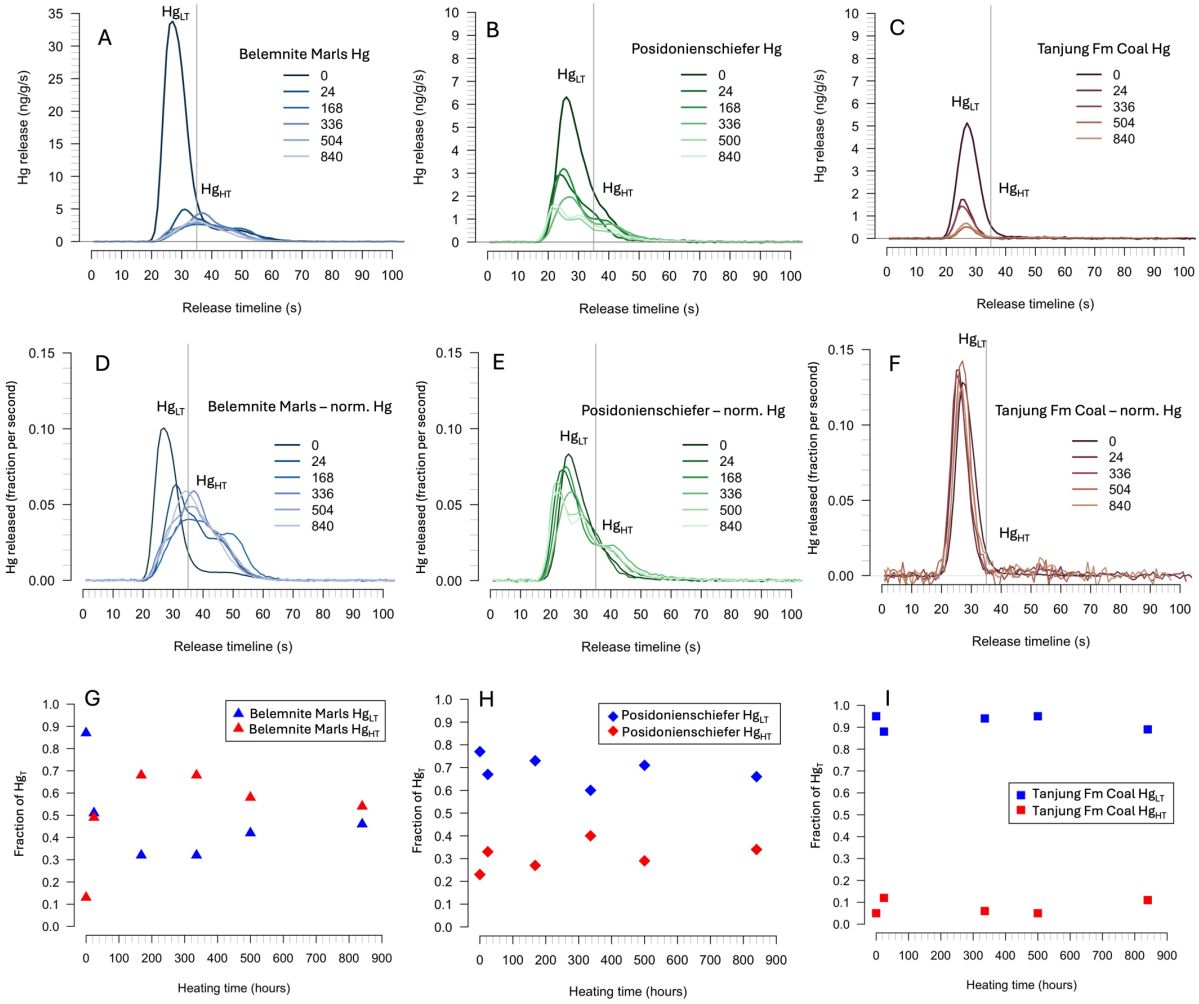


Figure 4.4. Thermal desorption and Hg release intensity for samples before and after pyrolysis (number labels by lines show heating time in hours). **A.** Hg release (in ng g-1 s-1) for the Belemnite Marls sub-samples. **B.** As panel A for the Posidonienschiefer. **C.** As panel A for the Tanjung Formation coal. **D.** Hg release intensity for the Belemnite Marls sub-samples, normalised to the total Hg release (Area) from each sub-sample. **E.** As panel D for the Posidonienschiefer. **F.** As panel D for the Tanjung Formation coal. **G.** Fraction of low-temperature Hg (Hg_{LT}) and high-temperature Hg (Hg_{HT}) – defined by their release stage with Hg_{LT} released first and Hg_{HT} released later in the TDP – compared to the heating time for the Belemnite Marls sub-samples. **H.** As panel G for the Posidonienschiefer. **I.** As panel G for the Tanjung Formation coal.

Formation coal sub-samples (Fig. 4.4F), which show identical and overlapping curves, with all Hg released at broadly the same intensity (max ≥0.1 fraction/seconds at second 30).

The proportion of Hg phases in the Tanjung Formation coal began at 95:5 Hg_{LT}:Hg_{HT} in the original untreated sample (Fig. 4.4I). Only a very subtle change in the proportion of Hg phases was observed during heating, as the proportion of Hg_{LT} and Hg_{HT} in the Tanjung

Formation coal sub-samples remained nearly stable at approximately 90:10 after heating for 24 to 840 hours.

4.3.3.3. Posidonienschiefer Hg behaviour

The original Posidonienschiefer sub-sample appears to yield a dominant, single-phase Hg release peak. However, Hg release is more prolonged compared to the main Hg release peak of the Belemnite Marls and the Tanjung Formation coal (Fig. 4.4A, B, C), indicating the presence of a Hg_{HT} phase. In contrast to the Belemnite Marls sub-samples that lost most of their Hg_{LT} after heating, the heated sub-samples of the Posidonienschiefer still show a main Hg peak release relatively early in the TDP (<30s). The heated sub-samples of the Posidonienschiefer (≥ 24 hours) display more complex TDPs, featuring bimodal peaks and 'shoulders', further supporting the presence of multiple Hg species (Fig. 4.4B, E).

Examining the distribution of Hg phases, the original Posidonienschiefer sub-sample exhibits a higher proportion of Hg_{HT} compared to the previously described samples, with a 77:23 ratio of Hg_{LT}:Hg_{HT} (Fig. 4.4H). Similar to the Tanjung Formation coal, the proportion of Hg phases in the Posidonienschiefer shows only subtle changes after heating, at approximately 70:30 Hg_{LT}:Hg_{HT}.

4.4. Discussion

In this study, we analysed three distinct sedimentary rocks, each representing different depositional environments and organic-matter (OM) types. The Belemnite Marls sample is an example of a calcareous marine mudrocks, dominated by relatively inert organic carbon, that contains pyrite due to low oxygen (dysoxic) conditions at the sediment-water interface upon deposition and potentially sulfidic conditions in pore waters after sulphate reduction (Schöllhorn et al., 2020). The Tanjung Formation coal is a lignin-rich coal deposited in a less

reducing fresh-water-dominated environment, where sulphate and particularly sulphides are scarce, and organic matter predominantly consists of plant-derived material. The Posidonienschiefer is a marine, highly organic-rich black shale, formed under euxinic conditions where sulphide was abundantly available in both the water column and sediment.

After isothermal heating of varying durations, distinct patterns of Hg loss emerged across the three lithologies, with the rate of Hg release being highest within the first 24 hours of heating at 325°C. The Belemnite Marls and Tanjung Formation coal released more than 70% of their Hg_T during this initial period, whereas the Posidonienschiefer exhibited slower Hg release, with only 40% of Hg_T volatilized (Fig. 4.2). These findings align with trends observed in similar experiments from previous studies (Liu et al., 2022; Chen et al., 2022), which also showed variations in Hg_T release efficiency. For example, clastic marine shales demonstrated less efficient Hg_T release curves compared to calcareous marine and lacustrine shales (Fig. 4.5).

4.4.1. Is the rate of Hg release from sediments related to different primary Hg speciation characteristics?

The mercury thermal desorption profiles (TDPs) of the samples allow us to see distinct differences in Hg phase stability across the three sediment types (Fig. 4.4A-F). These differences in Hg release rates can be directly linked to the Hg speciation in the sub-samples before heating and are illustrated as changes in the relative proportions of low-temperature (Hg_{LT}) and high-temperature (Hg_{HT}) phases (Fig. 4.4G, H, I). The rapid Hg_T release observed during the first 24 hours of heating in the Belemnite Marls and Tanjung Formation coal (Fig. 4.2C) corresponds closely to the dominance of the Hg_{LT} in these sub-samples. Specifically, the original sub-samples of the Belemnite Marls and Tanjung Formation coal with 87% and 95% Hg_{LT}, respectively, make the sedimentary Hg more susceptible to volatilization upon relatively modest heating. The TDPs further illustrate that the Belemnite Marls exhibit single-phase release patterns dominated by the loss of Hg_{LT} in the first 24 hours (Fig. 4.4A). For the Tanjung

Formation coal, the position of the Hg release peak suggests most Hg is present as Hg bound to OM or OM-associated sulphides (Frieling et al., 2024b). Moreover, the plots of the Tanjung Formation coal indicate that this Hg phase remains dominant throughout the heating experiment, despite a decreasing concentration (Fig. 4.4C).

By contrast, the slower Hg_T release observed in the Posidonienschiefer during the first 24 hours (Fig. 4.2C) is consistent with its higher proportion (>20%) of more thermally stable (Hg_{HT}) species prior to heating (Fig. 4.4H) compared to the Belemnite Marls (~13%, Fig. 4.4G) and Tanjung Formation coal (<10%, Fig. 4.4I). The Hg_{HT} complexes, which may include, for example, cinnabar (desorption temperature > 275°C *vs* Hg-OM > 225°C; Rumayor et al., 2015; Saniewska and Bełdowska, 2017) are more thermally stable than Hg associated with organic matter, making them less prone to volatilization during heating.

4.4.2. Sedimentary Hg speciation and primary depositional environment

The factors influencing Hg speciation in recent soft sediments have been extensively studied, including sulphur availability (e.g., Benoit et al., 1999; Fabbri et al., 2001), particle size variations linked to depositional environments (e.g., Boszke et al., 2004; Xu et al., 2021), and the proximity of depositional sites to pollution sources in modern settings (e.g., Wallschläger et al., 1998; Bindler et al., 2001). In this study, the samples primarily differ in their depositional settings, allowing us to investigate how the sedimentary environment may have influenced primary Hg speciation and how this characteristic ultimately may affect Hg behaviour during heating.

The Posidonienschiefer, characterized by a high proportion of Hg_{HT}, was deposited under euxinic conditions. In such environments, the uptake potential of Hg by sulphides is significantly enhanced due to the stronger chemical affinity of Hg^{2+} for sulphide (S^{2-}) compared to organic matter (Ravichandran, 2004; Bower et al., 2008). These conditions provide abundant

sulphide, thereby enabling Hg and other metals to bind and form sulphide minerals. This process may then result in a higher proportion of sulphide-bound or sulphide-hosted Hg in strata such as the Posidonienschiefer. If part of the Hg is present as cinnabar HgS, this may explain the larger proportion of Hg_{HT} compared to the other successions examined here. Similarly, the Belemnite Marls exhibit evidence of a substantial quantity of Hg_{HT}, in the original sample that becomes more significant after the isothermal heating process. While this may seem counterintuitive as the depositional environments were quite different in their oxidation regime, the presence of similar Hg phases could be attributed to the potential for sulphate reduction and sulphide production in pore waters in the Belemnite Marls sequence. Despite the dysoxic bottom-water conditions, the Belemnite Marls commonly contain some pyrite, likely deposited in sulfidic pore-waters. By contrast, the Tanjung Formation coal, deposited in a less reducing and notably low-salinity (fresh-water-dominated) environment, does not show a substantial proportion of Hg_{HT}. Thus, we may speculate that there may have been minimal sulphide available for Hg to bind with even in the more anoxic pore waters, leading to Hg being almost exclusively associated with OM. Despite the major differences in primary Hg speciation related to the environment of deposition and potential for the formation of sulphide minerals, both the Belemnite Marls and Tanjung Formation coal released Hg_T at similar efficiency in the first 24 hours of heating, which can be attributed to the dominance (~90%) of relatively low-temperature fractions of Hg, likely OM-associated Hg, in both these original untreated samples**.**

Although we cannot examine the TDPs for previously published maturation experiments, we postulate that the differences in Hg behaviour between the sample types in the previous studies of thermal maturation by Liu et al. (2022) and Chen et al. (2022) also reflect variations in the availability of sulphur and the type of OM present during deposition. The efficiency of Hg volatilization in sedimentary rocks deposited in marine euxinic environments, such as the

Proterozoic Xiamaling Formation (Liu et al., 2022) and the Cryogenian Datangpo Formation (Chen et al., 2022), aligns with our observations in the Posidonienschiefer (Fig. 4.5). Similarly, the Permian Talung Formation, which is a calcareous shale (Liu et al., 2022) exhibits the efficiency of Hg loss comparable to that recoded in the Belemnite Marls (Fig. 4.5). These findings suggest that depositional environments and early diagenesis play a crucial role in determining the proportion of organic-bound and higher temperature (potentially sulphide-mineral associated) Hg. We therefore consider it likely that the differences of Hg loss between these sample types in the Chen et al. (2022) and Liu et al. (2022) (Fig. 4.5) are, at least in part, explained by differences in initial Hg speciation, which in turn is related to the depositional environment from which the samples derive.

4.4.3. Thermally induced organic matter transformation and Hg release

The nature of organic matter (OM) available as a potential host phase for Hg has an influence on the type of products generated and released during thermal maturation and may also affect the mobilization and transport of Hg. The terrestrially sourced Tanjung Formation coal is mainly a gas-prone source rock, although it also generates bitumen due to its exceptional content of oil-prone liptinitic components (Davis et al., 2007; Kusuma and Darin, 1989). By contrast, marine OM, rich in oil-prone algal and bacterial biomass, such as the Posidonienschiefer, will generate a significantly higher proportion of liquid products relative to gas. This observation is especially relevant in the maturity range of our isothermal pyrolysis experiments that rather simulate the early to peak oil-generative phases (0.6–0.9% Ro) without extending into the gas window. Hence, the mobilization of Hg during thermal maturation of these different types of labile organic matter (Tanjung Formation coal and Posidonienschiefer), may be impacted by the relative amount of gas or liquid phases generated, with more efficient transport in the gas. By contrast, the Belemnite Marls sub-sample used in our study has little, if any, labile organic matter and is unlikely to generate cracking products that would be

involved in or facilitate the transport of Hg. The trends of Hg_T loss we observe in the various experimental heating intervals (after 24, 168, 336, 500, and 840 hours) in the Posidonienschiefer and Tanjung Formation coal (Fig. 4.2C) could consequently be related to the variable production of bitumen and hydrocarbon gas from the two different types of OM. Crucially, the processes that drive hydrocarbon formation and mobilize fluids in the subsurface may be critical for Hg mobilization after release from its original host phase.

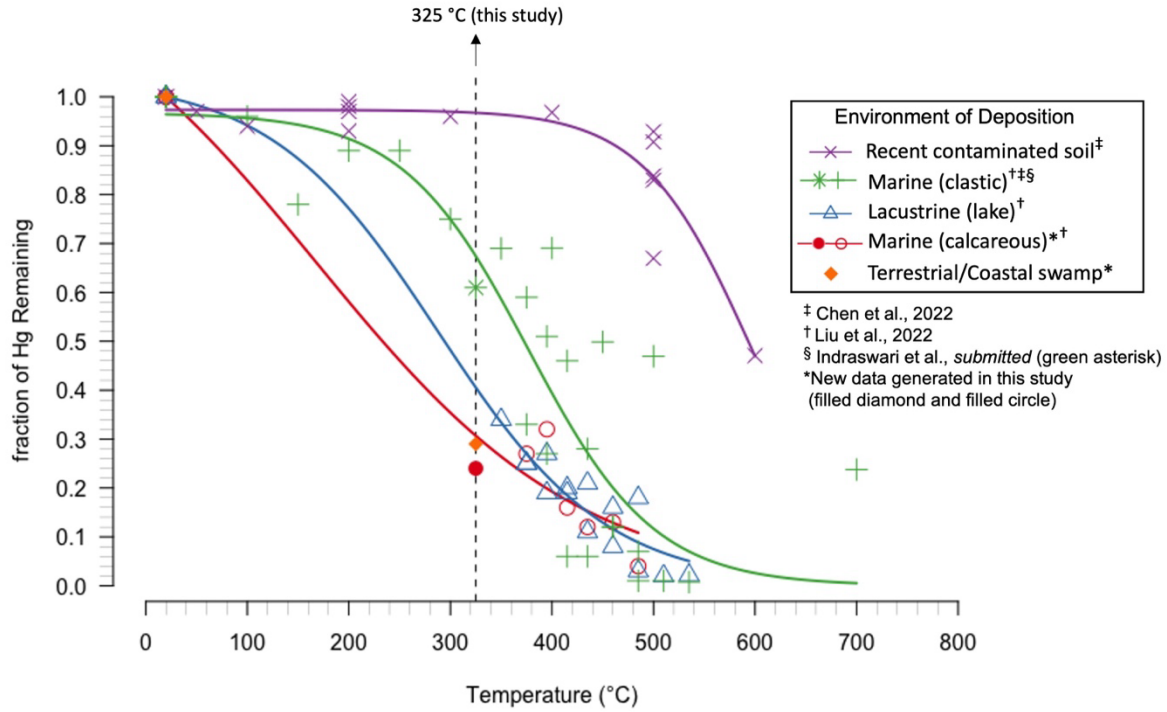


Figure 4.5. Mercury fraction remaining relative to the original concentration in different materials in response to artificial heating of less than 25 hours (previous studies used heating durations of ≤ 25 hours). Fitted lines are sigmoidal curves to represent cumulative Hg loss. Fraction of Hg remaining = $(1 / (1+ b \times e^{cx}))$, where x is peak exposure temperature, b and c are fitted constants. Orange filled diamond and red filled circle in 325°C are new data generated in this study.

4.4.4. Relevance to contact aureoles and burial-related maturation

In the contact aureoles associated with LIP dykes, various types of sedimentary rocks are intruded, ranging from organic-rich (e.g., Ecca group in Karoo basin: Aarnes et al., 2011; Svensen et al., 2007, 2015) to organic-lean sedimentary rocks (e.g., evaporites in Siberian Traps and the CAMP: Svensen et al., 2009; Heimdal et al., 2018). The amount of Hg volatilized and released from these contact aureoles is influenced by the type of sedimentary rocks intruded. For example, this study suggests that sedimentary rocks deposited under relatively less sulphidic and moderately reducing conditions may release Hg more efficiently upon heating than those formed in marine anoxic to euxinic settings, where strong sulphidic conditions can enhance Hg sequestration through HgS formation. This finding implies that we must be cautious in using Hg release to back-calculate carbon emissions, for example, as it requires careful consideration of the Hg speciation composition influenced by sedimentary depositional settings.

A similar notion applies to thermal maturation in natural systems related to burial or subsidence. For example, our findings support the proposal that the immobility of Hg in the naturally matured Posidonienschiefer samples (Cores B and C) observed by Indraswari et al. (2024) can now be explained by the inefficiency of Hg volatilization, likely in part due to the high proportion of Hg_{HT} in the immature core (Core A) that further increases with maturation in Cores B and C (Indraswari et al., *submitted*).

A useful comparison can be made between the experimental maturation of the Belemnite Marls in this chapter and the natural maturation trend observed in the organic-lean Lias Delta from cores A (%Ro ~0.5–0.7%) and B (%Ro ~1.5) in the Lower Saxony Basin, as discussed in Chapter 2 (with Lias Delta having an average TOC of 0.85% in immature core A). Unlike the significant increase in Hg concentrations and Hg/TOC observed in the Posidonienschiefer (Chapter 2), the Lias Delta exhibits minimal variation in both Hg concentrations and Hg/TOC

following natural burial-related maturation. Specifically, core A shows an average Hg concentration of 44.6 ppb and Hg/TOC of 47.8 ppb/%, while core B has 49.4 ppb Hg and Hg/TOC of 41.9 ppb/%. This minor increase in Hg signals between cores A and B might suggest that, unlike the experimental results from the Belemnite Marls, Hg was not effectively released during natural maturation in the Lias Delta. This differing behaviour of Hg in organic-lean sediments could be attributed to differences in Hg speciation, potentially influenced by variations in the primary depositional setting.

Our findings also highlight the critical importance of understanding sedimentary Hg speciation distribution (e.g., high-temperature versus low-temperature species) in immature rocks to aid the interpretation of the effects of thermal maturation in natural systems, either burial- or intrusion-related.

4.5. Conclusions and outlook

In order to better understand the behaviour for mercury during thermal maturation of sedimentary rocks, we conducted pyrolysis experiments involving isothermal heating at 325°C for varying durations (24–840 hours) on two sedimentary rocks, each representing different depositional environments and organic-matter (OM) types: the calcareous marine mudrocks of the poorly oxygenated shallow-marine Belemnite Marls and the Tanjung Formation coal from a coastal swamp. These materials were analysed and compared with the marine anoxic to euxinic Posidonienschiefer, which underwent the same experimental treatment in a previous broader study (Indraswari et al., *submitted*). We observe significant variability in Hg release efficiency, which we link to the initial Hg speciation (proportion of high-temperature stable Hg (Hg_{HT}) *vs* low-temperature stable Hg (Hg_{LT}) species) of the samples using thermal desorption profiles (TDPs). The TDPs reveal distinct differences in the Hg speciation between the Belemnite Marls sample (~13% Hg_{HT}), Tanjung Formation coal (<10% Hg_{HT}), and the

Posidonienschiefer (>20% Hg_{HT}). The initial Hg speciation appears to have been influenced by the depositional settings, possibly the availability of sulphide during and after deposition (in the water column or pore waters). These data directly connect the thermal stability of Hg phases to their volatilization potential after long-term exposure to heat. These results also suggest that the thermal desorption profiles (TDPs) can potentially be used to project the efficiency of Hg release under slow heating rates and isothermal conditions such as occur in deep basins and around igneous intrusions. Crucially, the differences in initial Hg speciation and resulting Hg release efficiency largely explain differences in Hg behaviour during isothermal heating in our sample set and may explain the significant differences in Hg loss observed within the sedimentary rock types in previous experiments (Liu et al., 2022; Chen et al., 2022) as well.

5. Conclusions and Future Work

5.1. Summary of results

As outlined in the introduction, the aim of this thesis is to explore the impact of sediment heating, thermal maturation, and hydrocarbon production on mercury (Hg) behaviour in sedimentary records. This has been achieved by combining an examination of natural cores with experimental work, employing Hg analysis (e.g., thermal desorption profiles), geochemical characterization (e.g., TOC and TS), and the measurement of Hg concentrations in oils and bitumen produced during experimental heating. These results are summarised below in reference to the four key questions laid out at the beginning of this thesis (Chapter 1, section 1.4.), along with the conclusions that can be drawn from this work towards answering these questions.

1. **How does natural subsidence-related thermally maturation affect sedimentary Hg?**

   Chapter 2 showed a > 2-fold increase in Hg concentrations is observed in mature and overmature cores from the Lower Toarcian Posidonienschiefer in the Lower Saxony Basin, Germany. In this chapter, we also found that the R^2 for Hg-TOC in cores B and C is lower than that in core A indicating there are likely changes in Hg speciation in the immature to the more mature cores. This change is demonstrated clearly in the TDPs presented in Chapter 3 from Hg-OM associated peaks in the immature core A to a more stable Hg-non-OM phase in mature and overmature cores.

2. **Does artificial thermal maturation affect sedimentary Hg in the same way as natural thermal maturation?**

The experimental work in Chapter 3 showed a ~65% drop in Hg concentration is observed in the Posidonienschiefer due to the release of volatilized gaseous Hg. The differences in Hg behaviour observed during pyrolysis experiments compared to cores B and C can be attributed to: (1) the distinction between open and closed systems in natural sedimentary basins versus experimental setups; (2) the higher temperatures used in the experiments compared to those typically experienced in most sedimentary basins; (3) the limited timescales of the experiments, which do not replicate the millions of years required for hydrocarbon generation during natural burial maturation. In addition to the initial Hg loss, we were also able to demonstrate reabsorption of Hg into the sediments using a simple experiment where we let closed tubes cool down before allowing the gas to escape. Although the reabsorption of Hg is observed the Hg appeared to re-associate with low-temperature Hg phases, which fundamentally differs from what we found in the naturally matured cores. From these pyrolysis experiments, we suggest that the artificial maturation experiments more closely mimic conditions in contact aureoles rather than subsidence-related thermal maturation, especially in terms of rapid volatilization and reabsorption of gaseous Hg. In the later Chapter 4, we did similar pyrolysis experiments to different types of samples. We found that there is a difference in volatilisation efficiency between different types of sedimentary rocks, with ~80% drops in Hg concentration observed in the Tanjung Formation Coal and Belemnite Marls under the same heating conditions. We explored whether this difference in Hg volatilisation efficiency comes from differences in initial Hg speciation, one of the factors that comes from the primary depositional settings.

3. **Is sedimentary Hg significantly affected by hydrocarbon production during thermal maturation?**

The findings from both natural and experimental conditions are consistent: in Chapter 2 we found that Hg concentrations in naturally produced oil from the Posidonienschiefer sediments have very low Hg concentrations (2–5 ppb) compared to the immature rock (50–150 ppb). In Chapters 3 and 4, we also found from the experiments that Hg does not partition into bitumen during early maturation. In the Posidonienschiefer and Tanjung Formation Coal, the Hg mass in the produced bitumen is less than 1% of the original Hg in the immature source rocks.

In conclusion, the low concentration of Hg in oils and produced bitumen showed Hg did not effectively partition into liquid hydrocarbons during maturation and may be considered nearly immobile under these circumstances. This notion could then explain the increasing Hg concentrations in the mature and overmature cores in the Lower Saxony Basin.

4. **What factors control the efficiency of Hg volatilisation and reabsorption during thermal maturation?**

The discussion in Chapter 2 highlighted how the low-permeability shale units in the subsidence-related basin create a ‘closed’ system, which likely prevents the effective mobilisation of Hg within the sedimentary basin. Overpressure, responsible for forming calcite- and pyrite-filled fractures and veins in specific Core B and C intervals, suggests that Hg may be redistributed into certain stratigraphic levels, possibly during or after hydrocarbon mobilisation. The reabsorption experiment in Chapter 3 demonstrated how Hg, once released from its original host, could be

efficiently (≥95%) redeposited into the sediment within ≤ 1 hour of cooling, shedding light on the mechanism of retained Hg in the Posidonienschiefer and notably the reabsorption seen around contact aureoles. Furthermore, with the help of thermal desorption profiles (TDPs), by comparing different sedimentary rocks in Chapter 4, it is shown that Hg mobility during subsurface heating is controlled by the stability of Hg host phases in sedimentary rocks, which is closely tied to their primary depositional environments. For instance, the Posidonienschiefer, deposited in sulphide-rich environments, contains a greater proportion of higher-temperature Hg phases (Hg_{HT}) than the Belemnite Marls and Tanjung Formation coal. These Hg_{HT} phases are not effectively volatilised, particularly in sedimentary basins with temperatures between 70–260°C.

5.2. Conclusions

In the natural burial sedimentary basin of Lower Saxony Basin, Germany, the mature cores of Lower Toarcian Posidonienschiefer revealed that thermal maturation increases Hg concentrations 132–157% higher than its immature cores. The artificial maturation in the lab showed the opposite, with a substantial loss of Hg, mainly through volatilisation. The Hg has been found to not significantly (<1% of Hg_T) partition into produced hydrocarbons with Posidonienschiefer-derived oils and bitumen produced during pyrolysis containing low Hg concentrations, showing that hydrocarbon production played a minor part in Hg mobilisation in early thermal maturation.

Additionally, experiments on Hg reabsorption demonstrated that gaseous Hg could be efficiently reabsorbed into sediments during cooling. However, in naturally matured core shales, Hg speciation appeared to transform into more thermally stable forms, limiting Hg mobility. This contrast suggests that, during burial maturation, Hg may not reabsorb into similar

phases but instead transition to more stable forms over time, which could further restrict its transport in low-permeability environments.

Finally, pyrolysis experiments on various sedimentary rocks, including the Posidonienschiefer, Belemnite Marls, and Tanjung Formation coal, revealed significant variability in Hg release efficiency, influenced by initial Hg speciation. Thermal desorption profiles (TDPs) indicated that depositional environments likely played a role in Hg speciation, with varying proportions of high-temperature stable Hg species across the samples. These findings suggest that the initial speciation of Hg in sediments can significantly influence its volatilisation potential during heating, offering a means to project Hg release efficiency in deep basins and areas affected by igneous intrusions. These results contribute to a better understanding of Hg behaviour during thermal maturation and highlight the need for caution when interpreting Hg concentrations in thermally altered sediments.

From the conclusions above, although the effect is not always straightforward and may vary between different types of sedimentary rocks and thermal maturation types (burial- or intrusion-related), this study managed to highlight several factors to consider when looking at the effect of thermal maturation on sedimentary Hg:

1. The importance of open and closed systems, the conduit with which the volatilised Hg could escape after being heated, and the possibility of Hg reabsorption in a closed system.
2. The temperatures that drive thermal maturation, especially the difference between subsidence- and intrusion-related heating, control Hg behaviour.
3. The initial chemical speciation of Hg in sedimentary rocks varies across different depositional environments and, through variable thermal stability of Hg species, influences volatilisation efficiency.

4. The different types of hydrocarbons produced during heating, with gas being more conducive to mobilising Hg than liquid (oil).

However, despite finding and resolving further complexity in Hg behaviour, this study underscores the notion that heating is a primary control on the Hg signal in the sedimentary deep-time record. Therefore, when using Hg anomalies as a proxy, the thermal maturation of the sediments should not be overlooked.

5.3. Future work

The observed differences between natural and artificial thermal maturation underscore the challenge of applying experimental results to real-world conditions, where the speciation and behaviour of Hg are influenced by complex interactions between temperature, pressure, time, primary depositional settings, and other geological factors. Future investigations involving even longer-duration thermal experiments at lower, more geologically realistic temperatures, notably not exceeding the thermal stability of at least some of the more common sedimentary Hg species (≤300 ºC), are necessary to replicate prolonged burial conditions. Such studies will be vital for understanding whether Hg undergoes gradual, diffusive loss over time, which could explain its mobility or immobility in natural settings, both in sedimentary basins or contact aureoles.

Additional exploration of the methodology or measurement analysis to enhance our understanding of mercury (Hg) speciation in sedimentary rocks would be useful. This methodology idea includes pairing thermal maturation experiments with gas detectors, such as CO_2 analysers, to monitor gas release and its correlation with Hg behaviour during heating. Detailed petrographic analysis could also be employed to examine Hg speciation at a finer scale, focusing on its association with specific mineral phases, such as pyrites. Combining gas

detection technology with high-resolution petrographic techniques will provide a more comprehensive understanding of Hg speciation, improving our ability to identify and quantify the processes controlling Hg behaviour and mobility during thermal maturation.

On how primary depositional settings influence the distribution of Hg_{HT} *vs* Hg_{LT}, it is essential to expand research to include more variation of depositional settings rather than focusing on just the three currently studied. Since clay minerals have been proposed to host Hg in sedimentary rocks low in organic carbon and sulphide contents (Kongchum et al., 2011; Percival et al., 2018; Shen et al., 2019b; Kalvoda et al., 2019), it would be particularly interesting to explore how clay mineral composition influences mercury concentration and speciation and subsequently volatilisation efficiency during thermal maturation. This broader approach could provide deeper insights into the complex interactions between sedimentary components and their effects on mercury cycling across diverse geological environments.

Bibliography

Aarnes, I., Fristad, K., Planke, S., & Svensen, H. (2011). The impact of host-rock composition on devolatilization of sedimentary rocks during contact metamorphism around mafic sheet intrusions. *Geochemistry, Geophysics, Geosystems*, *12*(10). https://doi.org/10.1029/2011GC003636

Abarghani, A., Gentzis, T., Liu, B., Khatibi, S., Bubach, B., & Ostadhassan, M. (2020). Preliminary investigation of the effects of thermal maturity on redox-sensitive trace metal concentration in the Bakken source rock, North Dakota. *American Chemical Society Omega*, *5*(13), 7135–7148. https://doi.org/10.1021/acsomega.9b03467

Anggara, F., Patria, A. A., Rahmat, B., Wibisono, H., Putera, M. Z. J., Petrus, H. T. B. M., Erviana, F., Handini, E., & Amijaya, D. H. (2024). Signature characteristics of coal geochemistry from the Eocene Tanjung Formation and the Miocene Warukin Formation, Barito Basin: Insights into geological control on coal deposition and future critical element prospection. *International Journal of Coal Geology*, *282*, 104423. https://doi.org/10.1016/j.coal.2023.104423

Ardakani, O. H., Hlohowskyj, S. R., Chappaz, A., Sanei, H., Liseroudi, M. H., & Wood, J. M. (2020). Molybdenum speciation tracking hydrocarbon migration in fine-grained sedimentary rocks. *Geochimica et Cosmochimica Acta*, *283*, 136–148. https://doi.org/10.1016/J.GCA.2020.06.006

Baldschun, R., Kockel, F., Best, G., Deneke, E., Frisch, U., Juergens, U., et al. (1996). Geotektonischer Atlas vonNW-Deutschland/Tectonic Atlas of NW Germany (scale 1:300,000). Bundesanstalt für Geowissenschaften und Rohstoffe, Hannover.

Baucon, A., Bednarz, M., Dufour, S., Felletti, F., Malgesini, G., Neto de Carvalho, C., Niklas, K. J., Wehrmann, A., Batstone, R., Bernardini, F., Briguglio, A., Cabella, R., Cavalazzi,

B., Ferretti, A., Zanzerl, H., & McIlroy, D. (2020). Ethology of the trace fossil Chondrites: Form, function and environment. *Earth-Science Reviews*, *202*, 102989. https://doi.org/10.1016/j.earscirev.2019.102989

Behar, F., Beaumont, V., & De B. Penteado, H. L. (2001). Rock-Eval 6 technology: performances and developments. *Oil & Gas Science and Technology*, *56*(2), 111–134. https://doi.org/10.2516/ogst:2001013

Benoit, J. M., Gilmour, C. C., Mason, R. P., & Heyes, A. (1999). Sulfide Controls on Mercury Speciation and Bioavailability to Methylating Bacteria in Sediment Pore Waters. *Environmental Science & Technology*, *33*(6), 951–957. https://doi.org/10.1021/es9808200

Benoit, J. M., Mason, R. P., Gilmour, C. C., & Aiken, G. R. (2001). Constants for mercury binding by organic matter isolates from the Florida Everglades. *Geochimica et Cosmochimica Acta*, *65*(24), 4445–4451. https://doi.org/10.1016/S0016-7037(01)00742-6

Berkowitz, N. (1997). Chapter 5 - Composition and chemical properties. In N. Berkowitz (Ed.), *Fossil Hydrocarbons: Chemistry and Technology* (pp. 83–120). Academic Press. https://doi.org/10.1016/B978-012091090-8/50005-8

Betz, D., Führer, F., Greiner, G., & Plein, E. (1987). Evolution of the Lower Saxony Basin. *Tectonophysics*, *137*(1–4), 127–170. https://doi.org/10.1016/0040-1951(87)90319-2

Bian, L., Chappaz, A., Schovsbo, N. H., Nielsen, A. T., & Sanei, H. (2022). High mercury enrichments in sediments from the Baltic continent across the late Cambrian: Controls and implications. *Chemical Geology, 599*, 120846. https://doi.org/10.1016/J.CHEMGEO.2022.120846

Bian, L., Chappaz, A., Wang, X., Amouroux, D., Schovsbo, N. H., Zheng, X., & Sanei, H. (2024). Improving mercury systematics with molybdenum and vanadium enrichments:

New insights from the Cambrian-Ordovician boundary. *Geophysical Research Letters, 51*, e2023GL107188. https://doi.org/10.1029/2023GL107188

Bin, C., Xiaoru, W., & Lee, F. S. C. (2001). Pyrolysis coupled with atomic absorption spectrometry for the determination of mercury in Chinese medicinal materials. *Analytica Chimica Acta*, *447*(1–2), 161–169. https://doi.org/10.1016/S0003-2670(01)01218-1

Bindler, R., Renberg, I., Appleby, P. G., Anderson, N. J., & Rose, N. L. (2001). Mercury Accumulation Rates and Spatial Patterns in Lake Sediments from West Greenland: A Coast to Ice Margin Transect. *Environmental Science & Technology*, *35*(9), 1736–1741. https://doi.org/10.1021/es0002868

Bjørlykke, K. (1989). *Sedimentology and petroleum geology* (B. Wahl, Trans.). Springer-Verlag.

Blumenberg, M., Zink, K. G., Scheeder, G., Ostertag-Henning, C., & Erbacher, J. (2019). Biomarker paleo-reconstruction of the German Wealden (Berriasian, Early Cretaceous) in the Lower Saxony Basin (LSB). *International Journal of Earth Sciences, 108,* 229–244. https://doi.org/10.1007/s00531-018-1651-5

Bohacs, K. M., Norton, I. O., Neal, J. E., & Gilbert, D. (2020). The accumulation of organic-matter-rich rocks within an earth system's framework: The integrated roles of plate tectonics, atmosphere, ocean, and biota through the Phanerozoic. In N. Scarselli, et al. (Eds.), *Regional Geology and Tectonics: Volume 1: Principles of Geologic Analysis* (pp. 721–744). Elsevier. https://doi.org/10.1016/B978-0-444-64134-2.00023-7

Boszke, L., Sobczynski, T., Glosinska, G., Kowalski, A., & Siepak, J. (2004). Distribution of mercury and other heavy metals in bottom sediments of the middle Odra River (Germany/Poland). *Polish Journal of Environmental Studies, 13*(5), 495–502.

Bower, J., Savage, K. S., Weinman, B., Barnett, M. O., Hamilton, W. P., & Harper, W. F. (2008). Immobilization of mercury by pyrite (FeS2). *Environmental Pollution*, *156*(2), 504–514. https://doi.org/10.1016/j.envpol.2008.01.011

Brink, H. J., Dürschner, H., & Trappe, H. (1992). Some aspects of the late and post-Variscan development of the Northwestern German Basin. *Tectonophysics*, *207*(1–2), 65–95. https://doi.org/10.1016/0040-1951(92)90472-I

Bromley, R. G., & Ekdale, A. A. (1984). Chondrites: a trace fossil indicator of anoxia in sediments. *Science, 224*(4651), 872–874. https://doi.org/10.1126/science.224.4651.872

Bruns, B., di Primio, R., Berner, U., & Littke, R. (2013). Petroleum system evolution in the inverted Lower Saxony Basin, northwest Germany: A 3D basin modeling study. *Geofluids*, *13*(2), 246–271. https://doi.org/10.1111/gfl.12016

Bryndzia, L. T. (2023). Elucidating the Role of Hydrocarbons in Cinnabar (HgS) Ore Formation: A Model for Hg Mineralization in the Terlingua Mining District, Big Bend National Park, SW Texas. *Economic Geology*, *118*(8), 1881–1897. https://doi.org/10.5382/econgeo.5022

Bryndzia, L. T., Burgess, J. M., & Bourdet, J. (2023). Predicting the Solubility of Mercury in Hydrocarbons. *SPE Journal, 28*(02), 859–875, SPE-212271-PA. https://doi.org/10.2118/212271-PA

Buatois, L. A., & Mángano, M. G. (2016). Ediacaran Ecosystems and the Dawn of Animals. In M. G. Mángano & L. A. Buatois (Eds.), *The Trace-Fossil Record of Major Evolutionary Events: Volume 1: Precambrian and Paleozoic* (pp. 27–72). Springer Netherlands. https://doi.org/10.1007/978-94-017-9600-2_2

Burnham, A. K. (2017). Pyrolysis in Closed Systems. In *Global Chemical Kinetics of Fossil Fuels* (pp. 205– 272). Springer International Publishing. https://doi.org/10.1007/978-3-319-49634-4_6

Celestino, R. (2019). Environmental change and carbon cycling during the Early Jurassic: A multi-proxy study on the Posidonienschiefer of NW Germany, (Doctoral dissertation). University of Exeter. Retrieved from http://hdl.handle.net/10871/36576

Celestino, R. F. S., Ruhl, M., Dickson, A. J., Idiz, E., Jenkyns, H. C., Leng, M. J., Mattioli, E., Minisini, D., & Hesselbo, S. P. (2024). Protracted carbon burial following the Early Jurassic Toarcian Oceanic Anoxic Event (Posidonia Shale, Lower Saxony Basin, Germany). *International Journal of Earth Sciences*, *113*(8), 2023–2041. https://doi.org/10.1007/s00531-024-02477-9

Chappaz, A., Lyons, T. W., Gregory, D. D., Reinhard, C. T., Gill, B. C., Li, C., & Large, R. R. (2014). Does pyrite act as an important host for molybdenum in modern and ancient euxinic sediments? *Geochimica et Cosmochimica Acta*, *126*, 112–122. https://doi.org/10.1016/j.gca.2013.10.028

Charbonnier, G., & Föllmi, K. B. (2017). Mercury enrichments in lower Aptian sediments support the link between Ontong Java large igneous province activity and oceanic anoxic episode 1a. *Geology*, *45*(1), 63–66. https://doi.org/10.1130/G38207.1

Chen, D., Ren, D., Deng, C., Tian, Z., & Yin, R. (2022). Mercury loss and isotope fractionation during high-pressure and high-temperature processing of sediments: Implication for the behaviors of mercury during metamorphism. *Geochimica et Cosmochimica Acta, 334*, 231–240. https://doi.org/10.1016/J.GCA.2022.08.010

Dahl, T. W., Chappaz, A., Hoek, J., McKenzie, C. J., Svane, S., & Canfield, D. E. (2017). Evidence of molybdenum association with particulate organic matter under sulfidic conditions. *Geobiology*, *15*(2), 311–323. https://doi.org/10.1111/gbi.12220

Dal Corso, J., Mills, B. J. W., Chu, D., Newton, R. J., Mather, T. A., Shu, W., et al. (2020). Permo–Triassic boundary carbon and mercury cycling linked to terrestrial ecosystem collapse. *Nature Communications, 11*(1), 2962. https://doi.org/10.1038/s41467-020-

16725-4

Davis, R. C., Noon, S. W., & Harrington, J. (2007). The petroleum potential of Tertiary coals from Western Indonesia: Relationship to mire type and sequence stratigraphic setting. *International Journal of Coal Geology*, *70*(1), 35–52. https://doi.org/10.1016/j.coal.2006.02.008

Dembicki, H. (2022). Chapter 2 - The formation of petroleum accumulations. In *Practical Petroleum Geochemistry for Exploration and Production (Second Edition)* (pp. 21–67). Elsevier. https://doi.org/10.1016/C2021-0-01572-8

Dickson, A. J., Idiz, E., Porcelli, D., & van den Boorn, S. H. J. M. (2020). The influence of thermal maturity on the stable isotope compositions and concentrations of molybdenum, zinc and cadmium in organic-rich marine mudrocks. *Geochimica et Cosmochimica Acta*, *287*, 205–220. https://doi.org/10.1016/j.gca.2019.11.001

Dickson, A. J., Idiz, E., Porcelli, D., Murphy, M. J., Celestino, R., Jenkyns, H. C., et al. (2022). No effect of thermal maturity on the Mo, U, Cd, and Zn isotope compositions of Lower Jurassic organic-rich sediments. *Geology*, *50*(5), 598–602. https://doi.org/10.1130/g49724.1

Espitalié, J., Laporte, J.L., Madec, M., Marquis, F., Leplat, P., Paulet, J., & Boutefeu, A. (1977). Méthode rapide de caractérisation des roches mètres, de leur potentiel pétrolier et de leur degré d'évolution. *Oil & Gas Science and Technology - Rev. IFP, 32*(1), 23–42. https://doi.org/10.2516/ogst:1977002

Evenick, J. C. (2021). Examining the relationship between Tmax and vitrinite reflectance: An empirical comparison between thermal maturity indicators. *Journal of Natural Gas Science and Engineering, 91*, 103946. https://doi.org/10.1016/J.JNGSE.2021.103946

Fabbri, D., Locatelli, C., Snape, C. E., & Tarabusi, S. (2001). Sulfur speciation in mercury-contaminated sediments of a coastal lagoon: the role of elemental sulfur. *Journal of Environmental Monitoring*, *3*(5), 483–486. https://doi.org/10.1039/B104477J

Fantasia, A., Föllmi, K. B., Adatte, T., Bernárdez, E., Spangenberg, J. E., & Mattioli, E. (2018). The Toarcian oceanic anoxic event in southwestern Gondwana: An example from the Andean Basin, northern Chile. *Journal of the Geological Society*, *175*(6), 883–902. https://doi.org/10.1144/jgs2018-008

Fendley, I. M., Frieling, J., Mather, T. A., Ruhl, M., Hesselbo, S. P., & Jenkyns, H. C. (2024). Early Jurassic large igneous province carbon emissions constrained by sedimentary mercury. *Nature Geoscience*, *17*(3), 241–248. https://doi.org/10.1038/s41561-024-01378-5

Fikri, H. N., Sachsenhofer, R. F., Bechtel, A., & Gross, D. (2022). Coal deposition in the Barito Basin (Southeast Borneo): The Eocene Tanjung Formation compared to the Miocene Warukin Formation. *International Journal of Coal Geology*, *263*, 104117. https://doi.org/10.1016/j.coal.2022.104117

Filby, R. H. (1994). Origin and nature of trace element species in crude oils, bitumens and kerogens: implications for correlation and other geochemical studies. In J. Parnell (Ed.), *Geofluids: Origin, Migration and Evolution of Fluids in Sedimentary Basins*, *Geological Society, London, Special Publications, 78*, 203–219. Geological Society, London. https://doi.org/10.1144/GSL.SP.1994.078.01.15

Fitzgerald, W. F., & Lamborg, C. H. (2013). Geochemistry of Mercury in the Environment. In H. D. Holland & K. K. Turekian (Eds.), *Treatise on Geochemistry: Second Edition* (Vol. 11, pp.91–129). Elsevier Inc. https://doi.org/10.1016/B978-0-08-095975-7.00904-9

French, K.L., Sepúlveda, J., Trabucho-Alexandre, J., Gröcke, D.R., & Summons, R.E. (2014). Organic geochemistry of the early Toarcian oceanic anoxic event in Hawsker

Bottoms, Yorkshire, England. *Earth and Planetary Science Letters*, *390*, 116–127. https://doi.org/10.1016/j.epsl.2013.12.033

Frieling, J., Mather, T. A., März, C., Jenkyns, H. C., Hennekam, R., Reichart, G.-J., Slomp, C. P., & van Helmond, N. A. G. M. (2023). Effects of redox variability and early diagenesis on marine sedimentary Hg records. *Geochimica et Cosmochimica Acta, 351*, 78–95. https://doi.org/10.1016/J.GCA.2023.04.015

Frieling, J., Svensen, H. H., & Mather, T. A. (2024a). Mercury efficiently volatilized but not completely removed from sediments around igneous intrusions. *Geology*. https://doi.org/10.1130/G52622.1

Frieling, J., Fendley, I. M., Nawaz, M. A., & Mather, T. A. (2024b). Assessment of Hg Speciation Changes in the Sedimentary Rock Record From Thermal Desorption Characteristics. *Geochemistry, Geophysics, Geosystems*, *25*(4). https://doi.org/10.1029/2024GC011502

Frimmel, A., Oschmann, W., & Schwark, L. (2004). Chemostratigraphy of the Posidonia Black Shale, SW Germany I. Influence of sea-level variation on organic facies evolution. *Chemical Geology*, *206*(3–4), 199–230. https://doi.org/10.1016/j.chemgeo.2003.12.007

Ganino, C., & Arndt, N.T. (2009). Climate changes caused by degassing of sediments during the emplacement of large igneous provinces. *Geology*, *37* (4), 323–326. https://doi.org/10.1130/G25325A.1

Gehrke, G. E., Blum, J. D., & Meyers, P. A. (2009). The geochemical behavior and isotopic composition of Hg in a mid-Pleistocene western Mediterranean sapropel. *Geochimica et Cosmochimica Acta*, *73*(6), 1651–1665. https://doi.org/https://doi.org/10.1016/j.gca.2008.12.012

Gluyas, J. G., & Swarbrick, R. E. (2021). *Petroleum geoscience*. John Wiley & Sons.

Goodarzi, F., Gentzis, T., Grasby, S. E., & Dewing, K. (2018). Influence of igneous intrusions on thermal maturity and optical texture: Comparison between a bituminous marl and a coal seam of the same maturity. *International Journal of Coal Geology*, *198*, 183–197. https://doi.org/10.1016/j.coal.2018.09.013

Gorbanenko, O. O, & Ligouis, B. (2014). Changes in optical properties of liptinite macerals from early mature to post mature stage in Posidonia Shale (Lower Toarcian, NW Germany). *International Journal of Coal Geology*, *133*, 47–59. https://doi.org/10.1016/j.coal.2014.09.007

Gorbanenko, O. O, & Ligouis, B. (2015). Variations of organo-mineral microfacies of Posidonia Shale from the Lower Saxony Basin and the West Netherlands Basin: Application to paleoenvironmental reconstruction. *International Journal of Coal Geology*, *152*, 78–99. https://doi.org/10.1016/j.coal.2015.09.011

Grasby, S. E., Shen, W., Yin, R., Gleason, J. D., Blum, J. D., Lepak, R. F., et al. (2017). Isotopic signatures of mercury contamination in latest Permian oceans. *Geology*, *45*(1), 55–58. https://doi.org/10.1130/G38487.1

Grasby, S. E., Them, T. R., Chen, Z., Yin, R., & Ardakani, O. H. (2019). Mercury as a proxy for volcanic emissions in the geologic record. *Earth-Science Reviews*, *196*(March), 102880. https://doi.org/10.1016/j.earscirev.2019.102880

Groysman, A. (2017). Corrosion problems and solutions in oil, gas, refining and petrochemical industry. *KOM – Corrosion and Material Protection Journal*, *61*(3), 100–117. https://doi.org/doi:10.1515/kom-2017-0013

Heimdal, T. H., Svensen, Henrik. H., Ramezani, J., Iyer, K., Pereira, E., Rodrigues, R., Jones, M. T., & Callegaro, S. (2018). Large-scale sill emplacement in Brazil as a trigger for the end-Triassic crisis. *Scientific Reports*, *8*(1), 141. https://doi.org/10.1038/s41598-017-18629-8

Hesselbo, S., & Jenkyns, H. (1995). A comparison of the Toarcian to Bajocian successions of Dorset and Yorkshire. In P. D. Taylor (Ed.), *Field geology of the British Jurassic* (pp. 105–150). Geological Society, London.

Hooker, J. N., Ruhl, M., Dickson, A. J., Hansen, L. N., Idiz, E., Hesselbo, S. P., & Cartwright, J. (2020). Shale anisotropy and natural hydraulic fracture propagation: An example from the Jurassic (Toarcian) Posidonienschiefer, Germany. *Journal of Geophysical Research: Solid Earth*, *125*(3), e2019JB018442. https://doi.org/10.1029/2019JB018442 https://doi.org/10.1029/2023GL107188

Hunt, J.M. (1996). *Petroleum Geochemistry and Geology* (2nd ed.). W.H. Freeman and Company.

Indraswari, A. O., Frieling, J., Mather, T. A., Dickson, A. J., Jenkyns, H. C., & Idiz, E. (2024). Investigating the Behavior of Sedimentary Mercury (Hg) During Burial-Related Thermal Maturation. *Geochemistry, Geophysics, Geosystems*, *25*(6). https://doi.org/10.1029/2024GC011555

Indraswari, A.O., Frieling, J., Idiz, E., Mather, T. A., Jenkyns, H. C., Robinson, S.A., & Dickson, A. J. (*Submitted*). Limited mercury (Hg) partitioning into bitumen and efficient gaseous Hg reabsorption in early thermal maturation of organic-rich mudrocks. *Submitted to Geochimica et Cosmochimica Acta*

Iyer, K., Schmid, D. W., Planke, S., & Millett, J. (2017). Modelling hydrothermal venting in volcanic sedimentary basins: Impact on hydrocarbon maturation and paleoclimate. *Earth and Planetary Science Letters*, *467*, 30–42. https://doi.org/https://doi.org/10.1016/j.epsl.2017.03.023

Jarvie, D. M. (2012). Shale resource systems for oil and gas: Part1—Shale-gas resource systems. In J. A. Breyer (Ed.), *Shale reservoirs—Giant resources for the 21st century*: *American Association of Petroleum Geologists Memoir*, *97*, 69–87. Tulsa, OK: The

American Association of Petroleum Geologists. https://doi.org/10.1306/13321446M973489

Jenkyns, H. C. (1985). The Early Toarcian and Cenomanian-Turonian anoxic events in Europe: comparisons and contrasts. *Geologische Rundschau, 74*(3), 505–518. https://doi.org/10.1007/BF01821208

Jenkyns, H. C. (1988). The early Toarcian (Jurassic) anoxic event; stratigraphic, sedimentary and geochemical evidence. *American Journal of Science*, *288*(2), 101–151. https://doi.org/10.2475/ajs.288.2.101

Jenkyns, H. C. (2010). Geochemistry of oceanic anoxic events. *Geochemistry, Geophysics, Geosystem*, *11*(3), Q03004. https://doi.org/10.1029/2009GC002788

Jiskra, M., Desgranges, M., & Petrova, M. V. (2021). Mercury stable isotopes constrain atmospheric sources to the Ocean. *Nature, 597*(September). https://doi.org/10.1038/s41586-021-03859-8

Jones, M. T., Percival, L. M. E., Stokke, E. W., Frieling, J., Mather, T. A., Riber, L., Schubert, B. A., Schultz, B., Tegner, C., Planke, S., & Svensen, H. H. (2019). Mercury anomalies across the Palaeocene–Eocene Thermal Maximum. *Climate of the Past, 15*(1), 217–236. https://doi.org/10.5194/cp-15-217-2019

Kalvoda, J., Kumpan, T., Qie, W., Frýda, J., & Bábek, O. (2019). Mercury spikes at the Devonian-Carboniferous boundary in the eastern part of the Rhenohercynian Zone (central Europe) and in the South China Block. *Palaeogeography, Palaeoclimatology, Palaeoecology*, *531*, 109221. https://doi.org/https://doi.org/10.1016/j.palaeo.2019.05.043

Kendall, B., Wang, S., Lillis, P., Xing, L., Zheng, W., & Zhu, C. (2023). Evaluation of the molybdenum isotope system as a petroleum tracer: The Phosphoria petroleum system,

western U.S.A. *Chemical Geology*, *617*, 121244. https://doi.org/10.1016/j.chemgeo.2022.121244

Kockel, F., Wehner, H., & Gerling, P. (1994). Petroleum Systems of the Lower Saxony Basin, Germany. In L. B. Magoon & W. G. Dow (Eds.), *The petroleum system—from source to trap*, *American Association of Petroleum Geologists Memoir* (Vol. 60). Tulsa, OK: The American Association of Petroleum Geologists. https://doi.org/10.1306/M60585C34

Kongchum, M., Hudnall, W. H., & Delaune, R. D. (2011). Relationship between sediment clay minerals and total mercury. *Journal of Environmental Science and Health, Part A*, *46*(5), 534–539. https://doi.org/10.1080/10934529.2011.551745

Kusuma, I., Darin, T. (1989). The hydrocarbon potential of the Lower Tanjung formation, Barito Basin, S.E. Kalimantan. In: *Proceedings Indonesian Petroleum Association 18th Annual Convention*. IPA89-11.09, pp. 1–32. https://doi.org/10.29118/ipa.2166.107.138

Lang, W. D., Spath, L. F., Cox, L. R., & Muir-Wood, H. M. (1928). The Belemnite Marls of Charmouth, a Series in the Lias of the Dorset Coast. *Quarterly Journal of the Geological Society of London*, *84*(1–4), 179–222. https://doi.org/10.1144/GSL.JGS.1928.084.01-04.06

Lash, G. G., & Engelder, T. (2005). An analysis of horizontal microcracking during catagenesis: Example from the Catskill delta complex. *American Association of Petroleum Geologists Bulletin*, *89*(11), 1433–1449. https://doi.org/10.1306/05250504141

Lee, S. H., & Park, Y. O. (2003). Gas-phase mercury removal by carbon-based sorbents. *Fuel Processing Technology, 84*(1–3), 197–206. https://doi.org/10.1016/S0378-3820(03)00055-1

Lewan, M. D., Winters, J. C., & Mcdonald, J. H. (1979). Generation of oil-like pyrolyzates from organic-rich shales. *Science, 203*(4383), 897–899.

http://www.jstor.org/stable/1747886

Lewan, M. D., & Maynard, J. (1982). Factors controlling enrichment of vanadium and nickel in the bitumen of organic sedimentary rocks. *Geochimica et Cosmochimica Acta*, *46*(12), 2547–2560. https://doi.org/10.1016/0016-7037(82)90377-5

Leythaeuser, D., Littke, R., Radke, M., & Schaefer, R. G. (1988). Geochemical effects of petroleum migration and expulsion from Toarcian source rocks in the Hils syncline area, NW-Germany. *Organic Geochemistry*, *13*(1–3), 489–502. https://doi.org/10.1016/0146-6380(88)90070-8

Li, X., Wang, Q., Zhang, W., & Yin, H. (2016). Contact metamorphism of shales intruded by a granite dike: Implications for shale gas preservation. *International Journal of Coal Geology*, *159*, 96–106. https://doi.org/10.1016/j.coal.2016.03.016

Li, J., Han, Z., Yan, Q., Wang, S., & Ge, S. (2019). Distribution and genesis of mercury in natural gas of large coal derived gas fields in China. *Petroleum Exploration and Development*, *46*(3), 463–470. https://doi.org/10.1016/S1876-3804(19)60027-3

Littke, R., Baker, D. R., & Leythaeuser, D. (1988). Microscopic and sedimentologic evidence for the generation and migration of hydrocarbons in Toarcian source rocks of different maturities. *Organic Geochemistry*, *13*(1–3), 549–559. https://doi.org/10.1016/0146-6380(88)90075-7

Littke, R., Leythaeuser, D., Rullkötter, J., & Baker, D. R. (1991). Keys to the depositional history of the Posidonia Shale (Toarcian) in the Hils Syncline, northern Germany. In R. V. Tyson & T. H. Pearson (Eds.), *Modern and Ancient Continental Shelf Anoxia*, *Geological Society Special Publication*, *58*, 311–333. Geological Society, London. https://doi.org/10.1144/GSL.SP.1991.058.01.20

Liu, Q. (2013). Mercury concentration in natural gas and its distribution in the Tarim Basin. *Science China Earth Sciences, 56*(8), 1371–1379. https://doi.org/10.1007/s11430-013-

4609-2

Liu, Q., Peng, W., Li, J., & Wu, X. (2020). Source and distribution of mercury in natural gas of major petroliferous basins in China. *Science China Earth Sciences*, *63*(5), 643–648. https://doi.org/10.1007/s11430-019-9596-6

Liu, Z., Tian, H., Yin, R., Chen, D., & Gai, H. (2022). Mercury loss and isotope fractionation during thermal maturation of organic-rich mudrocks. *Chemical Geology*, *612*(September), 121144. https://doi.org/10.1016/j.chemgeo.2022.121144

Lu, S.-T., & Kaplan, I. R. (1989). Pyrolysis of kerogens in the absence and presence of montmorillonite—II. Aromatic hydrocarbons generated at 200 and 300°C. *Organic Geochemistry*, *14*(5), 501–510. https://doi.org/10.1016/0146-6380(89)90030-2

Manceau, A., Merkulova, M., Murdzek, M., Batanova, V., Baran, R., Glatzel, P., et al. (2018). Chemical forms of mercury in pyrite: Implications for predicting mercury releases in acid mine drainage settings. *Environmental Science and Technology*, *52*(18), 10286–10296. https://doi.org/10.1021/acs.est.8b02027

Mandl, G., & Harkness, R. M. (1987). Hydrocarbon migration by hydraulic fracturing. In M. E. Jones & R. M. F. Preston (Eds.), *Deformation of Sediments and Sedimentary Rocks, Geological Society Special Publication*, *29*, 39–53. Geological Society, London. https://doi.org/10.1144/GSL.SP.1987.029.01.04

Meissner, F. F. (1978). Petroleum geology of the Bakken formation Williston basin, North Dakota and Montana. In D. Estelle & R. Miller (Eds.), *Montana Geological Society: 24th Annual Conference: 1978 Williston Basin Symposium* (pp. 207-227). Billings, MT: Montana Geological Society.

Mercone, D., Thomson, J., Croudace, I. W., & Troelstra, S. R. (1999). A coupled natural immobilisation mechanism for mercury and selenium in deep-sea sediments. *Geochimica et Cosmochimica Acta*, *63*(10), 1481–1488.

https://doi.org/https://doi.org/10.1016/S0016-7037(99)00063-0

Montero-Serrano, J. C., Föllmi, K. B., Adatte, T., Spangenberg, J. E., Tribovillard, N., Fantasia, A., & Suan, G. (2015). Continental weathering and redox conditions during the early Toarcian Oceanic Anoxic Event in the northwestern Tethys: Insight from the Posidonia Shale section in the Swiss Jura Mountains. *Palaeogeography, Palaeoclimatology, Palaeoecology, 429*, 83–99. https://doi.org/10.1016/J.PALAEO.2015.03.043

Moorcroft, D., & Tonnelier, N. (2016). Contact Metamorphism of Black Shales in the Thermal Aureole of a Dolerite Sill Within the Karoo Basin. In B. Linol & M. J. de Wit (Eds.), *Origin and Evolution of the Cape Mountains and Karoo Basin* (pp. 75–84). Springer International Publishing. https://doi.org/10.1007/978-3-319-40859-0_8

Mukherjee, A. B., Bhattacharya, P., Sarkar, A., & Zevenhoven, R. (2009). Mercury emissions from industrial sources in India and its effects in the environment. In R. Mason & N. Pirrone (Eds.), *Mercury fate and transport in the global atmosphere: Emissions, measurements and models* (pp. 81–112). Boston, MA: Springer US. https://doi.org/10.1007/978-0-387-93958-2_4

O'Connor, L. K., Robinson, S. A., Naafs, B. D. A., Jenkyns, H. C., Henson, S., Clarke, M., & Pancost, R. D. (2019). Late Cretaceous Temperature Evolution of the Southern High Latitudes: A TEX86 Perspective. *Paleoceanography and Paleoclimatology*, *34*(4), 436–454. https://doi.org/10.1029/2018PA003546

Outridge, P. M., Sanei, H., Stern, G. A., Hamilton, P. B., & Goodarzi, F. (2007). Evidence for control of mercury accumulation rates in Canadian High Arctic Lake sediments by variations of aquatic primary productivity. *Environmental Science and Technology*, *41*(15), 5259–5265. https://doi.org/10.1021/es070408x

Patria, A. A., Suhendra, R., Anggara, F., Agangi, A., Obrochta, S. P., & Setiawan, I. (2024). Association and textural-compositional evolution of pyrite-organic matter in coals of the Tarakan, Barito, and Pasir Basins, Kalimantan, Indonesia. *International Journal of Coal Geology*, *282*, 104442. https://doi.org/10.1016/j.coal.2023.104442

Percival, L. M. E., Witt, M. L. I., Mather, T. A., Hermoso, M., Jenkyns, H. C., Hesselbo, S. P., et al. (2015). Globally enhanced mercury deposition during the end-Pliensbachian extinction and Toarcian OAE: A link to the Karoo – Ferrar Large Igneous Province. *Earth and Planetary Science Letters*, *428*, 267–280. https://doi.org/http://dx.doi.org/10.1016/j.epsl.2015.06.064

Percival, L. M. E., Jenkyns, H. C., Mather, T. A., Dickson, A. J., Batenburg, S. J., Ruhl, M., et al. (2018). Does large igneous province volcanism always perturb the mercury cycle? Comparing the records of Oceanic Anoxic Event 2 and the end-Cretaceous to other Mesozoic events. *American Journal of Science*, *318*(8), 799–860. https://doi.org/10.2475/08.2018.01

Percival, L. M. E., Bergquist, B. A., Mather, T. A., & Sanei, H. (2021). Sedimentary mercury enrichments as a tracer of large igneous province volcanism. In R.E. Ernst, A.J. Dickson, A. Bekker (Eds.), *Large igneous provinces: A driver of global environmental and biotic changes, Geophysical Monograph Series* (Vol. 255, pp. 247–262). Washington, DC and Hoboken, NJ: American Geophysical Union and John Wiley and Sons, Inc. https://doi.org/10.1002/9781119507444.ch11

Peters, K. E., & Cassa, M. R. (1994). Applied source rock geochemistry. In L.B. Magoon & W.G. Dow (Eds.), *The petroleum system—from source to trap*, *American Association of Petroleum Geologists Memoir* (Vol. 60). Tulsa, OK: The American Association of Petroleum Geologists. https://doi.org/10.1306/M60585C5

Peters, K.E., Walters, C., & Moldowan, J. (2005). *The Biomarker Guide* (2nd ed.).

Cambridge: Cambridge University Press. https://doi.org/10.1017/CBO9780511524868

Pham, A. L. T., Morris, A., Zhang, T., Ticknor, J., Levard, C., & Hsu-Kim, H. (2014). Precipitation of nanoscale mercuric sulfides in the presence of natural organic matter: Structural properties, aggregation, and biotransformation. *Geochimica et Cosmochimica Acta*, *133*, 204–215. https://doi.org/10.1016/j.gca.2014.02.027

Poetz, S., Horsfield, B., Wilkes, H. (2014). Maturity-driven generation and transformation of acidic compounds in the organic-rich Posidonia shale as revealed by electrospray ionization Fourier transform ion cyclotron resonance mass spectrometry. *Energy Fuel, 28*(8), 4877– 4888. https://doi.org/10.1021/ef500688s

Pyle, D. M., & Mather, T. A. (2003). The importance of volcanic emissions for the global atmospheric mercury cycle. *Atmospheric Environment*, *37*(36), 5115–5124. https://doi.org/10.1016/j.atmosenv.2003.07.011

Qu, Y., Zhong, H., Liu, X., Zhang, W., & Chen, T. (2024). Coupling and decoupling between sedimentary mercury and organic carbon preservation in the oxygenated marine environment. *Geochemistry, Geophysics, Geosystems,* 25, e2023GC011201. https://doi.org/10.1029/2023GC011201

Raiswell, R., & Berner, R. A. (1987). Organic carbon losses during burial and thermal maturation of normal marine shales. *Geology*, *15*(9), 853–856. https://doi.org/10.1130/0091-7613(1987)15<853:OCLDBA>2.0.CO;2

Ravichandran, M. (2004). Interactions between mercury and dissolved organic matter - A review. *Chemosphere*, *55*(3), 319–331. https://doi.org/10.1016/j.chemosphere.2003.11.011

Reis, A. T., Coelho, J. P., Rodrigues, S. M., Rocha, R., Davidson, C. M., Duarte, A. C., & Pereira, E. (2012). Development and validation of a simple thermo-desorption technique for mercury speciation in soils and sediments. *Talanta, 99*, 363–368.

https://doi.org/10.1016/j.talanta.2012.05.065

Reis, A. T., Coelho, J. P., Rucandio, I., Davidson, C. M., Duarte, A. C., & Pereira, E. (2015). Thermo-desorption: A valid tool for mercury speciation in soils and sediments? *Geoderma, 237–238*, 98–104. https://doi.org/10.1016/J.GEODERMA.2014.08.019

Röhl, H. J., Schmid-Röhl, A., Oschmann, W., Frimmel, A., & Schwark, L. (2001). The Posidonia Shale (Lower Toarcian) of SW-Germany: An oxygen-depleted ecosystem controlled by sea level and palaeoclimate. *Palaeogeography, Palaeoclimatology, Palaeoecology*, *165*(1–2), 27–52. https://doi.org/10.1016/S0031-0182(00)00152-8

Rullkötter, J., Leythaeuser, D., Horsfield, B., Littke, R., Mann, U., Müller, P. J., et al. (1988). Organic matter maturation under the influence of a deep intrusive heat source: A natural experiment for quantitation of hydrocarbon generation and expulsion from a petroleum source rock (Toarcian shale, northern Germany). *Organic Geochemistry*, *13*(4–6), 847–856. https://doi.org/10.1016/0146-6380(88)90237-9

Rumayor, M., Diaz-Somoano, M., Lopez-Anton, M. A., & Martinez-Tarazona, M. R. (2013). Mercury compounds characterization by thermal desorption. *Talanta*, *114*, 318–322. https://doi.org/10.1016/j.talanta.2013.05.059

Rumayor, M., Diaz-Somoano, M., Lopez-Anton, M. A., & Martinez-Tarazona, M. R. (2015a). Application of thermal desorption for the identification of mercury species in solids derived from coal utilization. *Chemosphere*, *119*, 459–465. https://doi.org/10.1016/j.chemosphere.2014.07.010

Rumayor, M., Lopez-Anton, M. A., Díaz-Somoano, M., & Martínez-Tarazona, M. R. (2015b). A new approach to mercury speciation in solids using a thermal desorption technique. Fuel. 160, 525–530. https://10.1016/j.fuel.2015.08.028

Rumayor, M., Lopez-Anton, M. A., Díaz-Somoano, M., Maroto-Valer, M. M., Richard, J.-H., Biester, H., & Martínez-Tarazona, M. R. (2016). A comparison of devices using thermal

desorption for mercury speciation in solids. Talanta. 150, 272–277. https://10.1016/j.talanta.2015.12.058

Sanei, H., Grasby, S. E., & Beauchamp, B. (2012). Latest Permian mercury anomalies. *Geology*, *40*(1), 63–66. https://doi.org/10.1130/G32596.1

Saniewska, D., & Bełdowska, M. (2017). Mercury fractionation in soil and sediment samples using thermo-desorption method. *Talanta, 168*, 152–161. https://doi.org/10.1016/j.talanta.2017.03.026

Schmid-Röhl, A., Röhl, H. J., Oschmann, W., Frimmel, A., & Schwark, L. (2002). Palaeoenvironmental reconstruction of Lower Toarcian epicontinental black shales (Posidonia Shale, SW Germany): Global versus regional control. *Geobios*, *35*(1), 13–20. https://doi.org/10.1016/S0016-6995(02)00005-0

Schöllhorn, I., Adatte, T., van de Schootbrugge, B., Houben, A., Charbonnier, G., Janssen, N., & Föllmi, K. B. (2020). Climate and environmental response to the break-up of Pangea during the Early Jurassic (Hettangian-Pliensbachian); the Dorset coast (UK) revisited. *Global and Planetary Change*, *185*, 103096. https://doi.org/10.1016/j.gloplacha.2019.103096

Schroeder, W., Hamilton, M., & Stobart, S. (1985). The use of noble metals as collection media for mercury and its compounds in the atmosphere. *Reviews in Analytical Chemistry, 8*(3), 1. https://doi.org/10.1515/REVAC.1985.8.3.I

Schuster, P. F., Schaefer, K. M., Aiken, G. R., Antweiler, R. C., Dewild, J. F., Gryziec, J. D, et al. (2018). Permafrost stores a globally significant amount of mercury. *Geophysical Research Letters*, *45*, 1463–1471. https://doi.org/10.1002/2017GL075571

Schwark, L., & Frimmel, A. (2004). Chemostratigraphy of the Posidonia Black Shale, SW-Germany II. Assessment of extent and persistence of photic-zone anoxia using aryl isoprenoid distributions. *Chemical Geology*, *206*(3–4), 231–248.

https://doi.org/10.1016/j.chemgeo.2003.12.008

Sellwood, B. W. (1970). The relation of trace fossils to small scale sedimentary cycles in the British Lias. In Crimes, T. P., & Harper, J. C. (Eds.), *Trace fossils* (pp. 489–504). Seel House Press.

Sellwood, B. W. (1972). Regional environmental change across a Lower Jurassic stage-boundary in Britain. *Palaeontology*, *15*(1), 125–157.

Senglaub, Y., Littke, R., & Brix, M. R. (2006). Numerical modelling of burial and temperature history as an approach for an alternative interpretation of the Bramsche anomaly, Lower Saxony Basin. *International Journal of Earth Sciences, 95*(2), 204–224. https://doi.org/10.1007/s00531-005-0033-y

Shen, J., Algeo, T. J., Chen, J., Planavsky, N. J., Feng, Q., Yu, J., & Liu, J. (2019a). Mercury in marine Ordovician/Silurian boundary sections of South China is sulfide-hosted and non-volcanic in origin. *Earth and Planetary Science Letters*, *511*, 130–140. https://doi.org/10.1016/j.epsl.2019.01.028

Shen, J., Yu, J., Chen, J., Algeo, T.J., Xu, G.Z., Feng, Q., et al. (2019b). Mercury evidence of intense volcanic effects on land during the Permian-Triassic transition. *Geology 47*(12), 1117–1121. https://doi.org/10.1130/G46679.1

Shen, J., Feng, Q., Algeo, T. J., Liu, J., Zhou, C., Wei, W., et al. (2020). Sedimentary host phases of mercury (Hg) and implications for use of Hg as a volcanic proxy. *Earth and Planetary Science Letters*, *543*, 116333. https://doi.org/10.1016/j.epsl.2020.116333

Song, J., Littke, R., & Weniger, P. (2017). Organic geochemistry of the Lower Toarcian Posidonia Shale in NW Europe. *Organic Geochemistry*, *106*, 76–92. https://doi.org/10.1016/j.orggeochem.2016.10.014

Stock A., & Littke R. (2016). Geochemical composition of oils from the Gifhorn Trough and Lower Saxony Basin in comparison to Posidonia Shale source rocks from the Hils

Syncline *Northern Germany. German Journal of Geology, 167*, 315–331. https://doi.org/10.1127/zdgg/2016/0058

Svensen, H., Planke, S., Chevallier, L., Malthe-Sørenssen, A., Corfu, F., & Jamtveit, B. (2007). Hydrothermal venting of greenhouse gases triggering Early Jurassic global warming. *Earth and Planetary Science Letters*, *256*(3), 554–566. https://doi.org/10.1016/j.epsl.2007.02.013

Svensen, H., Bebout, G., Kronz, A., Li, L., Planke, S., Chevallier, L., & Jamtveit, B. (2008). Nitrogen geochemistry as a tracer of fluid flow in a hydrothermal vent complex in the Karoo Basin, South Africa. *Geochimica et Cosmochimica Acta*, *72*(20), 4929–4947. https://doi.org/https://doi.org/10.1016/j.gca.2008.07.023

Svensen, H., Planke, S., Polozov, A. G., Schmidbauer, N., Corfu, F., Podladchikov, Y. Y., & Jamtveit, B. (2009). Siberian gas venting and the end-Permian environmental crisis. *Earth and Planetary Science Letters*, *277*(3), 490–500. https://doi.org/10.1016/j.epsl.2008.11.015

Svensen, H. H., Planke, S., Neumann, E.-R., Aarnes, I., Marsh, J. S., Polteau, S., Harstad, H. H., Chevallier, L. (2015a). Sub-Volcanic Intrusions and the Link to Global Climatic and Environmental Changes, in: Breitkreuz, C., & Rocchi, S. (Eds.), Physical Geology of Shallow Magmatic Systems. Springer Cham, pp. 249–272. https://doi.org/10.1007/11157_2015_10

Svensen, H., Fristad, K. E., Polozov, A. G., & Planke, S. (2015b). Volatile generation and release from continental large igneous provinces. In A. Schmidt, K. Fristad, & L. Elkins-Tanton (Eds.), *Volcanism and Global Environmental Change* (pp. 177–192). Cambridge: Cambridge University Press. https://doi.org/10.1017/CBO9781107415683.015

Svensen, H. H., Jones, M. T., Percival, L. M. E., Grasby, S. E., & Mather, T. A. (2023a). Release of mercury during contact metamorphism of shale: Implications for understanding the impacts of large igneous province volcanism. *Earth and Planetary Science Letters*, *619*, 118306. https://doi.org/10.1016/j.epsl.2023.118306

Svensen, H. H., Jones, M. T., & Mather, T. A. (2023b). Large Igneous Provinces and the Release of Thermogenic Volatiles from Sedimentary Basins. *Elements*, *19*(5), 282–288. https://doi.org/10.2138/gselements.19.5.282

Tannenbaum, E., & Kaplan, I. R. (1985). Role of minerals in the thermal alteration of organic matter—I: Generation of gases and condensates under dry condition. *Geochimica et Cosmochimica Acta*, *49*(12), 2589–2604. https://doi.org/10.1016/0016-7037(85)90128-0

Them, T.R., Gill, B.C., Caruthers, A.H., Gröcke, D.R., Tulsky, E.T., Martindale, R.C., et al. (2017). High-resolution carbon isotope records of the Toarcian Oceanic Anoxic Event (Early Jurassic) from North America and implications for the global drivers of the Toarcian carbon cycle. *Earth and Planetary Science Letters*, *459*, 118–126. https://doi.org/10.1016/j.epsl.2016.11.021

Them, T. R., Jagoe, C. H., Caruthers, A. H., Gill, B. C., Grasby, S. E., Gröcke, D. R., et al. (2019). Terrestrial sources as the primary delivery mechanism of mercury to the oceans across the Toarcian Oceanic Anoxic Event (Early Jurassic). *Earth and Planetary Science Letters*, *507*, 62–72. https://doi.org/10.1016/j.epsl.2018.11.029

Thibodeau, A. M., Ritterbush, K., Yager, J. A., West, A. J., Ibarra, Y., Bottjer, D. J., et al. (2016). Mercury anomalies and the timing of biotic recovery following the end-Triassic mass extinction. *Nature Communications, 7*(1), 11147. https://doi.org/10.1038/ncomms11147

Tissot, B. P., & Welte, D. H. (1984). *Petroleum Formation and Occurrence*. Springer-Verlag. https://doi.org/10.1007/978-3-642-96446-6_5

UN Environment. (2019). *Global Mercury Assessment 2018*. UN Environment Programme, Chemicals and Health Branch Geneva, Switzerland. Retrieved from https://www.unep.org/resources/publication/global-mercury-assessment-2018

Varekamp, J. C., & Buseck, P. R. (1984). The speciation of mercury in hydrothermal systems, with applications to ore deposition *Geochimica et Cosmochimica Acta, 48*, 177–185. https://doi.org/10.1016/0016-7037(84)90359-4

Wallace, G. T. (1982). The association of copper, mercury and lead with surface-active organic matter in coastal seawater. *Marine Chemistry*, *11*(4), 379–394. https://doi.org/10.1016/0304-4203(82)90032-9

Wallschläger, D., Desai, M.V.M., Spengler, M. and Wilken, R.-D. (1998). Mercury Speciation in Floodplain Soils and Sediments along a Contaminated River Transect. *Journal of Environmental Quality, 27*, 1034-1044. https://doi.org/10.2134/jeq1998.00472425002700050008x

Wang, X., Cawood, P. A., Zhao, H., Zhao, L., Grasby, S. E., Chen, Z. Q., et al. (2018). Mercury anomalies across the end Permian mass extinction in South China from shallow and deep water depositional environments. *Earth and Planetary Science Letters*, *496*, 159–167. https://doi.org/10.1016/j.epsl.2018.05.044

Weedon, G. P., & Jenkyns, H. C. (1990). Regular and irregular climatic cycles and the Belemnite Marls (Pliensbachian, Lower Jurassic, Wessex Basin). *Journal of the Geological Society*, *147*(6), 915–918. https://doi.org/10.1144/gsjgs.147.6.0915

Weedon, G. P., & Jenkyns, H. C. (1999). Cyclostratigraphy and the Early Jurassic timescale: Data from the Belemnite Marls, Dorset, southern England. *GSA Bulletin*, *111*(12), 1823–1840. https://doi.org/10.1130/0016-7606(1999)111<1823:CATEJT>2.3.CO;2

Wilhelm, M., & Bloom, N. (2000). Mercury in petroleum. *Fuel Processing Technology*, *63*(1), 1–27. https://doi.org/10.1016/S0378-3820(99)00068-5

Wilhelm, S. M. (2001). Estimate of mercury emissions to the atmosphere from petroleum. *Environmental Science and Technology*, *35*(24), 4704–4710. https://doi.org/10.1021/es001804h

Wilhelm, S. M., Liang, L., & Kirchgessner, D. (2006). Identification and Properties of Mercury Species in Crude Oil. Energy & Fuels. 20(1), 180–186. https://doi.org/10.1021/ef0501391

Wilhelm, S. M., Liang, L., Cussen, D., & Kirchgessner, D. A. (2007). Mercury in crude oil processed in the United States (2004). Environmental Science and Technology. 41(13), 4509–4514. https:/doi.org/10.1021/es062742j

Windmöller, C. C., Wilken, R.-D., & Jardim, W. D. F. (1996). Mercury speciation in contaminated soils by thermal release analysis. Water, Air, and Soil Pollution, 89(3–4), 399–416. https://doi.org/10.1007/BF00171644

Witts, D., Hall, R., Nichols, G., & Morley, R. (2012). A new depositional and provenance model for the Tanjung Formation, Barito Basin, SE Kalimantan, Indonesia. *Journal of Asian Earth Sciences*, *56*, 77–104. https://doi.org/10.1016/j.jseaes.2012.04.022

Xu, J., Bland, G. D., Gu, Y., Ziaei, H., Xiao, X., Deonarine, A., Reible, D., Bireta, P., Hoelen, T. P., & Lowry, G. V. (2021). Impacts of Sediment Particle Grain Size and Mercury Speciation on Mercury Bioavailability Potential. *Environmental Science & Technology*, *55*(18), 12393–12402. https://doi.org/10.1021/acs.est.1c03572

Zettlitzer, M., Scholer, H. F., Eiden, R., & Falter, R. (1997). Determination of Elemental, Inorganic and Organic Mercury in North German Gas Condensates and Formation Brines. *International Symposium on Oilfield Chemistry, February 18–21, 1997, Houston, Texas*. https://doi.org/10.2118/37260-MS

Zimmermann, J., Franz, M., Schaller, A. & Wolfgramm, M. (2018). The Toarcian–Bajocian deltaic system in the North German Basin: Subsurface mapping of ancient deltas-morphology, evolution and controls. *Sedimentology*, *65*(3), 897–930. https://doi.org/10.1111/sed.12410

Appendices

Appendix 1 - Chapter 2 Supporting Information

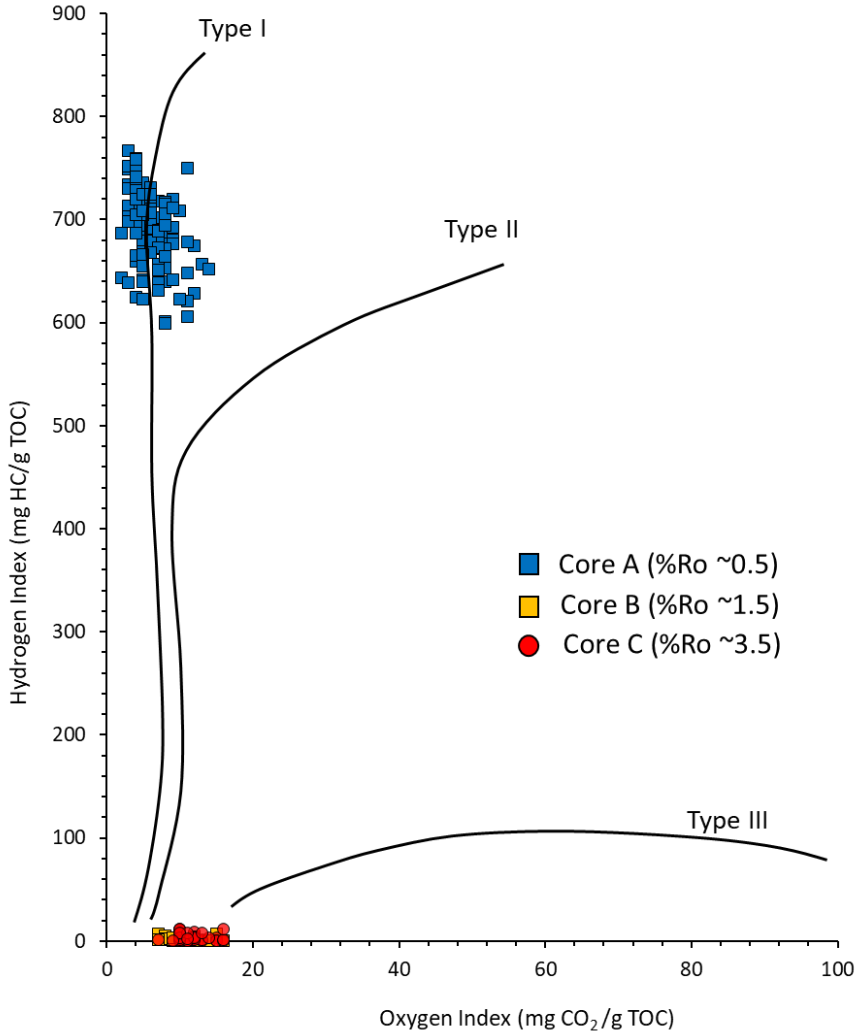


Figure 2.S1. Modified van Krevelen diagram (after Espitalié et al., 1977) showing the relationship between Hydrogen and Oxygen Indices for cores A, B, and C. The Posidonienschiefer from core A is mainly characterized by Type I/II kerogen. Cores B and C show mature and overmature states of the kerogen after thermal maturation. The HI/OI of Core B and C are hence no longer suitable parameters to determine the origin of organic matter.

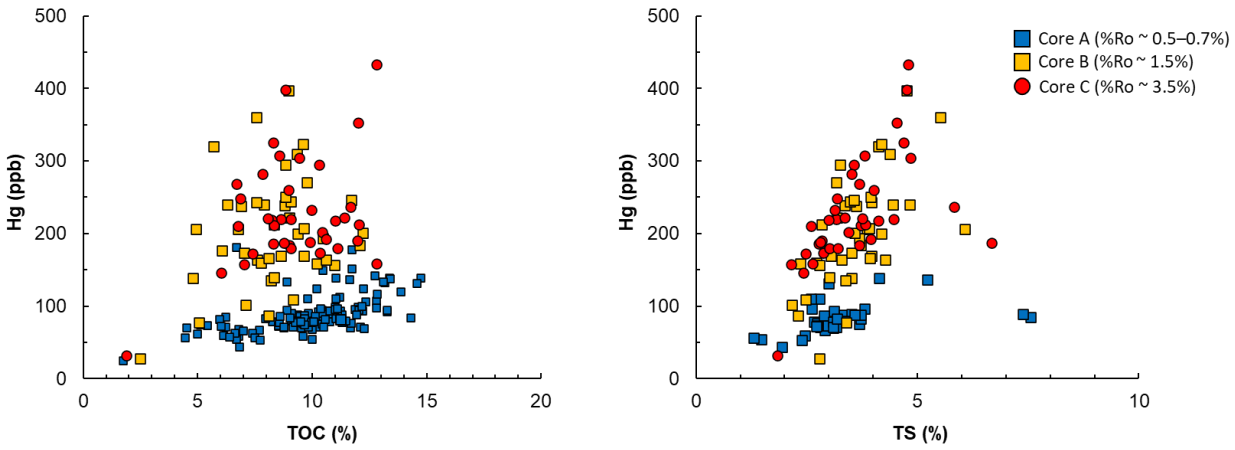


Figure 2.S2. Hg TOC (left), and TS (right) in cores A, B, and C. Hg vs TOC shows a weak correlation in core A and no correlation in cores B and C. Hg correlates only slightly better with TS for the 3 cores.

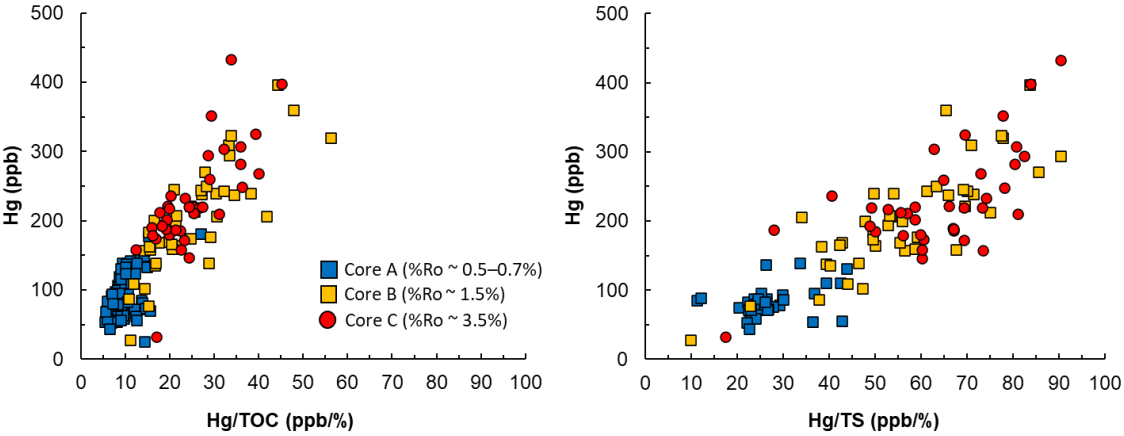


Figure 2.S3. Hg vs Hg/TOC and Hg/TS plots for the organic-rich PS sections in the 3 cores. Higher maturity cores (B and C) exhibit significantly higher Hg concentrations and Hg/TOC and Hg/TS ratios compared to the immature Core A data. Although none of the cores are above threshold values (~72 ppb/%TOC) for anomalous Hg/TOC values reported by Grasby et al., (2019), there is a clear trend towards those values with the higher maturity samples.

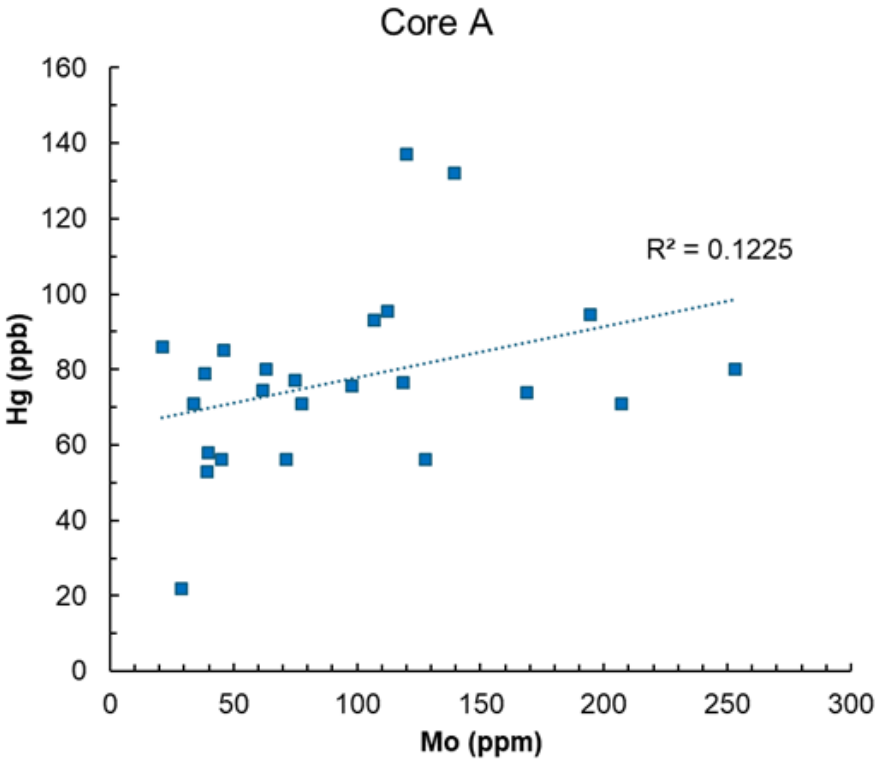


Figure 2.S4. Molybdenum versus mercury concentration in core A. The weak correlation between Hg and Mo supports a Hg supply limited system during deposition of Posidonienschiefer (cf. Bian et al., 2024). The variability in Mo concentrations suggest Hg supply was limiting over a wide range of reducing conditions.

Table 2.S1. Sampling resolution mercury (Hg) analyses in Posidonienschiefer for cores A, B, and C.

	Stratigraphic thickness (m)	Sample points	Interval/resolution (cm)
Core A	32	217	15
Core B	27.5	49	57
Core C	32.5	35	88

Table 2.S2. Correlation between Hg, TOC, and TS for cores A, B and C from the Posidonienschiefer.

		Core		
		A	B	C
Hg-TOC	N	114	42	35
	R	0.628	0.254	0.179
	R^2	0.395	0.065	0.032
	p	<0.001	<0.001	<0.001
Hg-TS	N	34	42	35
	R	0.373	0.603	0.521
	R^2	0.139	0.363	0.272
	p	<0.001	<0.001	<0.001
TS-TOC	N	34	42	35
	R	0.159	-0.1	0.256
	R^2	0.025	0.01	0.065
	p	<0.001	<0.001	<0.001

Appendix 2 - Chapter 3 Supporting Information

Table 3.S1. Mercury concentration data of sub-samples in reabsorption experiment in this study. Extracted Residue: pyrolysed bulk rock after solvent extraction of soluble organic matter. Bitumen: the total solvent-extractable organic matter. The gas loss is calculated using the difference: Hg loss as gas = 100% − %Hg in bitumen − %Hg in the sediments.

Heating time (hours)	Cooling time (minutes)	Hg				
0				74.6 ppb		
		Extracted Residues		Bitumen		Loss (as gas)
		ppb	% of total Hg	ppb	% of total Hg	% of total Hg
24	0	37.6	50.40	91.4	0.257	49.34
24	1	19.2	25.74	39.9	0.150	74.11
24	4	28.4	38.07	22.0	0.002	61.93
24	16	48.7	65.28	38.0	0.035	34.68
24	60	71.4	95.71	74.5	0.426	3.86

Appendix 3 – Data tables

A Data Chapter 2
B Data Chapter 3
C Data Chapter 4

A Data Chapter 2

Core	Depth (m)	TOC (wt%)	HI (mgHC/gTOC)	TS (wt%)	Hg (ppb)	Rock-Eval Data Source
A	1419.71	6.24		7.56	85	Hooker et al., 2020, Dickson et al., 2022
A	1419.74	8.26	718		78	Celestino, 2019
A	1420.05	10.73	674	7.38	89	Celestino, 2019
A	1420.26				74	
A	1420.38	11.66	705		70	Celestino, 2019
A	1420.51				77	
A	1420.62				90	
A	1420.63	13.28	734		92	Celestino, 2019
A	1420.74				83	
A	1420.85	11.31	713		85	Hooker et al., 2020, Dickson et al., 2022
A	1420.94				67	
A	1421.04				71	
A	1421.15				62	
A	1421.27				81	
A	1421.39				95	
A	1421.51				143	
A	1421.6	11.64	700	5.23	137	Celestino, 2019
A	1421.76	12.79	699		107	Celestino, 2019
A	1421.8				111	
A	1421.81	12.79			98	Hooker et al., 2020, Dickson et al., 2022
A	1421.91				112	
A	1422.02				102	
A	1422.14				102	

A	1422.24				116	
A	1422.35				113	
A	1422.43				102	
A	1422.63	11.19	698		112	Celestino, 2019
A	1422.79	13.37	657	4.14	139	Hooker et al., 2020, Dickson et al., 2022
A	1422.88				83	
A	1423	10.64	752		93	Hooker et al., 2020, Dickson et al., 2022
A	1423.22				109	
A	1423.34				79	
A	1423.66	9.53		3.1	70	Hooker et al., 2020, Dickson et al., 2022
A	1423.73	10.26	714		92	Celestino, 2019
A	1423.83	11.01	713		99	Celestino, 2019
A	1423.95				94	
A	1424.05				116	
A	1424.15				89	
A	1424.35				85	
A	1424.48				86	
A	1424.58				84	
A	1424.66	10.45	749		94	Celestino, 2019
A	1424.71				120	
A	1424.82	12.2	720	3.11	93	Hooker et al., 2020, Dickson et al., 2022
A	1424.92				100	
A	1425.03				112	
A	1425.13				96	
A	1425.23				88	
A	1425.44				99	

A	1425.58	9.38	695		88	This study
A	1425.7				85	
A	1425.8				74	
A	1425.91	9.65		2.67	78	Hooker et al., 2020, Dickson et al., 2022
A	1425.94	9.45	703		86	Celestino, 2019
A	1426.04				82	
A	1426.28				75	
A	1426.39				89	
A	1426.48				79	
A	1426.52	9.83	698	3.34	88	This study
A	1426.64				91	
A	1426.75	12.35	749		106	Celestino, 2019
A	1426.86				68	
A	1426.97				85	
A	1427.19	10.9	713	3.52	89	Celestino, 2019
A	1427.3				85	
A	1427.56	9.82	693		90	This study
A	1427.68				86	
A	1427.8				102	
A	1427.93	11.99	688		99	Celestino, 2019
A	1428.05	10.78	713		93	Celestino, 2019
A	1428.07	10.19	715	2.81	71	Hooker et al., 2020, Dickson et al., 2022
A	1428.17				86	
A	1428.27				84	
A	1428.33	10.44	687		92	This study
A	1428.43	10.78	708		79	Celestino, 2019

A	1428.55				67	
A	1428.66				79	
A	1428.77				73	
A	1428.9	11.03	730		83	Celestino, 2019
A	1429.03				74	
A	1429.07				90	
A	1429.19				113	
A	1429.25				88	
A	1429.37				93	
A	1429.49	9.61	701	2.74	76	This study
A	1429.61				82	
A	1429.7				75	
A	1429.84	11.22	736		93	Celestino, 2019
A	1430	10.42	708		89	Hooker et al., 2020, Dickson et al., 2022
A	1430.1				77	
A	1430.2	8.54	684		72	Celestino, 2019
A	1430.35	7.69	686	2.9	67	Celestino, 2019
A	1430.48				78	
A	1430.64				77	
A	1430.76				69	
A	1430.8	9.96			76	Hooker et al., 2020, Dickson et al., 2022
A	1430.9	10.47	724		80	Celestino, 2019
A	1431.14				68	
A	1431.26				68	
A	1431.43	10.43	696		75	Hooker et al., 2020, Dickson et al., 2022
A	1431.47	9.68	693	2.89	87	Celestino, 2019

A	1431.79				69	
A	1431.89	10.13	676		86	This study
A	1432.55	5.44	606	2.73	73	Celestino, 2019
A	1432.59	5.97			82	Hooker et al., 2020, Dickson et al., 2022
A	1432.69				62	
A	1432.8	6.24	675		71	This study
A	1432.92				56	
A	1433.12	7.4			63	Hooker et al., 2020, Dickson et al., 2022
A	1433.14	8.53	702	2.97	73	Celestino, 2019
A	1433.22				66	
A	1433.33				72	
A	1433.44	8.78	692		70	This study
A	1433.52				72	
A	1433.78				77	
A	1433.79	11.72	710		76	Hooker et al., 2020, Dickson et al., 2022
A	1433.9	10.01	694		68	Celestino, 2019
A	1434.02				64	
A	1434.11				88	
A	1434.32	9.2	696	3.09	79	Celestino, 2019
A	1434.46				77	
A	1434.65				58	
A	1434.75	9.83	713		71	Celestino, 2019
A	1434.86				74	
A	1434.97				87	
A	1435.02				67	
A	1435.3				56	

A	1435.45				64	
A	1435.47	9.63		3.69	75	Hooker et al., 2020, Dickson et al., 2022
A	1435.59				66	
A	1435.71	9.09	710		80	Celestino, 2019
A	1435.83	9.1	700		90	Celestino, 2019
A	1436.15	6.79	648		58	Hooker et al., 2020, Dickson et al., 2022
A	1436.21	6.12	636	2.46	59	Celestino, 2019
A	1436.33	5.12	623		74	Celestino, 2019
A	1436.44				71	
A	1436.59	4.51	601		70	Celestino, 2019
A	1436.77	7.5			56	Hooker et al., 2020, Dickson et al., 2022
A	1436.82				61	
A	1437.01	7.74	676	2.39	53	Hooker et al., 2020, Dickson et al., 2022
A	1437.06				63	
A	1437.59	6.78	676		68	Celestino, 2019
A	1437.71	6.71	653		54	Celestino, 2019
A	1437.84				70	
A	1438.1				62	
A	1438.22				63	
A	1438.35	9.16	689		71	Celestino, 2019
A	1438.6	6.01		2.71	72	Hooker et al., 2020, Dickson et al., 2022
A	1438.7	4.98	599		62	Celestino, 2019
A	1438.84				84	
A	1438.97				63	
A	1439.1				72	
A	1439.24	9.36	657		80	Hooker et al., 2020, Dickson et al., 2022

A	1439.3	6.98	625		66	Celestino, 2019
A	1439.4				91	
A	1439.52	10		1.48	54	Hooker et al., 2020, Dickson et al., 2022
A	1439.6	11.87	659		95	Celestino, 2019
A	1439.68				93	
A	1439.8				77	
A	1439.92	10.58			82	Hooker et al., 2020, Dickson et al., 2022
A	1440.02	8.56	652		77	Celestino, 2019
A	1440.12				85	
A	1440.24				99	
A	1440.36				81	
A	1440.64	10.37	681	3.8	96	Hooker et al., 2020, Dickson et al., 2022
A	1440.76	8.89	643		94	Celestino, 2019
A	1440.88	8.61	639		86	Celestino, 2019
A	1441.34	6.61	665		63	Hooker et al., 2020, Dickson et al., 2022
A	1441.49				84	
A	1441.6	9.68	640	3.72	83	This study
A	1441.8	9.97	655		77	Celestino, 2019
A	1441.92				62	
A	1442.03				74	
A	1442.17				154	
A	1442.27	11.31	623	3.72	88	Celestino, 2019
A	1442.42				80	
A	1442.6	9.68	672		74	Hooker et al., 2020, Dickson et al., 2022
A	1442.82				91	
A	1443.45				61	

A	1443.57	8.75	669	3.17	71	Celestino, 2019
A	1443.63				75	
A	1443.8				82	
A	1443.93	9.25	673		77	This study
A	1444.14	9.03	651		84	Celestino, 2019
A	1444.35	11.46	690	3.39	80	Hooker et al., 2020, Dickson et al., 2022
A	1444.72	12.05	713		94	Celestino, 2019
A	1445.26	11.09	672		93	This study
A	1445.39	11.94	679	3.58	88	This study
A	1445.58	12.18	697		100	Celestino, 2019
A	1445.98	10.07	673		78	This study
A	1446.08	10.5	642		71	Celestino, 2019
A	1446.18	12.09	668	3.09	71	Hooker et al., 2020, Dickson et al., 2022
A	1446.77	9.61	698		58	Celestino, 2019
A	1446.96	10.99	689		95	Hooker et al., 2020, Dickson et al., 2022
A	1447.17	11.1	694	2.61	96	Hooker et al., 2020, Dickson et al., 2022
A	1447.81	11.31	707		77	Hooker et al., 2020, Dickson et al., 2022
A	1448	7.97	642	3.18	83	This study
A	1448.36	9.5	666		79	Celestino, 2019
A	1448.46	8.9	631		133	Celestino, 2019
A	1448.66	13.18	705		132	Hooker et al., 2020, Dickson et al., 2022
A	1448.82	14.74	687		139	Celestino, 2019
A	1449	11.05	687	2.79	110	Celestino, 2019
A	1449.75	13.89	731		120	Hooker et al., 2020, Dickson et al., 2022
A	1450.05	4.44	687	1.31	56	Celestino, 2019
A	1450.22	11.74	705		178	Celestino, 2019

A	1450.53	12.85	752		116	Celestino, 2019
A	1450.6	11.75	767		151	Celestino, 2019
A	1450.73	10.47	728		149	Celestino, 2019
A	1450.95	12.74	720		142	Hooker et al., 2020, Dickson et al., 2022
A	1450.98	9.8	758	2.59	110	Celestino, 2019
A	1451.2	10.21	750		124	Celestino, 2019
A	1451.28	11.04	759		139	Celestino, 2019
A	1451.35	14.57	724	2.99	131	Hooker et al., 2020, Dickson et al., 2022
A	1451.38	13.4	724		138	Hooker et al., 2020, Dickson et al., 2022
A	1451.45	13.12	758		133	Celestino, 2019
A	1451.51	12.25	747		124	Celestino, 2019
A	1451.59	14.3	741		84	Celestino, 2019
B	1238.29	4.93	1	6.07	206	Hooker et al., 2020
B	1238.52	6.29	0	4.83	240	This study
B	1239.42	9.36	7	4.18	200	This study
B	1240.1	4.8	0	3.52	138.5	Hooker et al., 2020
B	1241.34	7.61	0	3.28	164	Hooker et al., 2020
B	1241.43				194	
B	1242.68	7.91	0	4.44	240	Hooker et al., 2020
B	1242.93				259	
B	1243.95				304	
B	1244.18				349	
B	1244.62	9.33	0	4.37	310	Hooker et al., 2020
B	1245.19				253	
B	1246.36	6.9	0	3.61	238	Hooker et al., 2020
B	1246.86	5.69	0	4.11	320	This study

B	1247.13				271	
B	1247.45	6.76	0	3.86	206.5	Hooker et al., 2020
B	1247.87	7.56	0	3.97	243	Hooker et al., 2020
B	1249.76	7.55	0	5.52	360.5	Hooker et al., 2020
B	1250.66	8.97	4	4.75	397	This study
B	1250.92	9.59	0	4.18	323.5	Hooker et al., 2020
B	1251.83	8.82	1	3.26	294.5	Hooker et al., 2020
B	1252.54	8.8	4	3.35	239	This study
B	1252.86	6.06	0	2.99	177	Hooker et al., 2020
B	1253.63	8.32	0	2.84	213	Hooker et al., 2020
B	1254.28	9.07	0	3.48	244	Hooker et al., 2020
B	1255.22	9.75	3	3.17	271	This study
B	1255.88	7.75	0	2.72	159.5	Hooker et al., 2020
B	1257.09	10.96	1	2.78	157	Hooker et al., 2020
B	1257.63				110	
B	1258.07	12.06	1	3.72	184	Hooker et al., 2020
B	1258.48	10.46	2	3.68	194	This study
B	1259.09	12.2	3	3.59	200.5	Hooker et al., 2020
B	1259.5	11.71	5	3.56	246	This study
B	1260.06	7.09	0	2.16	102	Hooker et al., 2020
B	1260.95	9.01	0	3.19	221.5	Hooker et al., 2020
B	1262.22	8.64	3	3.96	169.5	This study
B	1262.39	9.63	3	3.05	169	This study
B	1262.73	10.21	2	2.35	159	This study
B	1263	9.16	1	2.48	109	Hooker et al., 2020
B	1263.32	9.64	1	3.91	207.5	This study

B	1263.75	8.08	0	2.3	87	This study
B	1263.98	2.5	7	2.79	27.75	Hooker et al., 2020
B	1264.27	8.18	0	3.38	136	This study
B	1264.66	5.07	0	3.4	77.5	Hooker et al., 2020
B	1264.89	8.32	2	3.01	139.5	This study
B	1265.33	7.04	0	3.51	174	Hooker et al., 2020
B	1265.53	8.83	0	3.95	250	This study
B	1265.59	10.6	1	4.27	163.5	This study
B	1265.82	8.11	3	3.93	166	This study
C	3257.93	6.85		3.18	248.5	Hooker et al., 2020, Dickson et al., 2022
C	3259.99	8.97		4.01	260	Hooker et al., 2020, Dickson et al., 2022
C	3261.8	8.29		4.68	325.5	Hooker et al., 2020, Dickson et al., 2022
C	3263.3	10.29	9	3.57	294.5	Hooker et al., 2020, Dickson et al., 2022
C	3264.64	9.44		4.84	304	Hooker et al., 2020, Dickson et al., 2022
C	3266.29	12.01		4.53	352.5	Hooker et al., 2020, Dickson et al., 2022
C	3267.56	8.83		4.75	398	Hooker et al., 2020, Dickson et al., 2022
C	3269.23	8.56		3.81	307.5	Hooker et al., 2020, Dickson et al., 2022
C	3270.6	8.62		3.17	220	Hooker et al., 2020, Dickson et al., 2022
C	3272	12.81		4.79	433	Hooker et al., 2020, Dickson et al., 2022
C	3273.16	7.84	0	3.51	282	Hooker et al., 2020, Dickson et al., 2022
C	3274.54	9.96		3.14	233	Hooker et al., 2020, Dickson et al., 2022
C	3276.24	6.7		3.68	268.5	Hooker et al., 2020, Dickson et al., 2022
C	3276.81	6.77	3	2.59	210	Hooker et al., 2020, Dickson et al., 2022
C	3277.93	8.23		2.99	219	Hooker et al., 2020, Dickson et al., 2022
C	3278.88	7.38		2.48	172	Hooker et al., 2020, Dickson et al., 2022
C	3279.89	6.01		2.43	146.5	Hooker et al., 2020, Dickson et al., 2022

C	3280.6	7.03		2.15	158	Hooker et al., 2020, Dickson et al., 2022
C	3281.35	10.32	2	2.87	174	Hooker et al., 2020, Dickson et al., 2022
C	3282.47	9.01		3.69	184.5	Hooker et al., 2020, Dickson et al., 2022
C	3283.2	12.82	3	2.64	159	Hooker et al., 2020, Dickson et al., 2022
C	3283.64	10.44		3.44	202	Hooker et al., 2020, Dickson et al., 2022
C	3284.72	11.97		2.84	190	Hooker et al., 2020, Dickson et al., 2022
C	3285.78	8.34		3.72	211.5	Hooker et al., 2020, Dickson et al., 2022
C	3286.17	9.05	1	4.47	220	This study
C	3286.64	9.08	11	3.01	180	Hooker et al., 2020, Dickson et al., 2022
C	3287.27	11.66		5.83	236.5	Hooker et al., 2020, Dickson et al., 2022
C	3287.49	11.41	12	3.35	221.5	Hooker et al., 2020, Dickson et al., 2022
C	3287.66	8.31		2.77	186	Hooker et al., 2020, Dickson et al., 2022
C	3288.06	8.75	8	6.68	187	Hooker et al., 2020, Dickson et al., 2022
C	3288.44	11.11		3.2	179.5	Hooker et al., 2020, Dickson et al., 2022
C	3288.69	9.89	8	2.81	188.5	This study
C	3288.8	12.03	2	3.83	212.5	Hooker et al., 2020, Dickson et al., 2022
C	3288.89	8.06	12	3.76	220.5	This study
C	3289.1	11		4.12	217.5	Hooker et al., 2020, Dickson et al., 2022

B Data Chapter 3

Hg Pyrolysis Experiment - Table 3.4, Figures 3.3, 3.4, 3.5, 3.7A, 3.7B.

Sub-sample ID	PS-0	PS-1	PS-2	PS-3	PS-4	PS-5	PS-6
Heating time (h)	0	24	24	168	336	500	840
HI (mg HC/g TOC)	701	653	638	603	546	364	317
TOC (%)	8.85	8.65	7.73	7.99	7.3	6	6.07
Tmax (°C)	437	436	440	440	441	443	440
TR	0	0.07	0.09	0.14	0.22	0.48	0.55
TLE (mg/g sediment)	0.44	3.16	9.02	11.58	14.89	22.58	18.31
Hg in extracted residues (ppb)	74.6	48	41.1	41.45	33.05	22.55	28.5
Hg in extracted residues (% of total Hg)	100	64.34	55.09	55.56	44.3	30.23	38.2
Hg/TOC in extracted rock-residues (ppb/%)	8.43	5.55	5.32	5.19	4.53	3.76	4.7
Hg in bitumen(ppb)	-	128.95	44.15	11.1	22.95	40.95	39.75
Hg in bitumen (% of total Hg)	-	0.36	0.38	0.04	0.33	1	0.76
Hg loss (as gas) (% of total Hg)	-	35.29	44.53	44.4	55.36	68.77	61.04
Mercury mass (ng)	3.93	2.57	2.17	2.21	1.78	1.11	1.47
Start	2758	7356	55	9740	10416	480	718
End	2852	7461	135	9872.5	10555	567	814
Area	3530	2304	1870	1982	1598	959	1266
Peak height (instrument units)	288.1	153	136.6	162.1	104.8	60.7	74.8
Hg release (ppb) after >							
1sec	0.00	0.00	-0.02	0.00	0.00	0.00	0.04
2sec	0.01	0.00	-0.02	0.01	0.01	0.01	0.04
3sec	0.02	0.00	-0.01	0.01	0.01	0.01	0.04
4sec	0.02	0.01	-0.01	0.01	0.01	0.01	0.04
5sec	0.02	0.02	-0.01	0.01	0.01	0.01	0.04
6sec	0.02	0.02	-0.01	0.01	0.01	0.02	0.04
7sec	0.02	0.02	-0.01	0.01	0.01	0.02	0.04
8sec	0.02	0.02	-0.01	0.01	0.01	0.02	0.04
9sec	0.02	0.02	-0.01	0.01	0.01	0.02	0.04
10sec	0.02	0.02	0.00	0.01	0.02	0.02	0.04
11sec	0.03	0.02	0.00	0.01	0.02	0.02	0.04
12sec	0.03	0.03	0.00	0.01	0.02	0.02	0.04
13sec	0.04	0.03	0.00	0.01	0.02	0.03	0.04
14sec	0.04	0.03	0.00	0.01	0.02	0.03	0.04
15sec	0.04	0.03	0.00	0.01	0.02	0.03	0.04
16sec	0.04	0.03	0.00	0.02	0.02	0.03	0.04
17sec	0.06	0.03	0.01	0.10	0.03	0.10	0.13

18sec	0.16	0.06	0.27	0.41	0.12	0.39	0.48
19sec	0.48	0.27	0.86	1.07	0.34	0.96	1.17
20sec	1.22	0.72	2.06	2.32	0.79	1.98	2.32
21sec	2.70	1.50	4.00	4.19	1.59	3.31	3.89
22sec	5.25	2.77	6.59	6.74	2.75	4.71	5.59
23sec	9.14	4.55	9.53	9.82	4.24	6.04	7.23
24sec	14.25	6.86	12.54	13.14	6.07	7.20	8.77
25sec	20.21	9.58	15.47	16.33	8.10	8.22	10.14
26sec	26.30	12.61	18.20	19.18	10.25	9.12	11.32
27sec	32.19	15.76	20.67	21.57	12.38	9.98	12.39
28sec	37.54	18.80	22.95	23.58	14.36	10.89	13.49
29sec	42.38	21.60	25.08	25.25	16.08	11.87	14.65
30sec	46.68	23.99	27.03	26.70	17.51	12.88	15.86
31sec	50.43	26.11	28.78	27.94	18.73	13.87	17.02
32sec	53.73	27.97	30.42	29.08	19.76	14.77	18.12
33sec	56.56	29.69	31.95	30.14	20.64	15.57	19.10
34sec	59.00	31.30	33.36	31.16	21.47	16.28	19.93
35sec	61.12	32.82	34.66	32.16	22.23	16.89	20.73
36sec	62.98	34.21	35.84	33.13	22.98	17.43	21.41
37sec	64.65	35.54	36.82	34.08	23.74	17.96	22.10
38sec	66.15	36.77	37.67	34.97	24.48	18.47	22.74
39sec	67.52	37.95	38.32	35.79	25.24	18.94	23.37
40sec	68.70	39.08	38.84	36.55	25.97	19.35	23.96
41sec	69.71	40.16	39.26	37.22	26.70	19.74	24.54
42sec	70.56	41.15	39.54	37.78	27.35	20.09	25.05
43sec	71.24	42.05	39.74	38.28	27.96	20.42	25.51
44sec	71.74	42.83	39.93	38.68	28.50	20.69	25.88
45sec	72.15	43.53	40.10	39.03	28.97	20.92	26.21
46sec	72.44	44.11	40.20	39.31	29.38	21.09	26.47
47sec	72.69	44.60	40.29	39.53	29.74	21.21	26.71
48sec	72.87	44.97	40.36	39.74	30.04	21.35	26.93
49sec	73.03	45.29	40.46	39.91	30.31	21.45	27.11
50sec	73.16	45.56	40.53	40.04	30.53	21.57	27.25
51sec	73.27	45.78	40.59	40.14	30.74	21.65	27.40
52sec	73.38	45.99	40.65	40.23	30.91	21.73	27.50
53sec	73.47	46.15	40.70	40.31	31.03	21.81	27.60
54sec	73.55	46.27	40.74	40.39	31.16	21.87	27.66
55sec	73.63	46.40	40.77	40.47	31.29	21.93	27.74
56sec	73.68	46.50	40.82	40.55	31.38	21.96	27.77
57sec	73.75	46.60	40.87	40.63	31.48	21.99	27.86
58sec	73.82	46.70	40.91	40.67	31.56	22.01	27.91

59sec	73.88	46.78	40.93	40.72	31.62	22.05	27.96
60sec	73.91	46.87	40.96	40.78	31.68	22.06	27.99
61sec	73.98	46.94	40.97	40.83	31.75	22.11	28.04
62sec	74.04	46.99	41.00	40.86	31.80	22.12	28.07
63sec	74.08	47.09	41.03	40.89	31.86	22.14	28.12
64sec	74.13	47.14	41.05	40.96	31.90	22.17	28.16
65sec	74.18	47.19	41.08	40.98	31.95	22.19	28.20
66sec	74.21	47.25	41.08	41.01	32.00	22.23	28.23
67sec	74.25	47.30	41.08	41.03	32.04	22.26	28.25
68sec	74.28	47.34	41.08	41.07	32.07	22.28	28.27
69sec	74.30	47.39	41.08	41.12	32.11	22.29	28.32
70sec	74.32	47.43	41.08	41.13	32.14	22.33	28.32
71sec	74.34	47.45	41.08	41.15	32.17	22.34	28.32
72sec	74.35	47.46	41.08	41.18	32.18	22.34	28.36
73sec	74.37	47.49	41.08	41.20	32.20	22.35	28.36
74sec	74.40	47.52	41.08	41.22	32.23	22.38	28.36
75sec	74.42	47.56	41.08	41.23	32.27	22.41	28.39
76sec	74.43	47.59	41.08	41.24	32.30	22.42	28.39
77sec	74.45	47.61	41.08	41.26	32.31	22.43	28.39
78sec	74.46	47.62	41.08	41.27	32.34	22.44	28.39
79sec	74.46	47.65	41.08	41.28	32.36	22.45	28.39
80sec	74.46	47.67	41.08	41.28	32.39	22.47	28.39
81sec	74.46	47.68	41.08	41.29	32.41	22.48	28.40
82sec	74.47	47.70	41.08	41.29	32.41	22.48	28.42
83sec	74.47	47.70	41.08	41.30	32.43	22.49	28.42
84sec	74.47	47.71	41.08	41.32	32.43	22.50	28.42
85sec	74.48	47.71	41.10	41.32	32.45	22.52	28.42
86sec	74.49	47.73	41.10	41.32	32.47	22.52	28.43
87sec	74.49	47.76	41.10	41.32	32.48	22.52	28.45
88sec	74.50	47.78	41.10	41.32	32.51	22.53	28.45
89sec	74.53	47.79	41.10	41.32	32.53	22.54	28.46
90sec	74.53	47.80	41.10	41.33	32.55	22.54	28.47
91sec	74.53	47.81	41.10	41.33	32.55	22.55	28.47
92sec	74.53	47.82	41.10	41.34	32.58	22.55	28.47
93sec	74.53	47.84	41.10	41.35	32.60	22.55	28.47
94sec	74.54	47.85	41.10	41.37	32.61	22.55	28.47
95sec	74.55	47.86	41.10	41.37	32.63	22.55	28.47
96sec	74.55	47.88	41.10	41.38	32.64	22.55	28.47
97sec	74.55	47.88	41.10	41.38	32.66	22.80	28.48
98sec	74.55	47.89	41.10	41.38	32.67	22.80	28.48
99sec	74.55	47.89	41.10	41.38	32.68	22.80	28.48

100sec	74.57	47.92	41.10	41.38	32.69	22.80	28.48

Hg and Hetero+Polar Compounds in Oils - Figure 3.6

Well name*	Sample name+	Hg (ppb)+	%Hetero*	%Polar*	% (Hetero+Polar)
Steimbke-Ost 10	66.02	4	12.65	0.77	13.42
Wehrbleck-Ost 37	66.05	2.6	3.62	3.49	7.11
Barenburg 52	66.06	2.8	8.42	0	8.42
Suderbruch V 97	66.09	5.2	20.19	8.39	28.58
Suderbruch 11	66.18	3	9.08	3.76	12.84
Barver Süd 1	66.21	2.5	1.17	5.48	6.65

* data from Stock and Littke (2016)
+ data from Indraswari et al. (2024)

Hg Reabsorption Experiment - Table 3.S1, Figure 3.8

Sub-sample ID	PS-0_1	PS-0_2	PS-0-min	PS-1-min	PS-4-min	PS-16-min	PS-60-min
Heating time (h)	0	0	24	24	24	24	24
Cooling time (minutes)	-	-	0	1	4	16	60
Opening temperature (°C)	-	-	280	211	63	16	16
Hg in extracted residues (ppb)	74.3	74.9	37.6	19.2	28.4	48.7	71.4
Hg in extracted residues (% of total Hg)	100	100	50.4	25.74	38.07	65.28	95.71
Hg in bitumen(ppb)	-	-	91.4	39.9	22	38	74.5
Hg in bitumen (% of total Hg)	-	-	0.257	0.15	0.002	0.035	0.426
Hg loss (as gas) (% of total Hg)	-	-	49.34	74.11	61.93	34.68	3.86
Sample mass (mg)	52.5	52.8	54.9	50.7	55.4	52.4	53
Mercury mass (ng)	3.9	3.96	2	0.973	1.57	2.55	3.76
Start	2765	2751	2498	559	751	990	8138
End	2853	2851	2587	652	840	1071	8264
Area	3501	3558	1776	812	1314	2131	3373
Peak height (instrument units)	291.5	284.7	117.9	39.1	64.3	177.9	302.7
Hg release (ppb) after >							
1sec	0.01	-0.01	-0.01	0.03	0.00	0.01	-0.01
2sec	0.01	0.01	0.00	0.03	0.01	0.01	-0.01
3sec	0.01	0.02	0.00	0.04	0.01	0.01	-0.01
4sec	0.01	0.02	0.00	0.04	0.01	0.01	-0.01
5sec	0.01	0.02	0.00	0.04	0.01	0.01	-0.01
6sec	0.01	0.02	0.00	0.04	0.01	0.01	-0.01
7sec	0.01	0.02	0.01	0.04	0.01	0.01	-0.01
8sec	0.01	0.02	0.01	0.04	0.01	0.01	-0.01
9sec	0.01	0.02	0.01	0.04	0.01	0.01	-0.01
10sec	0.01	0.02	0.01	0.04	0.01	0.01	0.00
11sec	0.03	0.02	0.01	0.04	0.02	0.01	0.00
12sec	0.03	0.02	0.01	0.04	0.05	0.01	0.00
13sec	0.05	0.02	0.01	0.04	0.05	0.01	0.00
14sec	0.06	0.02	0.01	0.04	0.05	0.01	0.00
15sec	0.06	0.02	0.01	0.04	0.05	0.01	0.00
16sec	0.06	0.02	0.01	0.04	0.08	0.01	0.00
17sec	0.09	0.02	0.03	0.04	0.17	0.02	0.04
18sec	0.19	0.12	0.19	0.04	0.34	0.13	0.20

19sec	0.43	0.52	0.55	0.14	0.65	0.47	0.63
20sec	1.08	1.36	1.26	0.26	1.17	1.17	1.68
21sec	2.39	3.02	2.37	0.44	1.86	2.42	3.47
22sec	4.77	5.72	3.88	0.72	2.74	4.37	6.57
23sec	8.51	9.77	5.73	1.08	3.80	7.18	11.16
24sec	13.60	14.90	7.80	1.48	5.03	10.64	17.14
25sec	19.59	20.83	10.03	1.93	6.34	14.58	23.52
26sec	25.74	26.86	12.32	2.42	7.72	18.64	29.48
27sec	31.71	32.67	14.57	2.95	9.09	22.45	34.62
28sec	37.19	37.88	16.77	3.54	10.45	25.66	38.84
29sec	42.12	42.64	18.85	4.26	11.74	28.31	42.30
30sec	46.51	46.84	20.74	5.11	13.01	30.52	45.14
31sec	50.32	50.54	22.46	6.02	14.27	32.58	47.59
32sec	53.68	53.78	24.03	6.94	15.46	34.47	49.77
33sec	56.59	56.54	25.49	7.82	16.62	36.23	51.74
34sec	59.02	58.97	26.83	8.67	17.69	37.83	53.54
35sec	61.14	61.09	28.08	9.44	18.71	39.25	55.18
36sec	62.98	62.98	29.21	10.14	19.65	40.53	56.73
37sec	64.57	64.73	30.25	10.81	20.53	41.66	58.17
38sec	66.03	66.28	31.16	11.43	21.35	42.67	59.50
39sec	67.35	67.69	31.97	12.00	22.12	43.57	60.72
40sec	68.44	68.95	32.69	12.54	22.85	44.37	61.86
41sec	69.39	70.03	33.34	13.09	23.50	45.08	62.90
42sec	70.22	70.89	33.88	13.65	24.08	45.69	63.86
43sec	70.86	71.62	34.36	14.20	24.60	46.16	64.74
44sec	71.34	72.14	34.77	14.67	25.07	46.57	65.53
45sec	71.74	72.56	35.14	15.17	25.47	46.89	66.25
46sec	72.02	72.86	35.43	15.61	25.80	47.12	66.87
47sec	72.26	73.12	35.67	16.00	26.10	47.29	67.32
48sec	72.44	73.31	35.86	16.31	26.35	47.43	67.72
49sec	72.59	73.46	36.03	16.57	26.55	47.57	68.06
50sec	72.74	73.58	36.17	16.79	26.73	47.70	68.36
51sec	72.86	73.69	36.30	16.97	26.90	47.79	68.63
52sec	72.95	73.80	36.41	17.17	27.02	47.88	68.80
53sec	73.04	73.90	36.51	17.32	27.10	47.94	69.01
54sec	73.12	73.98	36.60	17.48	27.18	48.01	69.18
55sec	73.19	74.07	36.67	17.58	27.25	48.08	69.31
56sec	73.23	74.13	36.73	17.69	27.33	48.12	69.43
57sec	73.30	74.21	36.79	17.80	27.39	48.19	69.51
58sec	73.37	74.27	36.85	17.86	27.46	48.21	69.61
59sec	73.44	74.31	36.90	17.94	27.53	48.26	69.70

60sec	73.47	74.35	36.95	17.99	27.59	48.28	69.81
61sec	73.54	74.41	36.99	18.09	27.64	48.31	69.89
62sec	73.59	74.49	37.03	18.12	27.69	48.35	69.96
63sec	73.62	74.54	37.07	18.18	27.74	48.36	70.02
64sec	73.68	74.58	37.11	18.22	27.80	48.40	70.07
65sec	73.76	74.61	37.15	18.26	27.82	48.45	70.13
66sec	73.78	74.65	37.18	18.32	27.85	48.46	70.16
67sec	73.83	74.67	37.21	18.34	27.89	48.48	70.19
68sec	73.89	74.68	37.24	18.38	27.93	48.49	70.20
69sec	73.91	74.69	37.26	18.43	27.98	48.51	70.25
70sec	73.94	74.71	37.28	18.50	27.99	48.52	70.29
71sec	73.96	74.71	37.29	18.52	28.02	48.55	70.32
72sec	73.98	74.73	37.30	18.60	28.05	48.56	70.36
73sec	74.00	74.74	37.32	18.63	28.06	48.57	70.40
74sec	74.03	74.76	37.34	18.66	28.08	48.60	70.41
75sec	74.06	74.79	37.36	18.69	28.11	48.62	70.42
76sec	74.08	74.79	37.37	18.70	28.12	48.67	70.46
77sec	74.11	74.79	37.38	18.71	28.14	48.69	70.50
78sec	74.14	74.79	37.38	18.76	28.16	48.70	70.52
79sec	74.14	74.79	37.40	18.78	28.18	48.70	70.55
80sec	74.14	74.79	37.41	18.81	28.18	48.70	70.56
81sec	74.14	74.79	37.41	18.85	28.18	48.70	70.60
82sec	74.16	74.79	37.42	18.88	28.18	48.70	70.64
83sec	74.16	74.79	37.43	18.89	28.20	48.70	70.67
84sec	74.16	74.79	37.43	18.90	28.24	48.70	70.67
85sec	74.16	74.80	37.45	18.93	28.28	48.70	70.67
86sec	74.16	74.81	37.46	18.94	28.30	48.70	70.67
87sec	74.17	74.81	37.47	18.94	28.30	48.70	70.67
88sec	74.19	74.82	37.48	18.96	28.30	48.70	70.69
89sec	74.21	74.84	37.48	18.99	28.30	48.70	70.69
90sec	74.21	74.85	37.49	19.01	28.31	48.70	70.69
91sec	74.21	74.85	37.49	19.03	28.34	48.70	70.69
92sec	74.21	74.85	37.50	19.04	28.34	48.70	70.70
93sec	74.21	74.85	37.51	19.04	28.34	48.70	70.70
94sec	74.23	74.85	37.52	19.04	28.36	48.70	70.70
95sec	74.24	74.85	37.52	19.04	28.36	48.70	70.70
96sec	74.24	74.85	37.53	19.06	28.39	48.70	70.70
97sec	74.24	74.85	37.53	19.10	28.40	48.70	70.70
98sec	74.25	74.86	37.53	19.13	28.40	48.70	70.73
99sec	74.25	74.86	37.53	19.13	28.40	48.70	70.75
100sec	74.28	74.86	37.54	19.15	28.40	48.70	70.75

Hg TDP Natural Cores B and C - Figures 3.7C, D

Sample	C_3269.23	C_3270.60	C_3272.00	C_3273.16	C_3274.54	Averaged Core C
Well name	Core C (%Ro ~3.5%)					
Sample mass (mg)	51.85	49.75	51.5	52.25	50.1	51.09
Mercury concentration (ppb)	293.75	209.9	408.65	265.2	220.65	279.63
Mercury mass (ng)	15.2	10.45	21.05	13.85	11.05	14.32
Area	12285	8427	16985	11180	8920	11559.4
Hg release (ppb) after >						
1sec	-0.03	-0.02	0.00	0.02	-0.01	-0.01
2sec	-0.01	-0.01	0.00	0.04	-0.01	0.00
3sec	0.00	0.00	0.00	0.04	0.01	0.01
4sec	0.00	0.00	0.00	0.04	0.01	0.01
5sec	0.00	0.00	0.00	0.04	0.01	0.01
6sec	0.00	0.00	0.00	0.05	0.01	0.01
7sec	0.01	0.00	0.00	0.05	0.01	0.01
8sec	0.01	0.00	0.00	0.05	0.01	0.01
9sec	0.01	0.00	0.00	0.05	0.01	0.01
10sec	0.01	0.00	0.00	0.05	0.01	0.01
11sec	0.01	0.00	0.00	0.05	0.02	0.02
12sec	0.01	0.00	0.01	0.05	0.03	0.02
13sec	0.01	0.02	0.03	0.05	0.04	0.03
14sec	0.02	0.04	0.04	0.05	0.04	0.04
15sec	0.04	0.04	0.04	0.05	0.04	0.04
16sec	0.05	0.04	0.05	0.05	0.04	0.05
17sec	0.06	0.05	0.05	0.05	0.04	0.05
18sec	0.09	0.06	0.05	0.05	0.04	0.06
19sec	0.10	0.06	0.05	0.05	0.04	0.06
20sec	0.12	0.06	0.05	0.05	0.06	0.07
21sec	0.13	0.07	0.05	0.05	0.07	0.07
22sec	0.13	0.09	0.05	0.05	0.07	0.08
23sec	0.13	0.10	0.06	0.05	0.07	0.08
24sec	0.15	0.14	0.11	0.05	0.07	0.10
25sec	0.17	0.24	0.32	0.05	0.08	0.17
26sec	0.23	0.50	0.79	0.05	0.18	0.35
27sec	0.42	0.95	1.84	0.07	0.44	0.75
28sec	0.85	1.80	3.75	0.32	1.02	1.55
29sec	1.72	3.30	7.08	0.78	2.14	3.00
30sec	3.25	5.70	12.64	1.65	4.05	5.46
31sec	6.13	9.24	20.98	3.09	7.08	9.30

32sec	10.95	14.22	32.38	5.51	11.40	14.89
33sec	18.39	20.71	47.02	9.28	17.16	22.51
34sec	28.98	28.64	64.65	14.73	24.41	32.28
35sec	42.61	37.80	84.93	22.34	33.14	44.16
36sec	59.09	48.16	107.34	32.53	43.58	58.14
37sec	78.10	59.48	131.09	45.47	55.74	73.98
38sec	99.30	71.44	155.54	61.19	69.20	91.33
39sec	121.67	83.78	179.81	79.48	83.50	109.65
40sec	144.38	96.11	203.33	99.84	98.17	128.37
41sec	166.39	108.14	225.74	121.49	112.79	146.91
42sec	186.83	119.65	246.78	143.12	126.88	164.65
43sec	204.93	130.45	266.24	163.41	140.08	181.02
44sec	220.36	140.39	284.01	181.29	151.96	195.60
45sec	233.21	149.35	300.03	196.43	162.39	208.28
46sec	243.64	157.25	314.28	208.78	171.29	219.05
47sec	252.05	164.06	326.79	218.61	178.70	228.04
48sec	258.84	169.86	337.74	226.40	184.92	235.55
49sec	264.30	174.75	347.23	232.73	190.07	241.82
50sec	268.82	178.87	355.37	237.88	194.40	247.07
51sec	272.60	182.37	362.45	242.08	198.00	251.50
52sec	275.81	185.33	368.51	245.60	201.12	255.27
53sec	278.58	187.96	373.72	248.54	203.80	258.52
54sec	280.99	190.26	378.21	251.09	206.14	261.34
55sec	283.10	192.28	382.02	253.29	208.11	263.76
56sec	284.86	194.13	385.32	255.17	209.84	265.86
57sec	286.34	195.77	388.12	256.80	211.30	267.67
58sec	287.59	197.24	390.56	258.15	212.56	269.22
59sec	288.60	198.56	392.73	259.30	213.62	270.56
60sec	289.44	199.71	394.61	260.29	214.52	271.72
61sec	290.12	200.74	396.32	261.09	215.30	272.72
62sec	290.67	201.69	397.84	261.77	215.99	273.59
63sec	291.12	202.55	399.15	262.34	216.58	274.35
64sec	291.51	203.36	400.31	262.82	217.08	275.02
65sec	291.84	204.07	401.37	263.19	217.55	275.60
66sec	292.13	204.76	402.29	263.50	217.93	276.12
67sec	292.37	205.35	403.08	263.77	218.28	276.57
68sec	292.57	205.86	403.78	263.99	218.57	276.95
69sec	292.72	206.31	404.37	264.17	218.81	277.28
70sec	292.87	206.72	404.85	264.33	219.04	277.56
71sec	293.00	207.07	405.28	264.47	219.24	277.81
72sec	293.09	207.37	405.66	264.59	219.43	278.03

73sec	293.19	207.62	406.00	264.69	219.58	278.22
74sec	293.25	207.84	406.28	264.76	219.72	278.37
75sec	293.32	208.04	406.54	264.83	219.84	278.51
76sec	293.38	208.21	406.77	264.89	219.92	278.63
77sec	293.42	208.37	407.00	264.93	220.02	278.75
78sec	293.45	208.52	407.16	264.95	220.10	278.84
79sec	293.50	208.66	407.33	264.98	220.17	278.93
80sec	293.52	208.76	407.47	265.01	220.22	279.00
81sec	293.52	208.87	407.61	265.05	220.28	279.07
82sec	293.54	208.99	407.71	265.07	220.32	279.13
83sec	293.55	209.09	407.81	265.08	220.38	279.18
84sec	293.58	209.18	407.89	265.10	220.39	279.23
85sec	293.60	209.25	407.96	265.10	220.42	279.27
86sec	293.63	209.35	408.04	265.12	220.44	279.32
87sec	293.65	209.42	408.10	265.12	220.49	279.36
88sec	293.67	209.48	408.15	265.16	220.53	279.40
89sec	293.67	209.53	408.21	265.18	220.56	279.43
90sec	293.68	209.59	408.27	265.18	220.58	279.46
91sec	293.69	209.60	408.29	265.18	220.59	279.47
92sec	293.70	209.64	408.33	265.18	220.60	279.49
93sec	293.70	209.66	408.36	265.18	220.61	279.50
94sec	293.70	209.69	408.40	265.18	220.61	279.52
95sec	293.71	209.71	408.42	265.18	220.62	279.53
96sec	293.71	209.73	408.48	265.19	220.63	279.55
97sec	293.71	209.77	408.48	265.19	220.63	279.56
98sec	293.71	209.78	408.49	265.19	220.64	279.56
99sec	293.71	209.79	408.50	265.19	220.64	279.57
100sec	293.71	209.81	408.54	265.19	220.64	279.58

Sample	B_1247.87	B_1249.76	B_1250.66	B_1250.92	B_1251.83	Averaged Core B
Well name	Core B (%Ro ~1.5%)					
Sample mass (mg)	52.2	51.0	50.4	50.5	50.2	50.9
Mercury concentration (ppb)	230.30	354.05	377.10	315.25	275.03	310.35
Mercury mass (ng)	12	18.05	19	15.95	13.8	15.8
Area	9699	14555	15335	12845	11147	12716
Hg release (ppb) after >						
1sec	-0.01	-0.01	-0.01	0.01	0.01	0.00
2sec	-0.01	0.00	-0.01	0.02	0.01	0.00
3sec	0.01	0.01	0.00	0.02	0.02	0.01
4sec	0.01	0.01	0.00	0.02	0.03	0.01
5sec	0.01	0.01	0.01	0.02	0.03	0.01
6sec	0.01	0.02	0.01	0.02	0.03	0.02
7sec	0.01	0.02	0.01	0.02	0.03	0.02
8sec	0.01	0.02	0.01	0.02	0.03	0.02
9sec	0.01	0.02	0.01	0.02	0.03	0.02
10sec	0.01	0.02	0.01	0.02	0.03	0.02
11sec	0.01	0.02	0.01	0.02	0.03	0.02
12sec	0.03	0.03	0.01	0.02	0.04	0.03
13sec	0.03	0.05	0.01	0.02	0.04	0.03
14sec	0.03	0.05	0.02	0.02	0.04	0.03
15sec	0.04	0.05	0.02	0.02	0.04	0.04
16sec	0.05	0.05	0.05	0.02	0.04	0.04
17sec	0.05	0.06	0.06	0.02	0.05	0.05
18sec	0.06	0.07	0.06	0.02	0.05	0.05
19sec	0.08	0.07	0.06	0.02	0.05	0.05
20sec	0.09	0.07	0.06	0.03	0.05	0.06
21sec	0.10	0.07	0.06	0.03	0.06	0.06
22sec	0.10	0.07	0.06	0.03	0.26	0.10
23sec	0.34	0.10	0.36	0.22	1.03	0.41
24sec	1.44	0.20	1.43	0.87	3.24	1.44
25sec	3.95	0.65	3.89	2.70	7.47	3.73
26sec	8.25	1.72	8.88	6.62	14.18	7.93
27sec	14.45	3.99	17.40	13.21	23.25	14.46
28sec	22.73	8.39	29.82	22.40	33.96	23.46
29sec	32.91	15.71	46.00	34.06	45.67	34.87
30sec	44.79	25.97	65.09	47.91	57.93	48.34
31sec	57.89	39.16	86.02	63.49	70.43	63.40
32sec	71.63	54.69	107.75	80.43	83.15	79.53

33sec	85.40	72.19	129.51	98.17	95.93	96.24
34sec	98.75	91.11	150.66	116.20	108.54	113.05
35sec	111.35	111.05	170.86	134.04	120.82	129.62
36sec	123.05	131.38	189.78	151.46	132.61	145.66
37sec	133.76	151.56	207.48	168.03	143.79	160.92
38sec	143.52	171.08	223.88	183.59	154.32	175.28
39sec	152.39	189.53	238.92	197.91	164.17	188.59
40sec	160.35	206.71	252.83	211.10	173.35	200.87
41sec	167.57	222.60	265.64	223.06	181.83	212.14
42sec	174.04	237.06	277.44	233.88	189.72	222.43
43sec	179.88	250.19	288.20	243.66	197.01	231.78
44sec	185.11	261.94	297.91	252.39	203.69	240.21
45sec	189.87	272.54	306.68	260.20	209.74	247.81
46sec	194.19	282.04	314.49	267.16	215.30	254.64
47sec	198.18	290.46	321.42	273.37	220.33	260.75
48sec	201.85	297.94	327.57	278.82	224.94	266.22
49sec	205.18	304.53	332.95	283.57	229.17	271.08
50sec	208.21	310.35	337.70	287.77	233.05	275.41
51sec	210.89	315.55	341.90	291.41	236.57	279.26
52sec	213.18	320.12	345.61	294.62	239.76	282.66
53sec	215.17	324.13	348.93	297.41	242.68	285.66
54sec	216.91	327.68	351.93	299.95	245.32	288.36
55sec	218.38	330.83	354.56	302.20	247.74	290.74
56sec	219.68	333.61	356.86	304.14	249.94	292.85
57sec	220.81	336.14	358.90	305.81	251.95	294.72
58sec	221.83	338.32	360.74	307.24	253.80	296.39
59sec	222.79	340.29	362.37	308.41	255.47	297.87
60sec	223.61	342.03	363.80	309.37	257.02	299.17
61sec	224.36	343.52	365.06	310.20	258.40	300.31
62sec	225.04	344.85	366.18	310.87	259.69	301.33
63sec	225.66	346.00	367.15	311.43	260.84	302.22
64sec	226.21	347.03	368.01	311.92	261.93	303.02
65sec	226.66	347.91	368.81	312.35	262.87	303.72
66sec	227.08	348.67	369.51	312.69	263.75	304.34
67sec	227.44	349.31	370.17	313.02	264.55	304.90
68sec	227.75	349.87	370.75	313.32	265.26	305.39
69sec	228.04	350.34	371.26	313.59	265.94	305.84
70sec	228.29	350.76	371.74	313.81	266.57	306.23
71sec	228.52	351.14	372.17	314.00	267.15	306.60
72sec	228.70	351.48	372.60	314.15	267.68	306.92
73sec	228.83	351.76	372.97	314.29	268.16	307.20

74sec	228.98	352.02	373.30	314.41	268.61	307.46
75sec	229.10	352.23	373.62	314.51	269.01	307.69
76sec	229.19	352.41	373.87	314.60	269.38	307.89
77sec	229.27	352.56	374.14	314.68	269.75	308.08
78sec	229.34	352.73	374.39	314.74	270.08	308.25
79sec	229.40	352.83	374.62	314.81	270.38	308.41
80sec	229.44	352.92	374.82	314.85	270.67	308.54
81sec	229.51	353.02	374.98	314.89	270.93	308.67
82sec	229.56	353.10	375.14	314.96	271.19	308.79
83sec	229.61	353.16	375.26	314.99	271.44	308.89
84sec	229.68	353.24	375.42	315.00	271.66	309.00
85sec	229.72	353.31	375.55	315.03	271.87	309.10
86sec	229.78	353.36	375.64	315.05	272.07	309.18
87sec	229.82	353.40	375.75	315.08	272.24	309.26
88sec	229.87	353.43	375.87	315.11	272.41	309.34
89sec	229.90	353.49	375.95	315.12	272.57	309.40
90sec	229.91	353.54	376.04	315.13	272.71	309.47
91sec	229.93	353.55	376.10	315.13	272.84	309.51
92sec	229.95	353.58	376.19	315.16	272.96	309.57
93sec	229.97	353.61	376.23	315.16	273.09	309.61
94sec	229.99	353.64	376.27	315.19	273.21	309.66
95sec	230.03	353.64	376.33	315.21	273.32	309.71
96sec	230.05	353.66	376.39	315.23	273.42	309.75
97sec	230.07	353.68	376.44	315.23	273.52	309.79
98sec	230.10	353.68	376.49	315.23	273.62	309.82
99sec	230.11	353.70	376.54	315.23	273.71	309.86
100sec	230.13	353.72	376.59	315.23	273.81	309.90

C Data Chapter 4

Mercury fraction remaining *vs* artificial heating temperature – Figure 4.1.

SampleID	Tempe-rature (°C)	Environment of deposition	fHg remaining	References
Belemnite Marls	20	Marine (calcareous)	1.00	This study
Belemnite Marls	325	Marine (calcareous)	0.24	This study
Belemnite Marls	325	Marine (calcareous)	0.23	This study
Belemnite Marls	325	Marine (calcareous)	0.19	This study
Belemnite Marls	325	Marine (calcareous)	0.17	This study
Belemnite Marls	325	Marine (calcareous)	0.20	This study
Tanjung Formation	20	Terrestrial/Coastal swamp	1.00	This study
Tanjung Formation	325	Terrestrial/Coastal swamp	0.29	This study
Tanjung Formation	325	Terrestrial/Coastal swamp	0.24	This study
Tanjung Formation	325	Terrestrial/Coastal swamp	0.08	This study
Tanjung Formation	325	Terrestrial/Coastal swamp	0.12	This study
Posidonienschiefer	20	Marine (clastic)	1.00	Indraswari et al., *submitted*
Posidonienschiefer	325	Marine (clastic)	0.61	Indraswari et al., *submitted*
Posidonienschiefer	325	Marine (clastic)	0.56	Indraswari et al., *submitted*
Posidonienschiefer	325	Marine (clastic)	0.44	Indraswari et al., *submitted*
Posidonienschiefer	325	Marine (clastic)	0.31	Indraswari et al., *submitted*
Posidonienschiefer	325	Marine (clastic)	0.38	Indraswari et al., *submitted*
ZLDL	20	Marine (calcareous)	1.00	Liu et al., 2022
ZLDL	375	Marine (calcareous)	0.27	Liu et al., 2022
ZLDL	395	Marine (calcareous)	0.32	Liu et al., 2022
ZLDL	415	Marine (calcareous)	0.16	Liu et al., 2022
ZLDL	435	Marine (calcareous)	0.12	Liu et al., 2022
ZLDL	460	Marine (calcareous)	0.13	Liu et al., 2022
ZLDL	485	Marine (calcareous)	0.04	Liu et al., 2022
X491	20	Lacustrine (lake)	1.00	Liu et al., 2022
X491	350	Lacustrine (lake)	0.34	Liu et al., 2022
X491	375	Lacustrine (lake)	0.25	Liu et al., 2022
X491	395	Lacustrine (lake)	0.19	Liu et al., 2022
X491	415	Lacustrine (lake)	0.20	Liu et al., 2022
X491	435	Lacustrine (lake)	0.11	Liu et al., 2022
X491	460	Lacustrine (lake)	0.08	Liu et al., 2022
X491	485	Lacustrine (lake)	0.03	Liu et al., 2022
X491	510	Lacustrine (lake)	0.02	Liu et al., 2022
X491	535	Lacustrine (lake)	0.02	Liu et al., 2022
X491	585	Lacustrine (lake)	0.03	Liu et al., 2022
X491	610	Lacustrine (lake)	0.02	Liu et al., 2022
X491-2	20	Lacustrine (lake)	1.00	Liu et al., 2022
X491-2	375	Lacustrine (lake)	0.25	Liu et al., 2022
X491-2	395	Lacustrine (lake)	0.27	Liu et al., 2022
X491-2	415	Lacustrine (lake)	0.19	Liu et al., 2022
X491-2	435	Lacustrine (lake)	0.21	Liu et al., 2022

X491-2	460	Lacustrine (lake)	0.16	Liu et al., 2022
X491-2	485	Lacustrine (lake)	0.18	Liu et al., 2022
XJG	20	Marine (clastic)	1.00	Liu et al., 2022
XJG	375	Marine (clastic)	0.33	Liu et al., 2022
XJG	395	Marine (clastic)	0.27	Liu et al., 2022
XJG	415	Marine (clastic)	0.06	Liu et al., 2022
XJG	435	Marine (clastic)	0.06	Liu et al., 2022
XJG	460	Marine (clastic)	0.12	Liu et al., 2022
XJG	485	Marine (clastic)	0.07	Liu et al., 2022
XQ1-2	20	Marine (clastic)	1.00	Liu et al., 2022
XQ1-2	350	Marine (clastic)	0.69	Liu et al., 2022
XQ1-2	375	Marine (clastic)	0.59	Liu et al., 2022
XQ1-2	395	Marine (clastic)	0.51	Liu et al., 2022
XQ1-2	415	Marine (clastic)	0.46	Liu et al., 2022
XQ1-2	435	Marine (clastic)	0.28	Liu et al., 2022
XQ1-2	460	Marine (clastic)	0.12	Liu et al., 2022
XQ1-2	485	Marine (clastic)	0.01	Liu et al., 2022
XQ1-2	510	Marine (clastic)	0.01	Liu et al., 2022
XQ1-2	535	Marine (clastic)	0.01	Liu et al., 2022
XQ1-2	585	Marine (clastic)	0.01	Liu et al., 2022
XQ1-2	610	Marine (clastic)	0.01	Liu et al., 2022
WH	20	Marine (clastic)	1.00	Chen et al., 2022
WH	100	Marine (clastic)	0.96	Chen et al., 2022
WH	150	Marine (clastic)	0.78	Chen et al., 2022
WH	200	Marine (clastic)	0.89	Chen et al., 2022
WH	250	Marine (clastic)	0.89	Chen et al., 2022
WH	300	Marine (clastic)	0.75	Chen et al., 2022
WH	400	Marine (clastic)	0.69	Chen et al., 2022
WH	450	Marine (clastic)	0.50	Chen et al., 2022
WH	500	Marine (clastic)	0.47	Chen et al., 2022
WH	700	Marine (clastic)	0.24	Chen et al., 2022
GSS-4-200	20	Recent contaminated soil	1.00	Chen et al., 2022
GSS-4-200	200	Recent contaminated soil	0.93	Chen et al., 2022
GSS-4-200	200	Recent contaminated soil	0.98	Chen et al., 2022
GSS-4-200	200	Recent contaminated soil	0.97	Chen et al., 2022
GSS-4-200	200	Recent contaminated soil	0.99	Chen et al., 2022
GSS-4-CS	20	Recent contaminated soil	1.00	Chen et al., 2022
GSS-4-CS	50	Recent contaminated soil	0.97	Chen et al., 2022
GSS-4-CS	100	Recent contaminated soil	0.94	Chen et al., 2022
GSS-4-CS	300	Recent contaminated soil	0.96	Chen et al., 2022
GSS-4-CS	400	Recent contaminated soil	0.97	Chen et al., 2022
GSS-4-CS	500	Recent contaminated soil	0.67	Chen et al., 2022
GSS-4-CS	600	Recent contaminated soil	0.47	Chen et al., 2022
GSS-4-500	500	Recent contaminated soil	0.84	Chen et al., 2022
GSS-4-500	500	Recent contaminated soil	0.83	Chen et al., 2022
GSS-4-500	500	Recent contaminated soil	0.91	Chen et al., 2022
GSS-4-500	500	Recent contaminated soil	0.93	Chen et al., 2022

Rock-Eval data for Posidonienschiefer – Figure 4.2.

Sample ID	Posidoniencshiefer					
Heating time (hours)	0	24	168	336	500	840
HI (mg HC/g TOC)	701	645.5	603	546	364	317
OI (mg HC/g TOC)	12	9	5	6	10	13
S2 (mg HC/ g rock)	62.03	52.9	48.15	39.84	21.83	19.22
TOC (%)	8.85	8.19	7.99	7.3	6	6.07

Hg TDP Pyrolysis Experiment - Figures 4.5

Belemnite Marls sample

Sub-sample ID	BM-0	BM-24	BM-168	BM-336	BM-500	BM-840
Heating time (h)	0	24	168	336	500	840
Sample mass (mg)	51.1	53.1	50.7	51.3	52.3	51.9
Mercury concentration (ppb)	323.4	78.7	65.9	74.7	60.8	55.3
Mercury mass (ng)	16.5	4.18	3.34	3.83	3.18	2.87
Area	14610	3524	2819	3232	2680	2420
Maximum height curve	1468.2	223.1	113.7	191	130.4	142.5
Hg release (ppb) after >						
1sec	0.003	-0.020	0.007	0.018	0.004	0.002
2sec	0.003	-0.020	0.031	0.042	0.006	0.002
3sec	0.003	-0.020	0.031	0.042	0.006	0.002
4sec	0.003	-0.020	0.031	0.042	0.006	0.002
5sec	0.003	-0.020	0.031	0.047	0.016	0.010
6sec	0.003	-0.020	0.031	0.047	0.016	0.022
7sec	0.003	-0.020	0.031	0.047	0.016	0.022
8sec	0.003	-0.020	0.031	0.047	0.016	0.022
9sec	0.008	-0.004	0.031	0.047	0.016	0.022
10sec	0.008	0.004	0.031	0.047	0.016	0.022
11sec	0.008	0.031	0.031	0.047	0.016	0.022
12sec	0.008	0.048	0.031	0.047	0.016	0.022
13sec	0.008	0.060	0.045	0.052	0.059	0.022
14sec	0.008	0.060	0.045	0.052	0.071	0.022
15sec	0.008	0.066	0.045	0.052	0.071	0.022
16sec	0.008	0.066	0.078	0.052	0.073	0.022
17sec	0.008	0.094	0.078	0.052	0.073	0.022
18sec	0.008	0.120	0.078	0.052	0.083	0.037
19sec	0.026	0.120	0.078	0.052	0.083	0.052
20sec	0.297	0.120	0.095	0.052	0.112	0.082
21sec	1.694	0.120	0.141	0.052	0.193	0.194
22sec	6.686	0.215	0.237	0.181	0.328	0.338
23sec	18.551	0.443	0.425	0.725	0.626	0.642
24sec	38.814	0.971	0.789	1.753	1.200	1.199
25sec	66.843	2.024	1.408	3.179	2.123	1.961
26sec	98.806	3.751	2.284	4.922	3.430	2.975
27sec	131.193	6.238	3.516	6.821	5.073	4.297
28sec	162.608	9.587	4.971	8.815	7.039	5.889
29sec	191.896	13.690	6.752	10.909	9.211	7.768
30sec	217.535	18.448	8.733	13.134	11.526	10.037

31sec	238.655	23.377	11.018	15.604	13.967	12.652
32sec	254.788	28.090	13.422	18.347	16.537	15.561
33sec	266.517	32.369	15.988	21.590	19.270	18.723
34sec	274.761	36.105	18.606	25.317	22.140	21.971
35sec	280.741	39.602	21.262	29.404	25.063	25.209
36sec	285.152	42.989	23.907	33.714	27.997	28.287
37sec	288.494	46.277	26.529	38.111	30.934	31.187
38sec	291.184	49.314	29.108	42.355	33.782	33.879
39sec	293.434	52.070	31.690	46.276	36.361	36.302
40sec	295.441	54.549	34.246	49.751	38.774	38.606
41sec	297.326	56.791	36.738	52.776	40.984	40.748
42sec	299.067	58.941	39.098	55.503	43.103	42.746
43sec	300.780	61.093	41.285	58.004	45.129	44.550
44sec	302.517	63.227	43.344	60.322	47.102	46.201
45sec	304.217	65.349	45.382	62.513	49.010	47.702
46sec	305.911	67.403	47.369	64.555	50.767	49.048
47sec	307.615	69.331	49.360	66.437	52.411	50.187
48sec	309.291	71.037	51.410	68.123	53.875	51.139
49sec	310.937	72.533	53.440	69.580	55.134	51.900
50sec	312.529	73.754	55.449	70.749	56.210	52.577
51sec	313.989	74.801	57.337	71.705	57.121	53.114
52sec	315.354	75.607	59.066	72.395	57.888	53.560
53sec	316.509	76.254	60.620	72.952	58.483	53.912
54sec	317.577	76.775	61.848	73.400	58.958	54.179
55sec	318.515	77.168	62.819	73.723	59.359	54.377
56sec	319.303	77.464	63.529	73.959	59.642	54.553
57sec	319.964	77.691	64.063	74.119	59.877	54.693
58sec	320.503	77.850	64.489	74.294	60.066	54.766
59sec	321.022	78.017	64.778	74.440	60.234	54.838
60sec	321.472	78.126	65.021	74.520	60.337	54.893
61sec	321.793	78.231	65.177	74.579	60.419	54.941
62sec	322.055	78.312	65.342	74.617	60.470	54.975
63sec	322.245	78.369	65.458	74.666	60.515	54.989
64sec	322.406	78.411	65.528	74.679	60.539	55.001
65sec	322.554	78.481	65.622	74.679	60.584	55.023
66sec	322.678	78.498	65.649	74.685	60.635	55.064
67sec	322.733	78.539	65.675	74.693	60.651	55.080
68sec	322.798	78.539	65.728	74.693	60.685	55.111
69sec	322.876	78.539	65.738	74.700	60.695	55.126
70sec	322.956	78.547	65.761	74.700	60.701	55.159
71sec	323.023	78.547	65.775	74.700	60.701	55.163
72sec	323.045	78.559	65.798	74.700	60.701	55.163

73sec	323.089	78.559	65.798	74.700	60.701	55.163
74sec	323.109	78.559	65.798	74.700	60.701	55.173
75sec	323.135	78.573	65.816	74.700	60.701	55.173
76sec	323.143	78.573	65.842	74.700	60.701	55.173
77sec	323.171	78.573	65.842	74.700	60.701	55.173
78sec	323.178	78.573	65.855	74.700	60.701	55.175
79sec	323.182	78.573	65.869	74.700	60.709	55.175
80sec	323.215	78.573	65.869	74.700	60.727	55.175
81sec	323.215	78.573	65.869	74.700	60.743	55.208
82sec	323.215	78.576	65.869	74.700	60.743	55.246
83sec	323.216	78.596	65.869	74.700	60.743	55.246
84sec	323.231	78.625	65.869	74.700	60.743	55.256
85sec	323.236	78.641	65.869	74.700	60.743	55.259
86sec	323.236	78.641	65.869	74.700	60.743	55.259
87sec	323.240	78.641	65.869	74.700	60.743	55.266
88sec	323.240	78.641	65.869	74.700	60.743	55.266
89sec	323.271	78.641	65.869	74.700	60.743	55.266
90sec	323.271	78.641	65.869	74.700	60.743	55.266
91sec	323.271	78.641	65.871	74.700	60.743	55.266
92sec	323.271	78.674	65.886	74.700	60.743	55.266
93sec	323.271	78.700	65.886	74.700	60.771	55.266
94sec	323.282	78.700	65.886	74.700	60.771	55.266
95sec	323.282	78.700	65.886	74.700	60.771	55.269
96sec	323.282	78.700	65.886	74.700	60.774	55.278
97sec	323.287	78.700	65.886	74.700	60.776	55.298
98sec	323.309	78.700	65.886	74.700	60.787	55.298
99sec	323.332	78.700	65.892	74.700	60.788	55.298
100sec	323.362	78.700	65.892	74.700	60.800	55.298

Tanjung Formation coal

Sub-sample ID	TJ-0	TJ-24	TJ-336	TJ-500	TJ-840
Heating time (h)	0	24	336	500	840
Sample mass (mg)	49.2	52.4	50.6	50.6	50.3
Mercury concentration (ppb)	44.2	12.7	10.8	3.6	5.4
Mercury mass (ng)	2.57	0.663	0.546	0.182	0.272
Area	2080	536	441	147	220
Maximum height curve	266.8	73.4	58.8	21	27.5
Hg release (ppb) after >					
1sec	0.010	0.027	-0.038	0.013	-0.013
2sec	0.023	0.027	-0.033	0.013	0.015
3sec	0.023	0.027	-0.033	0.013	0.023
4sec	0.023	0.027	-0.033	0.022	0.028
5sec	0.023	0.027	-0.033	0.032	0.030
6sec	0.027	0.027	-0.033	0.032	0.050
7sec	0.027	0.027	-0.033	0.046	0.050
8sec	0.028	0.027	-0.033	0.046	0.050
9sec	0.028	0.027	-0.025	0.046	0.050
10sec	0.028	0.027	-0.005	0.046	0.050
11sec	0.028	0.027	0.019	0.046	0.050
12sec	0.028	0.027	0.019	0.046	0.050
13sec	0.028	0.027	0.019	0.046	0.050
14sec	0.028	0.027	0.040	0.046	0.050
15sec	0.028	0.027	0.040	0.046	0.050
16sec	0.028	0.027	0.040	0.046	0.050
17sec	0.028	0.027	0.062	0.046	0.050
18sec	0.028	0.027	0.062	0.046	0.050
19sec	0.028	0.027	0.062	0.046	0.050
20sec	0.028	0.027	0.089	0.046	0.050
21sec	0.174	0.201	0.296	0.046	0.110
22sec	0.764	0.653	0.775	0.068	0.244
23sec	2.183	1.477	1.573	0.211	0.467
24sec	4.840	2.806	2.809	0.499	0.855
25sec	9.165	4.571	4.235	0.904	1.383
26sec	15.085	6.339	5.617	1.410	2.026
27sec	21.794	7.850	6.845	1.931	2.691
28sec	28.407	9.033	7.849	2.419	3.255
29sec	34.279	9.939	8.641	2.818	3.683
30sec	39.181	10.504	9.165	3.067	4.029
31sec	43.133	10.869	9.543	3.256	4.284
32sec	45.987	11.081	9.821	3.369	4.445

33sec	47.924	11.214	9.953	3.421	4.574
34sec	49.159	11.266	10.035	3.472	4.658
35sec	49.975	11.334	10.043	3.484	4.735
36sec	50.512	11.350	10.079	3.495	4.775
37sec	50.869	11.385	10.085	3.509	4.825
38sec	51.108	11.424	10.132	3.509	4.831
39sec	51.286	11.459	10.151	3.509	4.831
40sec	51.358	11.525	10.169	3.509	4.831
41sec	51.432	11.575	10.169	3.509	4.845
42sec	51.521	11.622	10.169	3.509	4.854
43sec	51.575	11.694	10.189	3.509	4.875
44sec	51.647	11.769	10.189	3.509	4.875
45sec	51.730	11.777	10.211	3.509	4.908
46sec	51.758	11.827	10.259	3.509	4.938
47sec	51.822	11.876	10.295	3.509	4.960
48sec	51.847	11.908	10.328	3.509	4.977
49sec	51.894	11.953	10.362	3.509	5.004
50sec	51.924	11.981	10.403	3.512	5.010
51sec	51.986	12.014	10.464	3.512	5.014
52sec	52.022	12.028	10.494	3.523	5.039
53sec	52.072	12.120	10.541	3.553	5.103
54sec	52.100	12.181	10.582	3.563	5.158
55sec	52.132	12.219	10.627	3.600	5.183
56sec	52.132	12.270	10.627	3.600	5.217
57sec	52.162	12.309	10.627	3.600	5.254
58sec	52.211	12.346	10.627	3.600	5.287
59sec	52.254	12.381	10.627	3.600	5.295
60sec	52.254	12.457	10.635	3.600	5.315
61sec	52.260	12.457	10.646	3.600	5.332
62sec	52.281	12.460	10.646	3.600	5.344
63sec	52.292	12.482	10.665	3.600	5.344
64sec	52.292	12.497	10.692	3.600	5.344
65sec	52.300	12.497	10.711	3.600	5.353
66sec	52.300	12.497	10.741	3.600	5.353
67sec	52.300	12.509	10.741	3.600	5.353
68sec	52.300	12.517	10.751	3.600	5.353
69sec	52.300	12.548	10.751	3.600	5.372
70sec	52.300	12.552	10.751	3.600	5.372
71sec	52.300	12.552	10.752	3.600	5.395
72sec	52.300	12.552	10.755	3.600	5.395
73sec	52.300	12.560	10.755	3.600	5.395

74sec	52.300	12.582	10.762	3.600	5.395
75sec	52.300	12.598	10.770	3.600	5.395
76sec	52.300	12.607	10.781	3.600	5.395
77sec	52.300	12.623	10.785	3.600	5.395
78sec	52.300	12.632	10.785	3.600	5.395
79sec	52.300	12.666	10.785	3.600	5.395
80sec	52.300	12.679	10.785	3.600	5.395
81sec	52.300	12.700	10.785	3.600	5.395
82sec	52.300	12.700	10.800	3.600	5.395
83sec	52.300	12.700	10.800	3.600	5.395
84sec	52.300	12.700	10.800	3.600	5.395
85sec	52.300	12.700	10.800	3.600	5.395
86sec	52.300	12.700	10.800	3.600	5.395
87sec	52.300	12.700	10.800	3.600	5.395
88sec	52.300	12.700	10.800	3.600	5.397
89sec	52.300	12.700	10.800	3.600	5.400
90sec	52.300	12.700	10.800	3.600	5.400
91sec	52.300	12.700	10.800	3.600	5.400
92sec	52.300	12.700	10.800	3.600	5.400
93sec	52.300	12.700	10.800	3.600	5.400
94sec	52.300	12.700	10.800	3.600	5.400
95sec	52.300	12.700	10.800	3.600	5.400
96sec	52.300	12.700	10.800	3.600	5.400
97sec	52.300	12.700	10.800	3.600	5.400
98sec	52.300	12.700	10.800	3.600	5.400
99sec	52.300	12.700	10.800	3.600	5.400
100sec	52.300	12.700	10.800	3.600	5.400

Fraction Hg_T – Figures 4.5.

Sample	Heating hours	HgLT (Hg<35s)	HgHT (Hg>35s)
Posidonienschiefer	0	0.77	0.23
Posidonienschiefer	24	0.67	0.33
Posidonienschiefer	168	0.73	0.27
Posidonienschiefer	336	0.6	0.4
Posidonienschiefer	500	0.71	0.29
Posidonienschiefer	840	0.66	0.34
Tanjung Formation coal	0	0.95	0.05
Tanjung Formation coal	24	0.88	0.12
Tanjung Formation coal	336	0.94	0.06
Tanjung Formation coal	500	0.95	0.05
Tanjung Formation coal	840	0.89	0.11
Belemnite Marls	0	0.87	0.13
Belemnite Marls	24	0.51	0.49
Belemnite Marls	168	0.32	0.68
Belemnite Marls	336	0.32	0.68
Belemnite Marls	500	0.42	0.58
Belemnite Marls	840	0.46	0.54